The Dissertation Committee for Han Duc Tran
certifies that this is the approved version of the following dissertation:

A Computational Procedure for Analysis of Fractures in Two-dimensional Multi-field Media

Committee:

Mark E. Mear, Supervisor

Gregory J. Rodin

K. Ravi-Chandar

Chad M. Landis

John L. Tassoulas

A Computational Procedure for Analysis of Fractures in Two-dimensional Multi-field Media

by

Han Duc Tran, B.S., M.S.

DISSERTATION

Presented to the Faculty of the Graduate School of
The University of Texas at Austin
in Partial Fulfillment
of the Requirements
for the Degree of

DOCTOR OF PHILOSOPHY

THE UNIVERSITY OF TEXAS AT AUSTIN
December 2010

This dissertation is dedicated to my beloved wife Tuyet Hoa

and son Bao Huy.

Acknowledgments

I wish to express my appreciation and gratitude to my advisor Professor Mark E. Mear, for his excellent guidance and encouragement throughout this research.

I would also like to thank my Advisory Committee, Professors Gregory J. Rodin, K. Ravi-Chandar, Chad M. Landis, and John L. Tassoulas, for their helpful suggestions and comments. Further, my great appreciation goes to the NASA Marshall Space Flight Center and Vietnam Education Foundation for providing financial support for this work.

I would like to extend my thanks to all my colleagues and friends. In particular, I would like to thank Dr. Jaroon Rungamornrat for his friendship and help. Last but not least, I would like to thank my wife Tuyet Hoa, and my parents Van Hien and Cam Duong. Without their love and supports I would never finish this work.

A Computational Procedure for Analysis of Fractures in Two-dimensional Multi-field Media

Publication No. ____________________

Han Duc Tran, Ph.D.
The University of Texas at Austin, 2010

Supervisor: Mark E. Mear

A systematic procedure is followed to develop singularity-reduced integral equations for modeling cracks in two-dimensional, linear multi-field media. The class of media treated is quite general and includes, as special cases, anisotropic elasticity, piezoelectricity and magnetoelectroelasticity. Of particular interest is the development of a pair of weakly-singular, weak-form integral equations (IEs) for "generalized displacement" and "generalized stress"; these serve as the basis for the development of a Symmetric Galerkin Boundary Element Method (SGBEM). The implementation is carried out to allow treatment of general mixed boundary conditions, an arbitrary number of cracks, and multi-region domains (in which regions having different material properties are bonded together). Finally, a procedure for calculation of T-stress, the constant term in the asymptotic series expansion of crack-tip stress field, is developed for anisotropic elastic media.

The pair of weak-form boundary IEs that is derived (one for generalized displacement and the other one for generalized stress) are completely regularized in the sense that all kernels that appear are (at most) weakly-singular. This feature allows standard C^o elements to be utilized in the SGBEM, and such elements are employed everywhere except at the crack tip. A special crack-tip element is developed to properly model the asymptotic behavior of the relative crack-face displacements. This special element contains “extra” degrees of freedom that allow the generalized stress intensity factors to be directly obtained from the solution of the governing system of discretized equations. It should be noted that while the integral equations contain only weakly-singular kernels (and so are integrable in the usual sense) there remains a need to devise special integration techniques to accurately evaluate these integrals as part of the numerical implementation.

Various examples for crack problems are treated to illustrate the accuracy and versatility of the proposed procedure for both unbounded and finite domains and for both single-region and multi-region problems. It is found that highly accurate fracture data can be obtained using relatively course meshes.

Finally, this dissertation addresses the development of a numerical procedure to calculate T-stress for crack problems in general anisotropic elastic media. T-stress is obtained from the sum of crack-face displacements which are computed via a (regularized) integral equation of the boundary data. Two approaches for computing the derivative of the sum of crack-face displacements are proposed: one uses numerical differentiation, and the other one uses a weak-form integral equation. Various examples are examined to demonstrate that highly accurate results are obtained by means of both approaches.

Table of Contents

List of Tables

List of Figures

Chapter 1

Introduction

Computational fracture analysis has become an important aspect in engineering design and/or structural integrity assessment. Besides the well-recognized application in mechanical elastic materials, fracture analysis has recently received the increased interest of researchers and engineers in analyzing smart materials (e.g. piezoelectric or magnetoelectroelastic materials). These materials can be effectively employed for active structures, nondestructive testing devices, electronic devices, sensors and actuators and so on. Due to complicated behavior of the coupled electric-mechanical responses or electric-magnetic-mechanical responses, analytical solutions for crack problems in smart materials have been limited to relatively simple problems. Thus, it is both necessary and practical to have a numerical technique that can effectively perform the fracture analysis of a complex structural component to assure proper working condition during its lifetime.

For a great many fracture mechanics applications, any non-linear material behavior is contained within a region near the crack tip that is sufficiently small (as compared to other relevant dimensions of the structure) such that solutions based upon linear analysis can provide appropriate fracture data. Although the standard Finite Element Method (FEM) is a powerful tool for engineering analysis, it has significant drawbacks when applied to the modeling of cracks and, in particular, for the simulation of crack growth. This is due to the fact that the region around the crack front must be finely meshed in order to capture the singular crack tip fields. Perhaps more importantly, remeshing the domain around the crack can become quite complicated when the crack does not remain planar. Boundary Element Methods (BEM) are attractive alternatives to the FEM for fracture analysis since in the absence of a distributed source, only the boundary of the region requires discretization. A particularly effective BEM formulation for crack problems is the weakly-singular symmetric Galerkin boundary element method (SGBEM) for isotropic and anisotropic linear elasticity and piezoelectricity recently developed by Li *et al.* [42] and Rungamornrat and Mear [57], [56], [58]. However, as of yet, a two-dimensional weakly-singular SGBEM for cracks in anisotropic or piezoelectric or magnetoelectroelastic media [1] has not been developed. Moreover, two-dimensional analyses for crack problems are much less computationally expensive than three-dimensional analyses, yet they are often sufficient to provide the information relevant to a fracture-analysis based assessment of a structural component.

The main objective of the present work is to develop a weakly-singular Symmetric Galerkin Boundary Element Method (SGBEM) for solving two-dimensional boundary value problems involving cracks in multi-field media. While the method is analogous to the three-dimensional version for anisotropic elastic media and piezoelectric media that was developed by Li *et al.*, Rungamornrat and Mear (e.g. [42], [57], [56], [58]), the key ingredients employed are nontrivially distinct from the three-dimensional setting. The mathematical development is carried out for a fairly gen-

---

[1] All of these media are termed, as suggested by other authors, ‘multi-field’ media.

eral class of linear multi-field media that includes, as special cases, anisotropic elasticity, piezoelectricity and magnetoelectroelasticity. An additional objective of this work is to develop a computational procedure to calculate T-stress for crack problems in anisotropic elastic media. This method can be considered a ‘post-processing’ stage when T-stress is obtained from the solution of the governing system of equations of the problem. An important feature of the proposed method for T-stress determination is that all kernels appearing in the integral relations are weakly-singular.

1.1 Boundary integral equation methods for 2D crack problems

1.1.1 Elastic media

As mentioned earlier, BEM is well recognized as an effective numerical tool for linear elastic fracture analysis due to the fact that only the crack faces and the boundary of a body-force-free domain are discretized. Unfortunately, the conventional BEM cannot be applied to crack problems due to the fact that the displacement integral equation lacks information about traction on crack face (e.g. Cruse [17]) when a self-equilibrated traction is applied on the crack face. To overcome this difficulty, a traction integral equation must be employed either instead of or in addition to a displacement equation. Such a traction equation is obtained from the displacement equation via a constitutive relation and a proper limiting process. The resulting equation contains a hyper-singular kernel (of order $1/r^2$) which requires special theoretical and numerical treatments. Furthermore, the existence of strongly-singular integrals requires that the gradient of displacements be continuous (e.g. Martin [46]). Various studies have been done to directly perform the hyper-singular integrals. For SGBEM employing straight elements, the strongly-singular integrals can be analytically evaluated, e.g. Carini *et al.* [13] by implementing continuous piecewise-linear displacements and piecewise-constant tractions, Salvadori [59] utilized polynomial shape functions of arbitrary degree, Sirtori *et al.* [62] derived complex-variable formulation with continuous linear displacements and piecewise-constant tractions. To preserve the symmetry of the Galerkin approach for curved elements, Bonnet and Guiggiani [9] applied coordinate transformations in a two-dimensional space of intrinsic coordinates to directly evaluate the singular double integrals as a whole. Their proposed procedure was applied to 2D anisotropic potential problems and 2D isotropic elastic problems. Garcia *et al.* [29] employed both displacement and traction integral equations for a mixed collocation boundary element approach. They applied a decomposition for the strongly-singular integral into a regular integral and a singular one with (known) analytical solution. Their approach utilized discontinuous elements with the collocation nodes moving into the interior of the element to fulfill the C^1 continuous condition.

Another approach to alleviate the difficulties posed by hyper-singular kernels is to seek singularity-reduced traction integral equations via a regularization process. In an attempt to reduce the order of singular integrals, Richardson and Cruse [55] exploited the state of constant-stress to obtain a 'weakly-singular' stress integral equation. However, the nature of the smoothness requirement for the crack-face displacement remains unclear. In addition, their method requires higher-order elements other than standard quadratic elements to model problems having non-trivial stress solution. In the context of SGBEM, Frangi and Novati (e.g. [24], [25]) utilized a technique of integration by parts to regularize strongly-singular kernels into weakly-singular ones. Their technique included the utilization of piecewise continuous functions to model the traction. However, this procedure is only applicable for isotropic elasticity. Recently, Bonnet [8] presented a general regularization technique applicable to 2D and 3D elastostatics. His technique involved the regularization of hyper-singular integral by combining the (hyper-singular) kernel with a function to reduce the singular order of the whole integrand. However, it only showed the theoretical point-of-view for 2D general anisotropic elasticity without any numerical implementation. To the author's knowledge, there are no published works about the complete regularization of hyper-singular kernels for 2D crack problems in general anisotropic materials.

1.1.2 Piezoelectric and magnetoelectroelastic media

Due to the complicated essence of the governing equations of field quantities in piezoelectric or magnetoelectroelastic media for crack problems, analytical solutions are limited to very simple configurations of crack and applied load (e.g. Suo *et al.* [68], Pak [49], Gao *et al.* [26] [27], Wang and Mai [74]). It is therefore necessary to have computational techniques for the treatment of more complicated problems. BEM again shows a significant advantage for crack modeling in multi-field media. However, the fundamental solution for piezoelectric and magnetoelectroelastic media poses some difficulties due to the coupling responses of the mechanical-electric-magnetic fields. Pan [50] derived the fundamental solution for piezoelectric media utilizing a complex variable function method. Wang [76] presented the fundamental solutions for piezoelectric media as an extension of the Stroh formalism of 2D anisotropic elasticity (see also Liu *et al.* [44] for 2D magnetoelectroelastic media containing an elliptical cavity). Later, with the Radon transform technique [19], Wang and Zhang [79] and Denda and Wang [22] extended the results of anisotropic elasticity (e.g. [77], [78]) to obtain the fundamental solution for 2D and 3D piezoelectric media. With the same Radon transform technique, but in a distinct final form, Rungamornrat and Mear [57] presented the fundamental solution for 3D piezoelectric media. Similar to elastic media, another challenge of using BEM for multi-field crack modeling is that the conventional BEM experiences a mathematical degeneracy due to the lack of information on the crack face. To overcome this difficulty, Davi and Milazzo [18] utilized a 'multidomain' technique which decomposed the original domain into subregions (see also Groh and Kuna [33]). This method may become impractical for problems with complex configuration of cracks, and it is necessary to model the singular field in front of the crack tips. An alternative remedy is to employ the generalized traction integral equation, which contains strongly-singular kernels, either instead of, or in addition to the generalized displacement integral equation. In this context, Pan [50] developed a hyper-singular integral equation for generalized traction (i.e. elastic traction and electric displacement) for 2D piezoelectric media. He also introduced a treatment of hyper-singular integral utilizing special Gaussian quadrature formulae. Rajapakse and Xu [54] derived a strongly-singular integral equation for generalized traction by applying extended Lekhnitskii's formalism and distributed dislocation. Garcia *et* *al.* [31] [30] employed both generalized displacement and traction integral equation in a mixed collocation BEM with a decomposition of strongly-singular integral to 'reduce' the singularity. Their study utilized discontinuous quadratic elements to fulfill the C^1 continuous condition.

All the above difficulties can be alleviated by developing weakly-singular integral equations for both generalized displacement and traction. This technique, as mentioned in the previous section, was employed by Frangi and Novati [24] for 2D isotropic elasticity, Li *et al.* [42] for 3D isotropic elasticity, and Rungamornrat and Mear [58] [56] [57] for 3D anisotropic elasticity and piezoelectricity. The important features of the method is that all the kernels that appear in their final forms in the integral equations are weakly-singular and that the boundary data needs to be at most C^o. This allows standard isoparametric elements to be employed in the discretization. This method is extended in the present work for the general case of two-dimensional multi-field media to form a pair of weakly-singular weak-form integral equations for generalized displacement and traction.

1.1.3 T-stress calculation

Fracture behavior for elastic media conventionally focuses on the singular terms, i.e. stress intensity factors, in the Williams' expansion [83] of the asymptotic stress field near the crack tip. These quantities provide a measure of the dominant behavior of the stress field in the vicinity of the crack tip. However, various experimental studies (e.g. Williams and Ewing [82], Ueda *et al* [73]) and theoretical studies (e.g. Cotterell and Rice [16], Larsson and Carlsson [39], Melin [47]) have showed that the constant term, often called T-stress, has significant influence on crack initiation direction, path stability of crack growth, size and shape of the plastic zone at the crack tip and fracture toughness. Accurate determination of T-stress is indeed essential for crack growth simulation. Although the (weakly-singular) SGBEM can give a significant advantage for T-stress calculation, the present author is not aware of any published studies on T-stress calculation utilizing this method for general anisotropic elastic material.

For the sake of brevity and continuity, the overview of methods to calculate T-stress in elastic media developed in literature will be addressed in a later section. The details of this review will be presented at the beginning of Chapter 5 where the derivation of T-stress calculation utilizing integral equations and numerical implementation and results are presented as well.

1.2 Overview of the dissertation

This dissertation is organized into six chapters. In Chapter 2, a brief summary of the governing equations and generalized notation for field quantities of multi-field media is introduced. A systematic procedure for regularizing strongly-singular kernels that appear in the integral relations for displacement and traction will follow. The procedure includes the motivation for a specific decomposition of the strongly-singular kernels. A detailed process to solve for the solution of the weakly-singular kernels through a system of partial differential equations is presented. As a result, a pair of weakly-singular weak-form equations for displacement and traction are established.

Chapter 3 presents details of the numerical implementation of the SGBEM. The developed procedure is for both single-region and multiple-region domains. Due to the fact that all kernels that appear in their final forms in the integral equations are completely regularized in the order of $\ln r$ (r is the distance from a source point to a field point), standard quadratic isoparametric elements are employed for the discretization of the boundary and crack face. A special crack-tip element is developed for the discretization of the domain right behind the crack tips. This particular element expresses a proper asymptotic behavior of crack-face displacements. In addition, extra degrees of freedom are incorporated in this element. This allows stress intensity factors to be obtained directly from the solution of governing discretized system of equations. A technique for numerical integration of the weakly-singular integrals is then presented. The technique is initiated from the procedure proposed by Parreira and Guiggiani [51] with some modification for crack-tip elements. The chapter ends with a treatment of weakly-singular contour integration of the kernels.

In Chapter 4, numerical examples are presented to illustrate the accuracy and efficiency of the developed method. Examples are categorized into three sections: problems in anisotropic elastic medium, problems in piezoelectric medium, and problems in magnetoelectroelastic medium. It is demonstrated that the developed procedure can produce highly accurate solutions for the generalized stress intensity factors at crack tips in all three media.

Chapter 5 presents the development of a numerical procedure for T-stress calculation in anisotropic elastic medium. The procedure is developed based on the relation between the sum of crack-face displacements and T-stress. The sum of crack-face displacements are obtained by utilizing the (weakly-singular) integral relation developed in Chapter 2 through a ‘smoothing process’ by enforcing this relation in a weak sense. Two approaches for the calculation of T-stress are proposed. These approaches are distinguished by how the derivatives of the sum of crack-face displacements are taken. To demonstrate the accuracy of this method, numerical examples for both isotropic and anisotropic materials are examined. Excellent agreement with analytical solutions and with other authors in the literature are demonstrated. The last chapter addresses the conclusions and discussion of future extensions of the developed procedures.

Chapter 2

Weakly-singular Integral Equations for Displacement and Traction

2.1 Statement of 2D boundary value problems

Before beginning our development of integral relations governing a crack in a linear multi-field media, we summarize certain notation and definitions of terms that will be used throughout. With respect to a cartesian coordinate system $\{x_1, x_2, x_3\}$, the components of the displacement vector at any material point $\boldsymbol{x}$ in the body are denoted u_i (with $i \in \{1, 2, 3\}$) and any scalar potential fields that additionally serve to characterize the state of the body are ordered and denoted $\{u_4, u_5, ..., u_N\}$. For convenience, these quantities are combined to form a N-component vector u_I (with $I \in \{1, 2, ..., N\}$) termed the generalized displacement. Similarly, we introduce a generalized stress σ_{iJ} defined in terms the standard (mechanical) stress tensor σ_{ij} and vectors $\{\sigma_{i4}, \sigma_{i5}, ..., \sigma_{iN}\}$ that are associated with the multi-field characteristics of the material under consideration. Specific examples of multi-field behavior will be given in detail further below, but here we note in passing that for a piezoelectric medium (for which $N = 4$) u_4 is the electric potential and σ_{i4} is the electric induction vector.

The setting for this work is two-dimensional in the sense that all field quantities are assumed to be independent of x_3, and as such we describe the domain occupied by the body simply in terms of a region Ω of the x_1-x_2 plane. A generalized traction vector follows from the generalized stress as $t_J = \sigma_{\alpha J} n_\alpha$ in which n_α (with $\alpha \in \{1, 2\}$) is a unit vector normal to a particular surface (represented by a planar curve owing to the two-dimensional setting) passing through a particular point $\boldsymbol{x} \in \Omega$. For every point $\boldsymbol{x} \in \Omega$, the generalized field quantities are taken to be governed by an equation of equilibrium of the form[1]

$$\frac{\partial}{\partial x_\alpha} \sigma_{\alpha J}(\boldsymbol{x}) + f_J(\boldsymbol{x}) = 0 \tag{2.1}$$

along with a constitutive relation of the form

$$\sigma_{\alpha J}(\boldsymbol{x}) = E_{\alpha J K \beta} \frac{\partial}{\partial x_\beta} u_K(\boldsymbol{x}) \tag{2.2}$$

where x_α denotes the cartesian coordinates of the point $\boldsymbol{x}$, $E_{\alpha JK\beta}$ are generalized moduli that characterize the material behavior, and f_J is a generalized body force. For the development to follow, we require that the generalized moduli are such that $E_{\alpha JK\beta} = E_{\beta KJ\alpha}$ and that, for any nonzero vector $\boldsymbol{z} \in \mathbb{R}^2$, the matrix $(\boldsymbol{z}, \boldsymbol{z})_{JK} \equiv z_\alpha E_{\alpha JK\beta} z_\beta$ is invertible. We remark that, for convenience and brevity, the adjective 'generalized' will now be omitted when referring to the various field quantities and material constants which appear; the meaning of the quantities will be evident from the context of the discussion.

The equilibrium equation (2.1) and constitutive relation (2.2) pertain to a variety of media by means of a proper selection of the index N and the moduli

---

[1] Here and what follows, lower case Greek indices range from 1 to 2, lower case Latin indices range from 1 to 3, and upper case Latin indices range from 1 to N. Repeated indices imply summation over their range.

$E_{\alpha JK\beta}$. This selection will be discussed in the next section for particular cases. The theoretical development presented further below will be carried out within a general context based upon these relations. We remark that while the presentation above has involved the introduction of mechanical stress and physical displacements (as well as additional "multi-field effects"), the theory equally applies to simpler theories such as heat conduction and Darcy flow (see Appendix F). Nevertheless, the numerical examples to be presented in Chapter 4 will be restricted to elasticity, piezoelasticity and magnetoelectroelasticity and, for definiteness, we now delineate those theories in the context of the general expressions (2.1) and (2.2).

2.1.1 Discussion of specific media

Firstly, by selecting $N = 2$ or $N = 3$, the relations (2.1) and (2.2) address problems in elastic media. Specifically, $N = 2$ corresponds to *plane strain* problems in monoclinic elastic materials with the symmetry plane at $x_3 = 0$ (or, slightly general anisotropic material, Ting [72]), and $N = 3$ corresponds to *generalized plane strain* problems in general anisotropic elastic materials. For the latter case, the inplane displacements $\{u_1, u_2\}$ and the antiplane displacement $\{u_3\}$ are coupled although they are independent of x_3. For these two cases, the constants $E_{\alpha\varphi\kappa\beta}$ and $E_{\alpha jk\beta}$ denote the elastic moduli of the material for the case of $N = 2$ and $N = 3$, respectively.

Secondly, $N = 4$ corresponds to problems in linear piezoelectric media. Equilibrium equations in a two-dimensional linear and generally anisotropic piezoelectric domain consist of

$$\begin{aligned}\frac{\partial}{\partial x_\alpha}\sigma_{\alpha j}(\boldsymbol{x}) + F_j(\boldsymbol{x}) &= 0 \qquad (2.3)\\ \frac{\partial}{\partial x_\alpha}D_\alpha(\boldsymbol{x}) - Q(\boldsymbol{x}) &= 0 \qquad (2.4)\end{aligned}$$

where $\sigma_{\alpha j}$ and D_α are elastic stresses and electric displacements, respectively. F_j and Q are body force and electric charge, respectively.

The coupled constitutive relations for elastic stresses $\sigma_{\alpha j}$ and electric displacement D_α are stated as follows

$$\begin{aligned}\sigma_{\alpha j}(\boldsymbol{x}) &= C_{\alpha jk\beta}\frac{\partial}{\partial x_\beta}u_k(\boldsymbol{x}) + e_{\beta\alpha j}\frac{\partial}{\partial x_\beta}\phi(\boldsymbol{x}) \qquad (2.5)\\ D_\alpha(\boldsymbol{x}) &= e_{\alpha k\beta}\frac{\partial}{\partial x_\beta}u_k(\boldsymbol{x}) - \kappa_{\alpha\beta}\frac{\partial}{\partial x_\beta}\phi(\boldsymbol{x}) \qquad (2.6)\end{aligned}$$

where u_k are elastic displacements and ϕ is an electric potential; $C_{\alpha jk\beta}$ and $e_{\beta\alpha j}$ are elastic moduli and piezoelectric coefficients, respectively; $\kappa_{\alpha\beta}$ are dielectric constants.

By adopting notation introduced by Barnett and Lothe [6] for the analysis of piezoelectric problems, we can combine the above field quantities into generalized quantities as follows

$$u_K = \begin{cases} u_k & , \quad K = 1,2,3 \\ \phi & , \quad K = 4 \end{cases} \qquad (2.7)$$

$$\sigma_{\alpha J} = \begin{cases} \sigma_{\alpha j} & , \quad J = 1,2,3 \\ D_\alpha & , \quad J = 4 \end{cases} \qquad (2.8)$$

$$E_{\alpha JK\beta} = \begin{cases} C_{\alpha jk\beta} & , \quad J,K = 1,2,3 \\ e_{\beta\alpha j} & , \quad J = 1,2,3 \quad , \quad K = 4 \\ e_{\alpha k\beta} & , \quad J = 4 \quad , \quad K = 1,2,3 \\ -\kappa_{\alpha\beta} & , \quad J,K = 4 \end{cases} \qquad (2.9)$$

$$f_J = \begin{cases} F_j & , \quad J = 1,2,3 \\ -Q & , \quad J = 4 \end{cases} \qquad (2.10)$$

With the notation (2.7)-(2.10), the equilibrium equation (2.1) is the representation for the equations (2.3) and (2.4), and the constitutive equation (2.2) is the representation for the equations (2.5) and (2.6) in a piezoelectric medium.

Lastly, $N = 5$ corresponds to problems in magnetoelectroelastic media. Equilibrium equations of a two-dimensional linear and generally anisotropic magnetoelectroelastic domain consist of

$$\begin{aligned}
\frac{\partial}{\partial x_\alpha}\sigma_{\alpha j}(\boldsymbol{x}) + f_j(\boldsymbol{x}) &= 0 \qquad (2.11)\\
\frac{\partial}{\partial x_\alpha}D_{\alpha}(\boldsymbol{x}) + b_e(\boldsymbol{x}) &= 0 \qquad (2.12)\\
\frac{\partial}{\partial x_\alpha}B_{\alpha}(\boldsymbol{x}) + b_m(\boldsymbol{x}) &= 0 \qquad (2.13)
\end{aligned}$$

where $\sigma_{\alpha j}$, D_α and B_α are elastic stresses, electric displacements and magnetic inductions, respectively; f_j, b_e and b_m are body forces, electric charges and electric currents, respectively.

The coupled constitutive relations for elastic stresses $\sigma_{\alpha j}$, electric displacements D_α and magnetic inductions B_α are expressed as follows

$$\begin{aligned}
\sigma_{\alpha j}(\boldsymbol{x}) &= C_{\alpha jk\beta}\frac{\partial}{\partial x_\beta}u_k(\boldsymbol{x}) + e_{\beta\alpha j}\frac{\partial}{\partial x_\beta}\phi(\boldsymbol{x}) + h_{\beta\alpha j}\frac{\partial}{\partial x_\beta}\psi(\boldsymbol{x}) \qquad (2.14)\\
D_{\alpha}(\boldsymbol{x}) &= e_{\alpha k\beta}\frac{\partial}{\partial x_\beta}u_k(\boldsymbol{x}) - \kappa_{\alpha\beta}\frac{\partial}{\partial x_\beta}\phi(\boldsymbol{x}) - \beta_{\alpha\beta}\frac{\partial}{\partial x_\beta}\psi(\boldsymbol{x}) \qquad (2.15)\\
B_{\alpha}(\boldsymbol{x}) &= h_{\alpha k\beta}\frac{\partial}{\partial x_\beta}u_k(\boldsymbol{x}) - \beta_{\alpha\beta}\frac{\partial}{\partial x_\beta}\phi(\boldsymbol{x}) - \gamma_{\alpha\beta}\frac{\partial}{\partial x_\beta}\psi(\boldsymbol{x}) \qquad (2.16)
\end{aligned}$$

where u_k are elastic displacements, ϕ is an electric potential and ψ is a magnetic potential; $C_{\alpha jk\beta}$, $e_{\beta\alpha j}$ and $h_{\beta\alpha j}$ are elastic moduli, piezoelectric coefficients and piezo magnetic constants, respectively; $\kappa_{\alpha\beta}$ and $\beta_{\alpha\beta}$ are dielectric constants and electro magnetic constants, respectively; and $\gamma_{\alpha\beta}$ are magnetic permeabilities.

Similar to the problems of piezoelectric media, a notation described as follows is employed to group elastic, electric and magnetic field quantities into generalized quantities.

$$u_K = \begin{cases} u_k & , \quad K = 1,2,3 \\ \phi & , \quad K = 4 \\ \psi & , \quad K = 5 \end{cases} \tag{2.17}$$

$$\sigma_{\alpha J} = \begin{cases} \sigma_{\alpha j} & , \quad J = 1,2,3 \\ D_\alpha & , \quad J = 4 \\ B_\alpha & , \quad J = 5 \end{cases} \tag{2.18}$$

$$E_{\alpha JK\beta} = \begin{cases} C_{\alpha jk\beta} & , \quad J,K = 1,2,3 & \\ e_{\beta\alpha j} & , \quad J = 1,2,3 & , \quad K = 4 \\ e_{\alpha k\beta} & , \quad J = 4 & , \quad K = 1,2,3 \\ h_{\beta\alpha j} & , \quad J = 1,2,3 & , \quad K = 5 \\ h_{\alpha k\beta} & , \quad J = 5 & , \quad K = 1,2,3 \\ -\kappa_{\alpha\beta} & , \quad J,K = 4 & \\ -\beta_{\alpha\beta} & , \quad J = 4 & , \quad K = 5 \\ -\beta_{\beta\alpha} & , \quad J = 5 & , \quad K = 4 \\ -\gamma_{\alpha\beta} & , \quad J,K = 5 & \end{cases} \tag{2.19}$$

$$f_J = \begin{cases} F_j & , \quad J = 1,2,3 \\ b_e & , \quad J = 4 \\ b_m & , \quad J = 5 \end{cases} \tag{2.20}$$

with the notation (2.17) - (2.20), the equilibrium equation (2.1) is the representation for equations (2.11) - (2.13), and the constitutive equation (2.2) is the representation for equations (2.14) - (2.16) in a magnetoelectroelastic medium.

In all of the above cases, the symmetric condition for the material constants $E_{\alpha JK\beta} = E_{\beta KJ\alpha}$ is always satisfied. Specifically, this condition results from the symmetric property of the elastic moduli (i.e. $C_{\alpha jk\beta} = C_{\beta kj\alpha}$), the piezoelectric constants (i.e. $e_{\alpha k\beta} = e_{\alpha\beta k}$), the dielectric constants (i.e. $\kappa_{\alpha\beta} = \kappa_{\beta\alpha}$), the piezo magnetic constants (i.e. $h_{\alpha k\beta} = h_{\alpha\beta k}$), the electro magnetic constants (i.e. $\beta_{\alpha\beta} = \beta_{\beta\alpha}$), and the magnetic permeabilities (i.e. $\gamma_{\alpha\beta} = \gamma_{\beta\alpha}$).

2.2 Basic integral relations

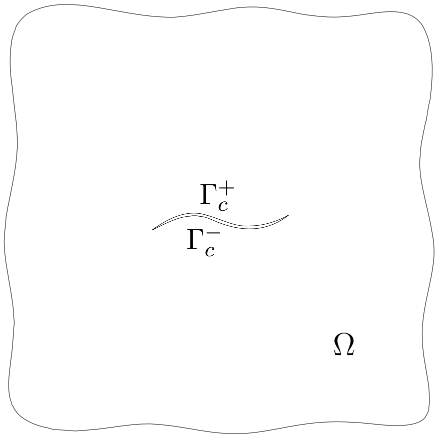

Figure 2.1: Schematic of an isolated crack in unbounded domain.

It is now assumed that the domain Ω occupies the whole plane, i.e. $\Omega = \mathbb{R}^2$ where $\mathbb{R}$ is a set of real numbers. This domain contains an isolated discontinuity of displacement as shown in Fig. 2.1. The discontinuity is represented simply in terms of an 'upper' and 'lower' curve Γ_c^+ and Γ_c^-, respectively, and these curves are geometrically coincident such that their unit normals (taken to be direct 'into' the discontinuity) satisfy $n_\alpha^+ = -n_\alpha^-$. It is further assumed that the tractions on discontinuity surfaces are self-equilibrated such that $t_J^+ = -t_J^-$, where t_J^+ and t_J^- refer to the traction applied to Γ_c^+ and Γ_c^- respectively. Based on this fact, with the denotation of $\Gamma_c \equiv \Gamma_c^+$ and $n_\alpha \equiv n_\alpha^+$, the relation between displacement at any point $\boldsymbol{x}$ in the domain and displacements on the surfaces of discontinuity, known as Somigliana's identity, is obtained for this special configuration (see details of the derivation of this identity in Appendix A).

$$u_P(\boldsymbol{x}) = -\int_{\Gamma_c} S^P_{\alpha J}(\boldsymbol{\xi} - \boldsymbol{x})\, n_\alpha(\boldsymbol{\xi})\, \Delta u_J(\boldsymbol{\xi})\, ds(\boldsymbol{\xi}) \tag{2.21}$$

where $S^P_{\alpha J}$ denotes the stress fundamental solution [2], $\Delta u_J(\boldsymbol{\xi}) \equiv u^+_J(\boldsymbol{\xi}) - u^-_J(\boldsymbol{\xi})$ denotes the relative difference of displacements crossing the discontinuity. The integral relation for the stress is readily obtained by taking the derivative of the displacement $\boldsymbol{u}$ in (2.21) with respect to $\boldsymbol{x}$ and utilizing the constitutive relation (2.2). The result is as follows

$$\sigma_{\zeta K}(\boldsymbol{x}) = \int_{\Gamma_c} \Sigma^{\zeta K}_{\alpha J}(\boldsymbol{\xi} - \boldsymbol{x})\, n_\alpha(\boldsymbol{\xi})\, \Delta u_J(\boldsymbol{\xi})\, ds(\boldsymbol{\xi}) \tag{2.22}$$

where

$$\Sigma^{\zeta K}_{\alpha J}(\boldsymbol{\xi} - \boldsymbol{x}) \equiv E_{\zeta K P \beta} \frac{\partial}{\partial \xi_\beta} S^P_{\alpha J}(\boldsymbol{\xi} - \boldsymbol{x}) \tag{2.23}$$

Note that, in (2.22), we used the fact of $\frac{\partial f}{\partial x_\beta} = -\frac{\partial f}{\partial \xi_\beta}$ where f is a function of $\boldsymbol{r} = \boldsymbol{\xi} - \boldsymbol{x}$.

The integral relations (2.21) and (2.22) contain strongly-singular kernel and hyper-singular kernel respectively when the source point $\boldsymbol{x}$ approaches the discontinuity surface. Specifically, the kernel $S^P_{\alpha J}$ in (2.21) has singularity of order $\mathcal{O}(1/r)$ and the kernel $\Sigma^{\zeta K}_{\alpha J}$ has singularity of order $\mathcal{O}(1/r^2)$ where r is the distance between the source point $\boldsymbol{x}$ and the field point $\boldsymbol{\xi}$. Proper treatments of these singular integrals are essential, particularly when the stress integral equation (2.22) is used to

---

[2] The utilization of both superscripts and subscripts in expressing the components of tensor valued quantities is simply a matter of notational convenience.

obtain the traction on the discontinuity surface where the integral is interpreted in terms of a Hadamaard finite part integral.

The above integral relations are applied for general discontinuity of displacement which can be either a dislocation (where Δu_I is prescribed) or a crack (where t_i is prescribed on the surfaces of the discontinuity). This dissertation will focus only on the latter case. For crack problems, the interesting quantity is the relative displacement on crack surface Δu_I which is related to the stress intensity factors at the crack tip. Thus, equation (2.21) does not receive attention in solving crack problems in unbounded domain since the displacements on crack faces are unknown. However, for the calculation of T-stress which will be discussed in details in Chapter 5, equation (2.21) is employed to obtain the integral equation for the summation of the crack-face displacements. Furthermore, the 'finite-domain' version of equation (2.21) (i.e. Somigliana's identity for finite domain), which will be presented at the end of this chapter, is useful for the problems of cracks in finite domains where a portion of the boundary has prescribed displacements. For all of these purposes, it is necessary to regularize both equations (2.21) and (2.22) to render them more suitable for numerical analysis. The technique, which is well known in the field of dislocation mechanics (e.g. Hirth and Lothe [35]; Lothe [45]) and more recently has been used for 3D crack problems in isotropic elasticity (e.g. Li and Mear [41], Xu and Ortiz [86]) anisotropic elasticity (e.g. Becache *et al* [7], Xu [85], Rungamornrat and Mear [58]) and piezoelectricity (e.g. Rungamornrat and Mear [57]), involves the utilization of integration by parts to reduce the 'strength' of singularity associated with the kernels. This technique is generalized here to obtain the weakly-singular integral equations for displacement and traction in multi-field media.

2.3 Regularization of singular integral relations

In this section, we propose a systematic procedure to regularize the strongly-singular kernel $S^P_{\alpha J}$ and the hyper-singular kernel $\Sigma^{\zeta K}_{\alpha J}$ (see equations (2.21) and (2.22)) based on a particular decomposition of these kernels. The regularized integral relations for the displacement and the stress will be the basis for constructing a pair of weakly-singular weak-form integral relations presented in the next section. For the purpose of simplicity and brevity, we present in this section the developments applicable to isolated crack. However, all of the derived equations can be straightforwardly extended to the problems of cracks in finite domains. This extension will be discussed at the end of this chapter.

2.3.1 Integral relation for displacement

Toward establishing the regularized form of the displacement integral equation (2.21), we note that, from the equilibrium equation of the 2D fundamental problem, the stress fundamental solution $S^P_{\alpha J}$ satisfies

$$\frac{\partial}{\partial \xi_\alpha} S^P_{\alpha J}(\boldsymbol{\xi} - \boldsymbol{x}) = -\delta_{JP}\delta(\boldsymbol{\xi} - \boldsymbol{x}) = -\delta_{JP}\frac{\partial}{\partial \xi_\alpha}\left[\frac{\partial}{\partial \xi_\alpha}\left(\frac{\ln r}{2\pi}\right)\right] \tag{2.24}$$

in which $\delta(\boldsymbol{\xi} - \boldsymbol{x})$ is the 2-D Dirac delta function center at $\boldsymbol{x}$ and $r = \|\boldsymbol{\xi} - \boldsymbol{x}\|$ is the distance between the source point $\boldsymbol{x}$ and the field point $\boldsymbol{\xi}$. Equation (2.24) motivates a decomposition of $S^P_{\alpha J}$ such that

$$S^P_{\alpha J}(\boldsymbol{\xi} - \boldsymbol{x}) = \tilde{S}^P_{\alpha J}(\boldsymbol{\xi} - \boldsymbol{x}) + H^P_{\alpha J}(\boldsymbol{\xi} - \boldsymbol{x}) \tag{2.25}$$

where

$$H^P_{\alpha J}(\boldsymbol{\xi} - \boldsymbol{x}) \equiv -\delta_{JP} \frac{\partial}{\partial \xi_\alpha} \Big(\frac{\ln r}{2\pi} \Big) = -\frac{\delta_{JP}}{2\pi} \frac{(\xi_\alpha - x_\alpha)}{r^2} \tag{2.26}$$

Then, from (2.24) and (2.25), it is obvious that

$$\frac{\partial}{\partial \xi_\alpha} \tilde{S}^P_{\alpha J}(\boldsymbol{\xi} - \boldsymbol{x}) = 0 \tag{2.27}$$

That is the kernel $\tilde{S}^P_{\alpha J}$ is divergence free *everywhere* including the source point $\boldsymbol{x}$. This feature implies the existence of a kernel G^P_J such that

$$\tilde{S}^P_{\alpha J}(\boldsymbol{\xi} - \boldsymbol{x}) = \epsilon_{\alpha\beta} \frac{\partial G^P_J(\boldsymbol{\xi} - \boldsymbol{x})}{\partial \xi_\beta} \tag{2.28}$$

where $\epsilon_{\alpha\beta}$ denotes the 2D alternating symbol (i.e. $\epsilon_{11} = \epsilon_{22} = 0$; $\epsilon_{12} = -\epsilon_{21} = 1$)

The important aspect of the representation (2.28) is that the kernel G^P_J is now a weakly-singular kernel in the sense that it is of order $\mathcal{O}(\ln r)$ when $r \to 0$. From (2.25), (2.26) and (2.28), we have the relation between the kernel G^P_J and the stress fundamental solution $S^P_{\alpha J}$ as

$$\epsilon_{\alpha\beta} \frac{\partial G^P_J(\boldsymbol{\xi} - \boldsymbol{x})}{\partial \xi_\beta} = S^P_{\alpha J}(\boldsymbol{\xi} - \boldsymbol{x}) + \delta_{JP} \frac{\partial}{\partial \xi_\alpha} \left(\frac{\ln r}{2\pi} \right) \tag{2.29}$$

Finally, using the constitutive relation (2.2) to replace the stress fundamental solution $S^P_{\alpha J}$ in (2.29) by the displacement fundamental solution, we obtain a system of partial differential equations to be solved for G^P_J as

$$\epsilon_{\alpha\beta} \frac{\partial G^P_J(\boldsymbol{\xi} - \boldsymbol{x})}{\partial \xi_\beta} = E_{\alpha JK\beta} \frac{\partial U^P_K(\boldsymbol{\xi} - \boldsymbol{x})}{\partial \xi_\beta} + \delta_{PJ} \frac{\partial}{\partial \xi_\alpha} \left(\frac{\ln r}{2\pi} \right) \tag{2.30}$$

Let us continue the process of regularization and defer the solving of (2.30) to obtain the solution for G^P_J to the next section. First, using (2.25) and (2.28) to re-express the fundamental solution $S^P_{\alpha J}$ in (2.21), with the note that $n_\alpha \epsilon_{\alpha\beta} \frac{\partial}{\partial \xi_\beta} = \frac{\partial}{\partial s}$ where s is the arc length, then performing an integration by parts, we obtain the expression of displacement at the source point $\boldsymbol{x}$ in terms of weakly-singular kernels as

$$u_P(\boldsymbol{x}) = \int_{\Gamma_c} G^P_J(\boldsymbol{\xi} - \boldsymbol{x})\, D\Delta u_J(\boldsymbol{\xi})\, ds(\boldsymbol{\xi}) - \int_{\Gamma_c} H^P_{\alpha J}(\boldsymbol{\xi} - \boldsymbol{x})\, n_\alpha(\boldsymbol{\xi})\, \Delta u_J(\boldsymbol{\xi})\, ds(\boldsymbol{\xi}) \tag{2.31}$$

where $D \equiv \frac{\partial}{\partial s}$ is the differential operator with respect to arc length. Note that for crack problems, which are the main target of this dissertation, the relative displacement Δu_J vanishes at the boundaries of the integration domain (i.e. crack tips). We also note that the kernel $H^P_{\alpha J} n_\alpha$ is weakly-singular (see proof in Appendix C) thus the integral relation (2.31) contains only weakly-singular kernels.

It is straightforward to take the limit of $\boldsymbol{x} \to \boldsymbol{y}$ where $\boldsymbol{y} \in \Gamma_c$, then equation (2.31) gives the expression for the summation of displacement at a point on crack surface as

$$\frac{1}{2}\Sigma u_P(\boldsymbol{y}) = \int_{\Gamma_c} G^P_J(\boldsymbol{\xi} - \boldsymbol{y})\, D\Delta u_J(\boldsymbol{\xi})\, ds(\boldsymbol{\xi}) - \int_{\Gamma_c} H^P_{\alpha J}(\boldsymbol{\xi} - \boldsymbol{y})\, n_\alpha(\boldsymbol{\xi})\, \Delta u_J(\boldsymbol{\xi})\, ds(\boldsymbol{\xi}) \tag{2.32}$$

where $\Sigma u_P(\boldsymbol{y}) \equiv u^+_P(\boldsymbol{y}) + u^-_P(\boldsymbol{y})$.

As mentioned earlier, the relation (2.32) is the starting point for the determination of T-stress that will be discussed further in Chapter 5.

2.3.2 Integral relation for stress

Similar to the case of displacement integral equation, the stress integral equation (2.22) is regularized as follows. Based on equations (2.23) and (2.24), we note that

$$\begin{aligned}\frac{\partial}{\partial\xi_\alpha}\Sigma^{\zeta K}_{\alpha J}(\boldsymbol{\xi}-\boldsymbol{x}) &= \frac{\partial}{\partial\xi_\alpha}\left[E_{\zeta KP\beta}\frac{\partial}{\partial\xi_\beta}S^{P}_{\alpha J}(\boldsymbol{\xi}-\boldsymbol{x})\right]\\ &= E_{\zeta KP\beta}\frac{\partial}{\partial\xi_\beta}\left[-\delta_{JP}\delta(\boldsymbol{\xi}-\boldsymbol{x})\right]\\ &= \frac{\partial}{\partial\xi_\alpha}\left[-E_{\zeta KJ\alpha}\delta(\boldsymbol{\xi}-\boldsymbol{x})\right] \qquad (2.33)\end{aligned}$$

and

$$\begin{aligned}\frac{\partial}{\partial\xi_\zeta}\Sigma^{\zeta K}_{\alpha J}(\boldsymbol{\xi}-\boldsymbol{x}) &= \frac{\partial}{\partial\xi_\zeta}\left[E_{\zeta KP\beta}\frac{\partial}{\partial\xi_\beta}\Big(E_{\alpha JM\gamma}\frac{\partial}{\partial\xi_\gamma}U^{P}_{M}(\boldsymbol{\xi}-\boldsymbol{x})\Big)\right]\\ &= \frac{\partial}{\partial\xi_\zeta}\left[E_{\alpha JM\gamma}\frac{\partial}{\partial\xi_\gamma}\Big(E_{\zeta KP\beta}\frac{\partial}{\partial\xi_\beta}U^{M}_{P}(\boldsymbol{\xi}-\boldsymbol{x})\Big)\right]\\ &= \frac{\partial}{\partial\xi_\zeta}\left[E_{\alpha JM\gamma}\frac{\partial}{\partial\xi_\gamma}S^{M}_{\zeta K}(\boldsymbol{\xi}-\boldsymbol{x})\right]\\ &= \frac{\partial}{\partial\xi_\gamma}\left[-E_{\alpha JM\gamma}\delta_{MK}\delta(\boldsymbol{\xi}-\boldsymbol{x})\right]\\ &= \frac{\partial}{\partial\xi_\gamma}\left[-E_{\gamma KJ\alpha}\delta(\boldsymbol{\xi}-\boldsymbol{x})\right]\\ &= \frac{\partial}{\partial\xi_\zeta}\left[-E_{\zeta KJ\alpha}\delta(\boldsymbol{\xi}-\boldsymbol{x})\right] \qquad (2.34)\end{aligned}$$

where, in (2.34), we employed the symmetric property of the displacement fundamental solution (i.e. $U^{P}_{M}(\boldsymbol{\xi}-\boldsymbol{x}) = U^{M}_{P}(\boldsymbol{\xi}-\boldsymbol{x})$) and of the generalized moduli (i.e. $E_{\alpha JK\gamma} = E_{\gamma KJ\alpha}$).

Equations (2.33) and (2.34) motivate a decomposition of the kernel $\Sigma^{\zeta K}_{\alpha J}$ such that

$$\Sigma^{\zeta K}_{\alpha J}(\boldsymbol{\xi}-\boldsymbol{x}) = \tilde{\Sigma}^{\zeta K}_{\alpha J}(\boldsymbol{\xi}-\boldsymbol{x}) - E_{\zeta KJ\alpha}\delta(\boldsymbol{\xi}-\boldsymbol{x}) \qquad (2.35)$$

Then, it is obvious that

$$\frac{\partial}{\partial\xi_\alpha}\tilde{\Sigma}^{\zeta K}_{\alpha J}(\boldsymbol{\xi}-\boldsymbol{x}) = 0 \quad \text{and} \quad \frac{\partial}{\partial\xi_\zeta}\tilde{\Sigma}^{\zeta \mathrm{K}}_{\alpha \mathrm{J}}(\boldsymbol{\xi}-\boldsymbol{x}) = 0 \qquad (2.36)$$

That is, the kernel $\tilde{\Sigma}^{\zeta K}_{\alpha J}$ is divergence free (with respect to ξ_α and ξ_ζ) *everywhere* including the source point $\boldsymbol{x}$. This feature implies the existence of a kernel C^K_J such that

$$\tilde{\Sigma}^{\zeta K}_{\alpha J}(\boldsymbol{\xi}-\boldsymbol{x}) = \epsilon_{\alpha\beta}\frac{\partial}{\partial\xi_\beta}\epsilon_{\zeta\gamma}\frac{\partial}{\partial\xi_\gamma}C^K_J(\boldsymbol{\xi}-\boldsymbol{x}) \tag{2.37}$$

where the kernel C^K_J is weakly-singular at $\boldsymbol{\xi} = \boldsymbol{x}$ in the sense that it is of order $\mathcal{O}(\ln r)$ as $r \to 0$. Combining equations (2.35) and (2.37), then replacing the kernel $\Sigma^{\zeta K}_{\alpha J}$ with the displacement fundamental solution U^P_M, we obtain a system of partial differential equations to be solved for the kernel C^K_J as

$$\epsilon_{\alpha\beta}\frac{\partial}{\partial\xi_\beta}\epsilon_{\zeta\gamma}\frac{\partial}{\partial\xi_\gamma}C^K_J(\boldsymbol{\xi}-\boldsymbol{x}) = E_{\zeta KP\beta}E_{\alpha JM\gamma}\frac{\partial^2 U^P_M(\boldsymbol{\xi}-\boldsymbol{x})}{\partial\xi_\beta\partial\xi_\gamma} + E_{\alpha JK\zeta}\delta(\boldsymbol{\xi}-\boldsymbol{x}) \tag{2.38}$$

Let us defer the solving of these equations until the next section, and continue with the process of regularization of the stress equation (2.22). We note that the equation (2.22) is still valid if the kernel $\Sigma^{\zeta K}_{\alpha J}$ is replaced by the kernel $\tilde{\Sigma}^{\zeta K}_{\alpha J}$ defined in (2.35) since, with any point $\boldsymbol{x}$ inside the domain (i.e. $\boldsymbol{x} \notin \Gamma_c$), the integral involving the Dirac delta function (i.e. the second term of (2.35)) will vanish. From this fact, equation (2.22) becomes

$$\begin{aligned}\sigma_{\zeta K}(\boldsymbol{x}) &= \int_{\Gamma_c}\epsilon_{\alpha\beta}\frac{\partial}{\partial\xi_\beta}\left[\epsilon_{\zeta\gamma}\frac{\partial}{\partial\xi_\gamma}C^K_J(\boldsymbol{\xi}-\boldsymbol{x})\right]n_\alpha(\boldsymbol{\xi})\Delta u_J(\boldsymbol{\xi})ds(\boldsymbol{\xi}) \\ &= \int_{\Gamma_c}\frac{\partial}{\partial s}\left[\epsilon_{\zeta\gamma}\frac{\partial}{\partial\xi_\gamma}C^K_J(\boldsymbol{\xi}-\boldsymbol{x})\right]\Delta u_J(\boldsymbol{\xi})ds(\boldsymbol{\xi}) \qquad (2.39)\end{aligned}$$

Then integrating by parts and utilizing the closing condition at crack tips (i.e. $\Delta u_J = 0$ at the crack tips), equation (2.39) becomes

$$\sigma_{\zeta K}(\boldsymbol{x}) \quad = \quad -\int_{\Gamma_c} \epsilon_{\zeta\gamma} \frac{\partial}{\partial \xi_\gamma} C_J^K(\boldsymbol{\xi} - \boldsymbol{x})\, D\Delta u_J(\boldsymbol{\xi}) ds(\boldsymbol{\xi}) \tag{2.40}$$

Next, with the note that $\frac{\partial C_J^K}{\partial \xi_\gamma} = -\frac{\partial C_J^K}{\partial x_\gamma}$ and $D\Delta u_J$ is the function of $\boldsymbol{\xi}$ only, equation (2.40) can be re-expressed as

$$\sigma_{\zeta K}(\boldsymbol{x}) \quad = \quad \epsilon_{\zeta\gamma} \frac{\partial}{\partial x_\gamma} \int_{\Gamma_c} C_J^K(\boldsymbol{\xi} - \boldsymbol{x})\, D\Delta u_J(\boldsymbol{\xi}) ds(\boldsymbol{\xi}) \tag{2.41}$$

Equation (2.41) is then utilized to obtain the traction acting at a point $\boldsymbol{y} \in \Gamma_c$ as follows

$$\begin{aligned} t_K(\boldsymbol{y}) \quad &= \quad \lim_{\boldsymbol{x} \to \boldsymbol{y}} n_\zeta(\boldsymbol{y}) \sigma_{\zeta K}(\boldsymbol{x}) \\ &= \quad \frac{\partial}{\partial s} \left(\int_{\Gamma_c} C_J^K(\boldsymbol{\xi} - \boldsymbol{y})\, D\Delta u_J(\boldsymbol{\xi}) ds(\boldsymbol{\xi}) \right) \end{aligned} \tag{2.42}$$

It is now straightforward to obtain the regularized equation for the traction acting at a point on the crack surface by forming the weak-form of (2.42). Indeed, by multiplying both sides of (2.42) with a continuous test function $\Delta \tilde{u}_K(\boldsymbol{y})$ chosen such that $\Delta \tilde{u}_K = 0$ at the boundary of Γ_c (i.e. crack tips), then integrating the result over Γ_c and finally integrating by parts, we get

$$\int_{\Gamma_c} t_K(\boldsymbol{y})\, \Delta \tilde{u}_K(\boldsymbol{y})\, ds(\boldsymbol{y}) = -\int_{\Gamma_c} D\Delta \tilde{u}_K(\boldsymbol{y}) \int_{\Gamma_c} C_J^K(\boldsymbol{\xi} - \boldsymbol{y})\, D\Delta u_J(\boldsymbol{\xi})\, ds(\boldsymbol{\xi})\, ds(\boldsymbol{y}) \tag{2.43}$$

2.3.3 Solution for G_J^P and C_J^K

The integral relations for displacement and traction have been regularized in the sense that their final forms (i.e. equations (2.32) and (2.43)) contain only weakly-singular kernels G_J^P and C_J^K which are of order $\mathcal{O}(\ln r)$. These kernels are determined via a system of partial differential equations (2.30) and (2.38). In this section, we apply the Radon transform [3] to solve these equations. The application of Radon transform to obtain the displacement fundamental solution for 2D anisotropic elasticity was first used in the work of C. Y. Wang [75]. Before extending this technique to solve the weakly-singular kernels G_J^P and C_J^K, we summarize the use of Radon transform to obtain the displacement fundamental solution which is a slightly different approach from that of Wang [75].

The governing equation for the displacement fundamental solution takes the form

$$E_{\alpha IJ\beta}\frac{\partial^2}{\partial\xi_\alpha\partial\xi_\beta}U_J^P(\boldsymbol{\xi}-\boldsymbol{x}) = -\delta_{IP}\,\delta(\boldsymbol{\xi}-\boldsymbol{x}) \tag{2.44}$$

Applying the Radon transform to (2.44), with the notation $(\boldsymbol{z},\boldsymbol{z})_{IJ} \equiv z_\alpha E_{\alpha IJ\beta} z_\beta$, we get

$$(\boldsymbol{z},\boldsymbol{z})_{IJ}\frac{\partial^2}{\partial p^2}\widehat{U}_J^P(\boldsymbol{z}, p-\boldsymbol{z}\cdot\boldsymbol{x}) = -\delta_{IP}\,\delta(p-\boldsymbol{z}\cdot\boldsymbol{x}) \tag{2.45}$$

where $\hat{f}(\boldsymbol{z}, p-\boldsymbol{z}\cdot\boldsymbol{x})$ denotes the transform of a function $f(\boldsymbol{\xi}-\boldsymbol{x})$ (in the transform space $\{p,\boldsymbol{z}\}$ with p is a scalar and $\boldsymbol{z}$ is a unit vector). From (2.45), solution to $\partial^2\widehat{U}_J^P/\partial p^2$ in the transform space is obtained as

$$\frac{\partial^2}{\partial p^2}\widehat{U}_J^P(\boldsymbol{z}, p-\boldsymbol{z}\cdot\boldsymbol{x}) = -(\boldsymbol{z},\boldsymbol{z})^{-1}_{PJ}\,\delta(p-\boldsymbol{z}\cdot\boldsymbol{x}) \tag{2.46}$$

---

[3] Summary of some Radon transform applications that are relevant to our developed procedure are presented in Appendix B

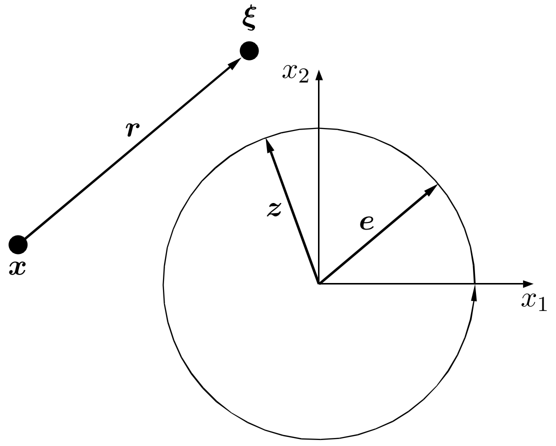

Figure 2.2: Schematic of contour integration for the displacement fundamental solution.

where $(\boldsymbol{z},\boldsymbol{z})^{-1}$ denotes the inverse of the tensor $(\boldsymbol{z},\boldsymbol{z})$. Applying the inverse Radon transform to (2.46), we obtain the displacement fundamental solution

$$U_J^P(\boldsymbol{\xi}-\boldsymbol{x}) = -\frac{1}{4\pi^2}\oint_{\|\boldsymbol{z}\|=1}(\boldsymbol{z},\boldsymbol{z})^{-1}_{PJ}\ln|\boldsymbol{z}\cdot(\boldsymbol{\xi}-\boldsymbol{x})|d\boldsymbol{z} \tag{2.47}$$

in which the contour integral is to be evaluated over a unit circle $\|\boldsymbol{z}\|=1$ as shown schematically in Fig. 2.2. Note that the kernel U_J^P is singular only at $\boldsymbol{\xi}=\boldsymbol{x}$ and is of order $\mathcal{O}(\ln r)$ as $r\to 0$. For the convenience of numerical evaluation of the kernels that will be discussed later in Chapter 3, with the denotation of $r\equiv\|\boldsymbol{\xi}-\boldsymbol{x}\|$ and $\boldsymbol{e}\equiv(\boldsymbol{\xi}-\boldsymbol{x})/r$, the integral on the right-hand side of (2.47) is split into two components as

$$U_J^P(\boldsymbol{\xi}-\boldsymbol{x}) = -\frac{1}{4\pi^2}\oint_{\|\boldsymbol{z}\|=1}(\boldsymbol{z},\boldsymbol{z})^{-1}_{PJ}(\ln r+\ln|\boldsymbol{z}\cdot\boldsymbol{e}|)d\boldsymbol{z} \tag{2.48}$$

2.3.3.1 Kernel G_J^P

After taking the Radon transform of (2.30), we obtain

$$\epsilon_{\alpha\beta} z_\beta \frac{\partial}{\partial p} \widehat{G}_J^P(\boldsymbol{z}, p - \boldsymbol{z}\cdot\boldsymbol{x}) \quad = \quad E_{\alpha JK\beta} z_\beta \frac{\partial}{\partial p} \widehat{U}_K^P(\boldsymbol{z}, p - \boldsymbol{z}\cdot\boldsymbol{x}) + \delta_{JP} z_\alpha \frac{\partial}{\partial p} \widehat{\left(\frac{\ln r}{2\pi}\right)} \tag{2.49}$$

Note that $\ln r/2\pi$ is the solution of 2D Laplace's equation, i.e.

$$\frac{\partial^2}{\partial \xi_\alpha \partial \xi_\alpha}\left(\frac{\ln r}{2\pi}\right) = \delta(\boldsymbol{\xi} - \boldsymbol{x}) \tag{2.50}$$

then by taking the Radon transform of (2.50), with the note that $z_\alpha z_\alpha = 1$, we get the result

$$\frac{\partial^2}{\partial p^2} \widehat{\left(\frac{\ln r}{2\pi}\right)} = \delta(p - \boldsymbol{z}\cdot\boldsymbol{x}) \tag{2.51}$$

Returning to the equation (2.49), we continue to take the derivative with respect to p. Utilizing (2.46) and (2.51), we obtain the result expressed in a vector format as

$$\boldsymbol{z} \times \frac{\partial^2}{\partial p^2} \widehat{\boldsymbol{G}}_J^P(\boldsymbol{z}, p - \boldsymbol{z}\cdot\boldsymbol{x}) = \boldsymbol{\Phi}_J^P \, \delta(p - \boldsymbol{z}\cdot\boldsymbol{x}) \tag{2.52}$$

where '×' is a standard vector cross product; $\hat{\boldsymbol{G}}_J^P$ and $\boldsymbol{\Phi}_J^P$ are vectors being perpendicular to and in the plane of problem, respectively, with their components defined as

$$\left[\widehat{\boldsymbol{G}}_J^P\right]_m = \delta_{3m} \widehat{G}_J^P \tag{2.53}$$

and

$$\left[\boldsymbol{\Phi}_J^P\right]_\alpha = -E_{\alpha JK\beta} z_\beta (\boldsymbol{z}, \boldsymbol{z})_{PK}^{-1} + \delta_{JP} z_\alpha \quad ; \quad \left[\boldsymbol{\Phi}_{\mathrm{J}}^{\mathrm{P}}\right]_3 = 0 \tag{2.54}$$

The fact of $\boldsymbol{z} \cdot \boldsymbol{z} = 1$ leads to the result of

$$\begin{aligned} \boldsymbol{z} \cdot \boldsymbol{\Phi}_J^P &= -z_\alpha E_{\alpha JK\beta} z_\beta (\boldsymbol{z}, \boldsymbol{z})_{PK}^{-1} + \delta_{JP} z_\alpha z_\alpha \\ &= -(\boldsymbol{z}, \boldsymbol{z})_{JK} (\boldsymbol{z}, \boldsymbol{z})_{PK}^{-1} + \delta_{JP} = 0 \end{aligned} \tag{2.55}$$

Then utilizing the vector identity $\boldsymbol{u} \times (\boldsymbol{v} \times \boldsymbol{w}) = (\boldsymbol{u} \cdot \boldsymbol{w})\boldsymbol{v} - (\boldsymbol{u} \cdot \boldsymbol{v})\boldsymbol{w}$ and the result of (2.55), we obtain

$$\boldsymbol{z} \times (\boldsymbol{z} \times \boldsymbol{\Phi}_J^P) = (\boldsymbol{z} \cdot \boldsymbol{\Phi}_J^P) - (\boldsymbol{z} \cdot \boldsymbol{z}) \boldsymbol{\Phi}_J^P = -\boldsymbol{\Phi}_J^P \tag{2.56}$$

The combination of (2.52) and (2.55) leads to a particular solution of (2.49) as

$$\frac{\partial^2}{\partial p^2} \widehat{\boldsymbol{G}}_J^P (\boldsymbol{z}, p - \boldsymbol{z} \cdot \boldsymbol{x}) = -\boldsymbol{z} \times \boldsymbol{\Phi}_J^P \, \delta(p - \boldsymbol{z} \cdot \boldsymbol{x}) \tag{2.57}$$

When we take the inversion of Radon transform, the solution (2.57) in the transformed space is transformed to that in the physical space as

$$\boldsymbol{G}_J^P (\boldsymbol{\xi} - \boldsymbol{x}) = -\frac{1}{4\pi^2} \oint_{\|\boldsymbol{z}\|=1} \boldsymbol{z} \times \boldsymbol{\Phi}_J^P \left(\ln r + \ln |\boldsymbol{z} \cdot \boldsymbol{e}| \right) \, d\boldsymbol{z} \tag{2.58}$$

where the contour integral, similarly to the case of displacement fundamental solution, is taken over a unit circle in the plane of problem. Expressing in terms of the components, and utilizing the identity $\epsilon_{\alpha\beta} z_\alpha z_\beta = 0$, we get the final form of the kernel G_J^P as

$$G_J^P (\boldsymbol{\xi} - \boldsymbol{x}) = -\frac{1}{4\pi^2} \epsilon_{\alpha\beta} E_{\alpha JK\rho} \oint_{\|\boldsymbol{z}\|=1} z_\beta z_\rho (\boldsymbol{z}, \boldsymbol{z})_{PK}^{-1} \left(\ln r + \ln |\boldsymbol{z} \cdot \boldsymbol{e}| \right) \, d\boldsymbol{z} \tag{2.59}$$

As in the case for the displacement fundamental solution (2.47), the kernel G_J^P is singular only at $\boldsymbol{\xi} = \boldsymbol{x}$ and is of order $\mathcal{O}(\ln r)$ as $r \to 0$.

2.3.3.2 Kernel C_J^K

After taking the Radon transform of (2.38) along with the utilization of (2.46), the result is expressed in the vector format as

$$\left[\boldsymbol{z}\hat{\times}\frac{\partial^2}{\partial p^2}\widehat{\boldsymbol{C}}_J^K(\boldsymbol{z}, p-\boldsymbol{z}\cdot\boldsymbol{x})\right]\check{\times}\boldsymbol{z} = \boldsymbol{\Lambda}_J^K\,\delta(p-\boldsymbol{z}\cdot\boldsymbol{x}) \tag{2.60}$$

where $\widehat{\boldsymbol{C}}_J^K$ and $\boldsymbol{\Lambda}_J^K$ are second order tensors defined as

$$\begin{aligned} \left[\widehat{\boldsymbol{C}}_J^K\right]_{mt} &= \delta_{3m}\delta_{3t}\widehat{C}_J^K && (2.61)\\ \left[\boldsymbol{\Lambda}_J^K\right]_{\alpha\zeta} &= E_{\alpha JK\zeta} - E_{\alpha JM\gamma}\; E_{\zeta KP\beta}\; z_\gamma z_\beta\; (\boldsymbol{z},\boldsymbol{z})^{-1}_{MP} && (2.62)\\ \left[\boldsymbol{\Lambda}_J^K\right]_{3i} &= 0 \quad ; \quad \left[\boldsymbol{\Lambda}^{\mathrm{K}}_{\mathrm{J}}\right]_{\mathrm{i3}} \;=\; 0 && (2.63) \end{aligned}$$

and the generalized cross product '$\hat{\times}$' between any vector $\boldsymbol{z}$ and any second order tensor $\boldsymbol{A}$, and the generalized cross product '$\check{\times}$' between any second order tensor $\boldsymbol{A}$ and any vector $\boldsymbol{z}$ are defined component-wise as

$$\begin{aligned} \left[\boldsymbol{z}\hat{\times}\boldsymbol{A}\right]_{ij} &= \epsilon_{imn} z_m A_{nj} && (2.64)\\ \left[\boldsymbol{A}\check{\times}\boldsymbol{z}\right]_{ij} &= \epsilon_{jmn} z_m A_{in} && (2.65) \end{aligned}$$

The fact of $\boldsymbol{z}\cdot\boldsymbol{z} = 1$ leads to the results of

$$\left[\boldsymbol{\Lambda}_J^K\right]^T\boldsymbol{z} = \left[\boldsymbol{\Lambda}_J^K\right]_{\beta\alpha} z_\beta = E_{\beta JK\alpha} z_\beta - E_{\alpha KP\rho} z_\rho (\boldsymbol{z},\boldsymbol{z})_{JM} (\boldsymbol{z},\boldsymbol{z})^{-1}_{MP} = 0 \tag{2.66}$$

$$\left[\boldsymbol{\Lambda}_J^K\right]\boldsymbol{z} = \left[\boldsymbol{\Lambda}_J^K\right]_{\alpha\beta} z_\beta = E_{\alpha JK\beta} z_\beta - E_{\alpha JM\gamma} z_\gamma (\boldsymbol{z},\boldsymbol{z})_{KP} (\boldsymbol{z},\boldsymbol{z})^{-1}_{MP} = 0 \tag{2.67}$$

Utilizing the vector-tensor identities generalized for the operators (2.64) and (2.65)

$$\begin{aligned} \boldsymbol{u}\hat{\times}(\boldsymbol{v}\hat{\times}\boldsymbol{A}) &= \boldsymbol{v}\otimes(\boldsymbol{A}^T\boldsymbol{u}) - (\boldsymbol{u}\cdot\boldsymbol{v})\boldsymbol{A} && (2.68)\\ (\boldsymbol{A}\check{\times}\boldsymbol{u})\check{\times}\boldsymbol{v} &= (\boldsymbol{A}\boldsymbol{v})\otimes\boldsymbol{u} - (\boldsymbol{u}\cdot\boldsymbol{v})\boldsymbol{A} && (2.69) \end{aligned}$$

and the results of (2.66) and (2.67), we obtain

$$\left[\boldsymbol{z}\hat{\times}(\boldsymbol{z}\hat{\times}\boldsymbol{\Lambda}_J^K)\check{\times}\boldsymbol{z}\right]\check{\times}\boldsymbol{z} \quad = \quad \boldsymbol{\Lambda}_J^K \tag{2.70}$$

The combination of (2.60) and (2.70) leads to a particular solution for $\frac{\partial^2}{\partial p^2}\widehat{\boldsymbol{C}}_J^K$ as

$$\frac{\partial^2}{\partial p^2}\widehat{\boldsymbol{C}}_J^K(\boldsymbol{z}, p - \boldsymbol{z}\cdot\boldsymbol{x}) \quad = \quad \left[(\boldsymbol{z}\hat{\times}\boldsymbol{\Lambda}_J^K)\check{\times}\boldsymbol{z}\right]\,\delta(p - \boldsymbol{z}\cdot\boldsymbol{x}) \tag{2.71}$$

By taking the inversion of Radon transform, the solution (2.71) in the transformed space is transformed to that in the physical space as

$$\boldsymbol{C}_J^K(\boldsymbol{\xi} - \boldsymbol{x}) \quad = \quad \frac{1}{4\pi^2}\oint_{\|\boldsymbol{z}\|=1}(\boldsymbol{z}\hat{\times}\boldsymbol{\Lambda}_J^K)\check{\times}\boldsymbol{z}(\ln r + \ln|\boldsymbol{z}\cdot\boldsymbol{e}|)\;d\boldsymbol{z} \tag{2.72}$$

where the contour integral, similar to the case of the displacement fundamental solution, is taken over a unit circle in the plane of problem. Expressed in component format, with the note that $\boldsymbol{z}$ is a planar vector (i.e. $z_3 = 0$) and $\left[\boldsymbol{\Lambda}_J^K\right]_{3i} = 0 = \left[\boldsymbol{\Lambda}_J^K\right]_{i3}$, equation (2.72) becomes

$$C_J^K(\boldsymbol{\xi} - \boldsymbol{x}) = \frac{1}{4\pi^2}\oint_{\|\boldsymbol{z}\|=1}\epsilon_{\alpha\beta}\epsilon_{\zeta\gamma}z_\alpha z_\zeta\left[\boldsymbol{\Lambda}_J^K\right]_{\beta\gamma}(\ln r + \ln|\boldsymbol{z}\cdot\boldsymbol{e}|)\;d\boldsymbol{z} \tag{2.73}$$

After employing the identity $\epsilon_{\alpha\beta}\epsilon_{\zeta\gamma} = \delta_{\alpha\zeta}\delta_{\beta\gamma} - \delta_{\alpha\gamma}\delta_{\beta\zeta}$ and given the fact that $z_\gamma z_\beta\left[\boldsymbol{\Lambda}_J^K\right]_{\beta\gamma} = (\boldsymbol{z},\boldsymbol{z})_{JK} - (\boldsymbol{z},\boldsymbol{z})_{KP}(\boldsymbol{z},\boldsymbol{z})_{JM}(\boldsymbol{z},\boldsymbol{z})_{MP}^{-1} = 0$ and $\boldsymbol{z}\cdot\boldsymbol{z} = 1$, equation (2.73) is simplified as

$$C_J^K(\boldsymbol{\xi} - \boldsymbol{x}) = \frac{1}{4\pi^2}\oint_{\|\boldsymbol{z}\|=1}\left[\boldsymbol{\Lambda}_J^K\right]_{\beta\beta}(\ln r + \ln|\boldsymbol{z}\cdot\boldsymbol{e}|)\;d\boldsymbol{z} \tag{2.74}$$

With (2.62) and employing the fact of $(\boldsymbol{z},\boldsymbol{z})_{PM}\;(\boldsymbol{z},\boldsymbol{z})_{PM}^{-1} = N$ where N is the dimension of media, the expression of C_J^K is written in the form similar to the expression of G_J^P in (2.59) as

$$C_J^K(\boldsymbol{\xi} - \boldsymbol{x}) = -\frac{1}{4\pi^2}A_{J\beta P}^{K\gamma M}\oint_{\|\boldsymbol{z}\|=1}z_\beta z_\gamma\;(\boldsymbol{z},\boldsymbol{z})_{PM}^{-1}(\ln r + \ln|\boldsymbol{z}\cdot\boldsymbol{e}|)\;d\boldsymbol{z} \tag{2.75}$$

where $A^{K\gamma M}_{J\beta P}$ is a constant (which depends only on the material constants) given by

$$A^{K\gamma M}_{J\beta P} = E_{\eta K P\beta} E_{\eta J M\gamma} - \frac{1}{N} E_{\nu J K\nu} E_{\beta P M\gamma} \tag{2.76}$$

Note that the kernel C^K_J is also singular only at $\boldsymbol{\xi} = \boldsymbol{x}$ and is of order $\mathcal{O}(\ln r)$ as $r \to 0$.

2.3.3.3 Summary of the kernels

Let $K^{I\alpha}_{J\beta}$ be defined by

$$K^{I\alpha}_{J\beta} \equiv -\frac{1}{4\pi^2} \oint_{\|\boldsymbol{z}\|=1} (\boldsymbol{z},\boldsymbol{z})^{-1}_{IJ}\, z_\alpha z_\beta (\ln r + \ln|\boldsymbol{z}\cdot\boldsymbol{e}|)\; d\boldsymbol{z} \tag{2.77}$$

Then the displacement fundamental solution U^P_J, the kernel G^P_J and the kernel C^K_J are now expressed in succinct form as

$$\begin{aligned} U^P_J(\boldsymbol{\xi}-\boldsymbol{x}) &= K^{P\alpha}_{J\alpha} && (2.78)\\ G^P_J(\boldsymbol{\xi}-\boldsymbol{x}) &= \epsilon_{\zeta\alpha} E_{\zeta JK\beta}\; K^{P\alpha}_{K\beta} && (2.79)\\ C^K_J(\boldsymbol{\xi}-\boldsymbol{x}) &= A^{K\gamma M}_{J\beta P}\; K^{P\beta}_{M\gamma} && (2.80) \end{aligned}$$

in which $A^{K\gamma M}_{J\beta P}$ is given by (2.76).

For the special case of isotropic material in elastic media, these kernels will reduce to much simpler forms in terms of the Young's modulus E and the Poisson ration ν of the material. Details of this reduction are presented in Appendix D.

2.4 Cracks in a finite domain

The weak-form integral equation for the unknown relative displacement $\Delta\boldsymbol{u}$ on crack surfaces (i.e. equation (2.43)) has been developed. This equation is the basis for a computational procedure to obtain all quantities of interest (e.g. crack-face displacements, stress intensity factors) in problems of isolated cracks. As mentioned earlier, our main interest is for the problems of cracks in finite domains which contain embedded cracks and/or edged cracks. The derivation of singularity-reduced integral equations needed for these finite-domain problems is very similar to that of isolated cracks. For that reason, in this section, we only provide a brief explanation of how to apply the established results for crack problems in finite domains.

Consider a homogeneous finite two-dimensional domain which contains embedded and/or surface breaking cracks as shown schematically in Fig. 2.3. The ordinary boundary of the domain, denoted as Γ_o, includes two parts: Γ_t on which tractions are prescribed and Γ_u on which displacements are prescribed. The crack faces which are geometrically coincident are denoted as Γ_c^+ and Γ_c^- representing the 'upper' and 'lower' face, respectively. Similar to the case of isolated cracks, a single crack face is sufficient for describing the crack due to the geometrically coincident property of the crack faces and the fact that the interesting quantity on crack faces is the relative displacement. Also, attention is restricted to cases of no body force existing in the domain and the traction prescribed on the crack is self-equilibrated such that $t_I^+ = -t_I^-$ where t_I^+ and t_I^- refer to the traction applied on Γ_c^+ and Γ_c^- respectively. The total boundary of the domain is denoted as $\Gamma = \Gamma_o \cup \Gamma_c$.

Somigliana's identity for the displacement u_P at a point $\boldsymbol{x}$ in the domain for this configuration is given as

$$u_P(\boldsymbol{x}) = \int_{\Gamma_o} U_J^P(\boldsymbol{\xi} - \boldsymbol{x})\, t_J(\boldsymbol{\xi})\, ds(\boldsymbol{\xi}) - \int_{\Gamma} S_{\alpha J}^P(\boldsymbol{\xi} - \boldsymbol{x})\, n_\alpha(\boldsymbol{\xi})\, v_J(\boldsymbol{\xi})\, ds(\boldsymbol{\xi}) \qquad (2.81)$$

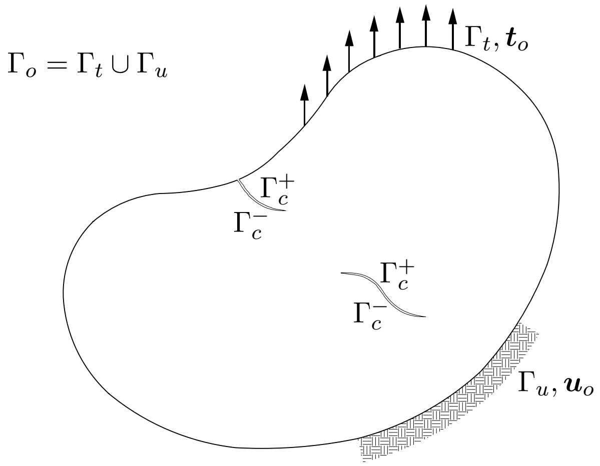

Figure 2.3: Schematic of a bounded domain containing embedded and edged cracks.

where

$$v_J(\boldsymbol{\xi}) \quad = \quad \begin{cases} u_J(\boldsymbol{\xi}) & , \quad \boldsymbol{\xi} \in \Gamma_o \\ \Delta u_J(\boldsymbol{\xi}) & , \quad \boldsymbol{\xi} \in \Gamma_c \end{cases} \tag{2.82}$$

The stress at the point $\boldsymbol{x}$ is then obtained by taking the derivative of (2.81) with respect to $\boldsymbol{x}$

$$\sigma_{\zeta K}(\boldsymbol{x}) = -\int_{\Gamma_o} S^J_{\zeta K}(\boldsymbol{\xi} - \boldsymbol{x})\, t_J(\boldsymbol{\xi})\, ds(\boldsymbol{\xi}) + \int_{\Gamma} \Sigma^{\zeta K}_{\alpha J}(\boldsymbol{\xi} - \boldsymbol{x})\, n_\alpha(\boldsymbol{\xi})\, v_J(\boldsymbol{\xi})\, ds(\boldsymbol{\xi}) \tag{2.83}$$

In the above integral equations, as stated for the case of isolated cracks, U^P_J and $S^P_{\alpha J}$ are fundamental solutions for displacement and stress, respectively, and $\Sigma^{\zeta K}_{\alpha J}$ is defined in (2.23). The kernel U^P_J is weakly-singular in the order of $\mathcal{O}(\ln r)$, thus it does not need to be regularized. However, the kernels $S^P_{\alpha J}$ and $\Sigma^{\zeta K}_{\alpha J}$ must be regularized so that the equations (2.81) and (2.83) are suitable for numerical evaluation.

Let us start with the displacement equation (2.81) first. While this equation is not of interest for isolated crack problems, it is useful for problems of finite domain where a portion of the ordinary boundary has prescribed displacement and an SGBEM is adopted for numerical implementation. In this context, a symmetric formulation is achieved when both displacement and traction equations are employed. Utilizing the decomposition (2.25) and integrating the term associated with $S^P_{\alpha J}$ in (2.81) by parts, then forming the limit of $\boldsymbol{x} \to \boldsymbol{y}$, where $\boldsymbol{y} \in \Gamma_o$, we get the result as

$$\begin{aligned} \frac{1}{2}u_P(\boldsymbol{y}) &= \int_{\Gamma_o} U^P_J(\boldsymbol{\xi}-\boldsymbol{y})t_J(\boldsymbol{\xi})ds(\boldsymbol{\xi}) + \int_{\Gamma} G^P_J(\boldsymbol{\xi}-\boldsymbol{y})Dv_J(\boldsymbol{\xi})ds(\boldsymbol{\xi}) \\ &- \int_{\Gamma} n_\alpha(\boldsymbol{\xi})H^P_{\alpha J}(\boldsymbol{\xi}-\boldsymbol{y})v_J(\boldsymbol{\xi})ds(\boldsymbol{\xi}) \end{aligned} \tag{2.84}$$

The weak-form integral equation for displacement is then obtained by multiplying (2.84) with a test function $\tilde{t}_P$ and integrating the result over the ordinary boundary as

$$\begin{aligned} \frac{1}{2}\int_{\Gamma_o} u_P(\boldsymbol{y})\,\tilde{t}_P(\boldsymbol{y})\,ds(\boldsymbol{y}) &= \int_{\Gamma_o} \tilde{t}_P(\boldsymbol{y}) \int_{\Gamma_o} U^P_J(\boldsymbol{\xi}-\boldsymbol{y})t_J(\boldsymbol{\xi})\,ds(\boldsymbol{\xi})\,ds(\boldsymbol{y}) \\ &+ \int_{\Gamma_o} \tilde{t}_P(\boldsymbol{y}) \int_{\Gamma} G^P_J(\boldsymbol{\xi}-\boldsymbol{y})Dv_J(\boldsymbol{\xi})\,ds(\boldsymbol{\xi})\,ds(\boldsymbol{y}) \\ &- \int_{\Gamma_o} \tilde{t}_P(\boldsymbol{y}) \int_{\Gamma} n_\alpha(\boldsymbol{\xi})H^P_{\alpha J}(\boldsymbol{\xi}-\boldsymbol{y})v_J(\boldsymbol{\xi})\,ds(\boldsymbol{\xi})\,ds(\boldsymbol{y}) \end{aligned} \tag{2.85}$$

Now consider the stress equation (2.83). Similar to the case of isolated cracks, the decompositions (2.25) and (2.35) are utilized for the kernel $S^J_{\zeta K}$ and the kernel $\Sigma^{\zeta K}_{\alpha J}$, respectively. An integration by parts is performed to obtain the singularity-reduced integral relation for the stress at a point $\boldsymbol{x}$ inside the domain. Finally, the traction integral equation at a point $\boldsymbol{y}$ on the boundary Γ is obtained by forming the product of $\sigma_{\zeta K}(\boldsymbol{x})n_{\zeta}(\boldsymbol{y})$ and then taking the limit of $\boldsymbol{x} \rightarrow \boldsymbol{y}$ with the result as

$$\begin{aligned} c(\boldsymbol{y})t_K(\boldsymbol{y}) &= D\int_{\Gamma_o} G_K^J(\boldsymbol{\xi}-\boldsymbol{y})t_J(\boldsymbol{\xi})ds(\boldsymbol{\xi}) - \int_{\Gamma_o} n_\alpha(\boldsymbol{y})H_{\alpha K}^J(\boldsymbol{\xi}-\boldsymbol{y})t_J(\boldsymbol{\xi})ds(\boldsymbol{\xi}) \\ &+ D\int_{\Gamma} C_J^K(\boldsymbol{\xi}-\boldsymbol{y})\, Dv_J(\boldsymbol{\xi})ds(\boldsymbol{\xi}) \end{aligned} \tag{2.86}$$

where $c = 1/2$ for $\boldsymbol{y} \in \Gamma_o$ and $c = 1$ for $\boldsymbol{y} \in \Gamma_c$.

From (2.86), the weak-form integral equation for traction is obtained by multiplying both sides with a test function $\tilde{v}_K$, then integrating over the entire boundary Γ, and finally integrating by parts. The final result is as follows

$$\begin{aligned} -\int_{\Gamma} c(\boldsymbol{y})t_K(\boldsymbol{y})\tilde{v}_K(\boldsymbol{y})ds(\boldsymbol{y}) &= \int_{\Gamma} D\tilde{v}_K(\boldsymbol{y})\int_{\Gamma} C_J^K(\boldsymbol{\xi}-\boldsymbol{y})Dv_J(\boldsymbol{\xi})ds(\boldsymbol{\xi})ds(\boldsymbol{y}) \\ &+ \int_{\Gamma} D\tilde{v}_K(\boldsymbol{y})\int_{\Gamma_o} G_K^J(\boldsymbol{\xi}-\boldsymbol{y})t_J(\boldsymbol{\xi})ds(\boldsymbol{\xi})ds(\boldsymbol{y}) \\ &+ \int_{\Gamma} \tilde{v}_K(\boldsymbol{y})n_\alpha(\boldsymbol{y})\int_{\Gamma_o} H_{\alpha K}^J(\boldsymbol{\xi}-\boldsymbol{y})t_J(\boldsymbol{\xi})ds(\boldsymbol{\xi})ds(\boldsymbol{y}) \end{aligned} \tag{2.87}$$

where

$$\tilde{v}_K(\boldsymbol{y}) = \begin{cases} \tilde{u}_K(\boldsymbol{y}) & , \quad \boldsymbol{y} \in \Gamma_o \\ \Delta\tilde{u}_K(\boldsymbol{y}) & , \quad \boldsymbol{y} \in \Gamma_c \end{cases} \tag{2.88}$$

in which $\tilde{u}_K$ and $\Delta\tilde{u}_K$ are test functions associated with Γ_o and Γ_c, respectively.

Chapter 3

SGBEM for Analysis of Fractures in Two-dimensional Multi-field Media

From the weakly-singular weak-form integral equations (IEs) for generalized displacement and stress derived in Chapter 2, a well-known numerical technique called Symmetric Galerkin Boundary Element Method is developed in this chapter. The procedure is also extended for the domain occupying multiple regions. Since the kernels appeared in the IEs are all weakly-singular of order $\mathcal{O}(\ln r)$, standard isoparametric quadratic elements are employed everywhere on the boundaries, interfaces (for multi-region problems) and crack faces except right behind crack tips where a special crack-tip element is developed to accurately capture the asymptotic behavior of the relative crack-face displacements. By utilizing special shape functions, the crack-tip elements directly provide generalized stress intensity factors as a part of the solution of the governing discretized equations. For evaluating the weakly-singular double line integrals when constructing the coefficient matrix of the discretized equations, transformations of the integration variables are used to eliminate the singularity so that standard Gaussian integration is sufficient to get the desirable accuracy. Also, an algorithm for numerical calculation of the weakly-singular kernels which are in the form of a contour integral is developed to efficiently and accurately obtain the kernels.

Consider a homogeneous finite 2D domain which contains either embedded or surface breaking cracks (or both) as shown schematically in Figure 3.1. The ordinary boundary of the domain denoted as Γ_o contains two parts: Γ_t on which tractions are prescribed and Γ_u on which displacements are prescribed. The crack faces which are geometrically coincident are denoted as Γ_c^+ and Γ_c^- representing the 'upper' face and the 'lower' face, respectively. As mentioned in Chapter 2, only a single crack face is needed for our derived equations and we denote this crack face as $\Gamma_c \equiv \Gamma_c^+$. It should be reminded that, as stated in the derivation of integral equations in Chapter 2, the assumptions of no body force existing in the domain and of self-equilibrated prescribed traction on crack faces (i.e. $\boldsymbol{t}^+ = -\boldsymbol{t}^-$, where $\boldsymbol{t}^+$ and $\boldsymbol{t}^-$ are the tractions applying on Γ_c^+ and Γ_c^-, respectively) are still applied here after.

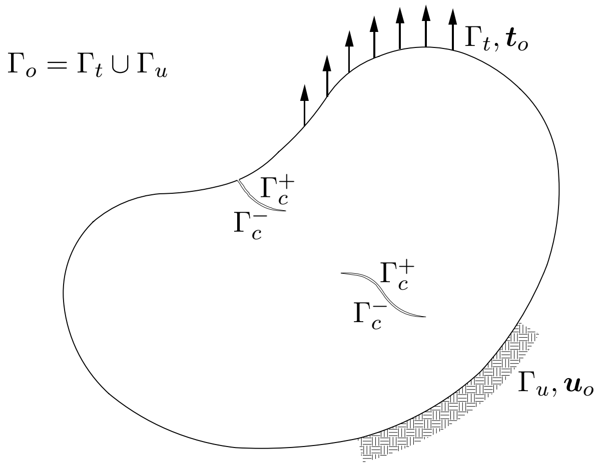

Figure 3.1: Schematic of a bounded domain containing embedded and edged cracks.

For convenience, a summary of the equations that were developed in Chapter 2 is restated here. These equations, include the weakly-singular weak-form integral equations for displacement and traction and the expression of the weakly-singular kernels, are the basis for the development of the SGBEM for single-region and multiple-region problems that will be discussed further below.

Integral equation for displacement

$$\begin{aligned}\frac{1}{2}\int_{\Gamma_o} u_P(\boldsymbol{y})\,\tilde{t}_P(\boldsymbol{y})\,ds(\boldsymbol{y}) \;&=\; \int_{\Gamma_o} \tilde{t}_P(\boldsymbol{y}) \int_{\Gamma} G_J^P\; Dv_J(\boldsymbol{\xi})\; ds(\boldsymbol{\xi})\,ds(\boldsymbol{y}) \\ &-\; \int_{\Gamma_o} \tilde{t}_P(\boldsymbol{y}) \int_{\Gamma} n_\alpha(\boldsymbol{\xi})\; H_{\alpha J}^P\; v_J(\boldsymbol{\xi})\; ds(\boldsymbol{\xi})\,ds(\boldsymbol{y}) \\ &+\; \int_{\Gamma_o} \tilde{t}_P(\boldsymbol{y}) \int_{\Gamma_o} U_J^P\; t_J(\boldsymbol{\xi})\; ds(\boldsymbol{\xi})\,ds(\boldsymbol{y}) \qquad (3.1)\end{aligned}$$

Integral equation for traction

$$\begin{aligned}-\int_{\Gamma} c(\boldsymbol{y}) t_K(\boldsymbol{y})\tilde{v}_K(\boldsymbol{y}) ds(\boldsymbol{y}) \;&=\; \int_{\Gamma} D\tilde{v}_K(\boldsymbol{y}) \int_{\Gamma} C_J^K\; Dv_J(\boldsymbol{\xi})\; ds(\boldsymbol{\xi}) ds(\boldsymbol{y}) \\ &+\; \int_{\Gamma} D\tilde{v}_K(\boldsymbol{y}) \int_{\Gamma_o} G_K^J\; t_J(\boldsymbol{\xi})\; ds(\boldsymbol{\xi}) ds(\boldsymbol{y}) \\ &+\; \int_{\Gamma} \tilde{v}_K(\boldsymbol{y}) n_\alpha(\boldsymbol{y}) \int_{\Gamma_o} H_{\alpha K}^J\; t_J(\boldsymbol{\xi})\; ds(\boldsymbol{\xi}) ds(\boldsymbol{y})\end{aligned} \qquad (3.2)$$

where

$$v_J(\boldsymbol{\xi}) = \begin{cases} u_J(\boldsymbol{\xi}) & , \;\boldsymbol{\xi} \in \Gamma_o \\ \Delta u_J(\boldsymbol{\xi}) & , \;\boldsymbol{\xi} \in \Gamma_c \end{cases} \quad , \quad \tilde{v}_K(\boldsymbol{y}) = \begin{cases} \tilde{u}_K(\boldsymbol{y}) & , \;\boldsymbol{y} \in \Gamma_o \\ \Delta\tilde{u}_K(\boldsymbol{y}) & , \;\boldsymbol{y} \in \Gamma_c \end{cases} \qquad (3.3)$$

and where

$$c(\boldsymbol{y}) = \begin{cases} \frac{1}{2} & , \;\boldsymbol{y} \in \Gamma_o \\ 1 & , \;\boldsymbol{y} \in \Gamma_c \end{cases} \qquad (3.4)$$

Weakly-singular kernels $\{U_J^P, G_J^P, C_J^K\}$ appeared in (3.1) and (3.2)

$$U_J^P(\boldsymbol{\xi}-\boldsymbol{y}) = K_{J\alpha}^{P\alpha} \tag{3.5}$$

$$G_J^P(\boldsymbol{\xi}-\boldsymbol{y}) = \epsilon_{\zeta\alpha} E_{\zeta JK\beta}\, K_{K\beta}^{P\alpha} \tag{3.6}$$

$$C_J^K(\boldsymbol{\xi}-\boldsymbol{y}) = A_{J\beta P}^{K\gamma M}\, K_{M\gamma}^{P\beta} \tag{3.7}$$

where $E_{\zeta JK\beta}$ are the material constants,

$$A_{J\beta P}^{K\gamma M} = E_{\eta KP\beta} E_{\eta JM\gamma} - \frac{1}{N} E_{\eta JK\eta} E_{\beta PM\gamma} \tag{3.8}$$

and

$$K_{J\beta}^{I\alpha} = \frac{-1}{4\pi^2} \oint_{\|\boldsymbol{z}\|=1} (\boldsymbol{z},\boldsymbol{z})_{IJ}^{-1}\ z_\alpha z_\beta \big(\ln r + \ln|\boldsymbol{z}\cdot\boldsymbol{e}|\big)\ d\boldsymbol{z} \tag{3.9}$$

in which $r = ||\boldsymbol{\xi}-\boldsymbol{y}||$, $(\boldsymbol{z},\boldsymbol{z})_{IJ} = z_\alpha E_{\alpha IJ\beta} z_\beta$, and the contour integral is to be evaluated over a unit circle $\|\boldsymbol{z}\| = 1$.

We note that the quantity

$$H_{\alpha J}^P(\boldsymbol{\xi}-\boldsymbol{y}) = -\frac{1}{2\pi}\frac{(\xi_\alpha - y_\alpha)\delta_{PJ}}{r^2} \tag{3.10}$$

together with either the normal $\boldsymbol{n}(\boldsymbol{\xi})$ or the normal $\boldsymbol{n}(\boldsymbol{y})$ is of order $\mathcal{O}(1)$ (see proof in Appendix C).

3.1 Symmetric formulation for single-region problems

The symmetric formulation for the single-region problems is derived by applying the integral equations (3.1) and (3.2) on different boundaries of the domain. Specifically, we apply the displacement equation (3.1) on Γ_u where displacements are prescribed (i.e. taking $\tilde{\boldsymbol{t}} = \boldsymbol{0}$ on Γ_t). Next, we apply the traction equation (3.2) on Γ_t where tractions are prescribed (i.e. taking $\tilde{\boldsymbol{v}} = \boldsymbol{0}$ on $\Gamma_u \cup \Gamma_c$). And finally, we apply the traction equation (3.2) on Γ_c where tractions are also prescribed (i.e. taking $\tilde{\boldsymbol{v}} = \boldsymbol{0}$ on $\Gamma_u \cup \Gamma_t$). The resulting symmetric system of integral equations can be expressed as

$$\begin{array}{ccccccc}
\mathcal{B}_{uu}(\tilde{\boldsymbol{t}}, \boldsymbol{t}) & + & \bar{\mathcal{A}}_{ut}(\tilde{\boldsymbol{t}}, \boldsymbol{u}) & + & \bar{\mathcal{A}}_{uc}(\tilde{\boldsymbol{t}}, \Delta\boldsymbol{u}) & = & \mathcal{R}_1(\tilde{\boldsymbol{t}}) \\
\mathcal{A}_{tu}(\tilde{\boldsymbol{u}}, \boldsymbol{t}) & + & \mathcal{D}_{tt}(\tilde{\boldsymbol{u}}, \boldsymbol{u}) & + & \mathcal{D}_{tc}(\tilde{\boldsymbol{u}}, \Delta\boldsymbol{u}) & = & \mathcal{R}_2(\tilde{\boldsymbol{u}}) \\
\mathcal{A}_{cu}(\Delta\tilde{\boldsymbol{u}}, \boldsymbol{t}) & + & \mathcal{D}_{ct}(\Delta\tilde{\boldsymbol{u}}, \boldsymbol{u}) & + & \mathcal{D}_{cc}(\Delta\tilde{\boldsymbol{u}}, \Delta\boldsymbol{u}) & = & \mathcal{R}_3(\Delta\tilde{\boldsymbol{u}})
\end{array} \tag{3.11}$$

where the integral operators $\mathcal{A}_{pq}, \bar{\mathcal{A}}_{pq}, \mathcal{B}_{pq}$ and $\mathcal{D}_{pq}$ (with $p, q \in \{u, t, c\}$) are defined as

$$\mathcal{B}_{pq}(\boldsymbol{X}, \boldsymbol{Y}) = -\int_{\Gamma_p} X_I(\boldsymbol{y}) \int_{\Gamma_q} U_J^I \; Y_J(\boldsymbol{\xi}) \; ds(\boldsymbol{\xi}) \, ds(\boldsymbol{y}) \tag{3.12}$$

$$\begin{aligned}
\mathcal{A}_{pq}(\boldsymbol{X}, \boldsymbol{Y}) &= -\int_{\Gamma_p} DX_k(\boldsymbol{y}) \int_{\Gamma_q} G_K^L \; Y_L(\boldsymbol{\xi}) \; ds(\boldsymbol{\xi}) \, ds(\boldsymbol{y}) \\
&\quad - \int_{\Gamma_p} X_K(\boldsymbol{y}) \; n_\alpha(\boldsymbol{y}) \int_{\Gamma_q} H_{\alpha K}^L \; Y_L(\boldsymbol{\xi}) \; ds(\boldsymbol{\xi}) \, ds(\boldsymbol{y})
\end{aligned} \tag{3.13}$$

$$\begin{aligned}
\bar{\mathcal{A}}_{pq}(\boldsymbol{X}, \boldsymbol{Y}) &= -\int_{\Gamma_p} X_K(\boldsymbol{y}) \int_{\Gamma_q} G_L^K \; DY_L(\boldsymbol{\xi}) \; ds(\boldsymbol{\xi}) \, ds(\boldsymbol{y}) \\
&\quad + \int_{\Gamma_p} X_K(\boldsymbol{y}) \int_{\Gamma_q} H_{\alpha L}^K \; n_\alpha(\boldsymbol{\xi}) \; Y_L(\boldsymbol{\xi}) \; ds(\boldsymbol{\xi}) \, ds(\boldsymbol{y})
\end{aligned} \tag{3.14}$$

$$\mathcal{D}_{pq}(\boldsymbol{X}, \boldsymbol{Y}) = -\int_{\Gamma_p} DX_K(\boldsymbol{y}) \int_{\Gamma_q} C_L^K \; DY_L(\boldsymbol{\xi}) \; ds(\boldsymbol{\xi}) \, ds(\boldsymbol{y}) \tag{3.15}$$

and the operators $\mathcal{R}_1, \mathcal{R}_2$ and $\mathcal{R}_3$ on the right hand side of (3.11) are defined as

$$\mathcal{R}_1(\tilde{\boldsymbol{t}}) = -\mathcal{C}_u(\tilde{\boldsymbol{t}}, \boldsymbol{u}) + \mathcal{B}_{ut}(\tilde{\boldsymbol{t}}, \boldsymbol{t}) - \bar{\mathcal{A}}_{uu}(\tilde{\boldsymbol{t}}, \boldsymbol{u}) \tag{3.16}$$

$$\mathcal{R}_2(\tilde{\boldsymbol{u}}) = \mathcal{C}_t(\tilde{\boldsymbol{u}}, \boldsymbol{t}) - \mathcal{A}_{tt}(\tilde{\boldsymbol{u}}, \boldsymbol{t}) - \mathcal{D}_{tu}(\tilde{\boldsymbol{u}}, \boldsymbol{u}) \tag{3.17}$$

$$\mathcal{R}_3(\Delta\tilde{\boldsymbol{u}}) = 2\mathcal{C}_c(\Delta\tilde{\boldsymbol{u}}, \boldsymbol{t}) - \mathcal{A}_{ct}(\Delta\tilde{\boldsymbol{u}}, \boldsymbol{t}) - \mathcal{D}_{cu}(\Delta\tilde{\boldsymbol{u}}, \Delta\boldsymbol{u}) \tag{3.18}$$

where

$$\mathcal{C}_p(\boldsymbol{X}, \boldsymbol{Y}) = \frac{1}{2}\int_{\Gamma_p} X_I(\boldsymbol{y})\; Y_I(\boldsymbol{y})\, ds(\boldsymbol{y}) \tag{3.19}$$

With the properties of the kernels that were discussed in Chapter 2, it is clear to have

$$\mathcal{B}_{pp}(\boldsymbol{X}, \boldsymbol{Y}) = \mathcal{B}_{pp}(\boldsymbol{Y}, \boldsymbol{X}) \tag{3.20}$$

$$\mathcal{D}_{pp}(\boldsymbol{X}, \boldsymbol{Y}) = \mathcal{D}_{pp}(\boldsymbol{Y}, \boldsymbol{X}) \tag{3.21}$$

$$\bar{\mathcal{A}}_{pq}(\boldsymbol{X}, \boldsymbol{Y}) = \mathcal{A}_{qp}(\boldsymbol{Y}, \boldsymbol{X}) \tag{3.22}$$

$$\mathcal{D}_{pq}(\boldsymbol{X}, \boldsymbol{Y}) = \mathcal{D}_{qp}(\boldsymbol{Y}, \boldsymbol{X}) \tag{3.23}$$

then the governing system of integral equation (3.11) for a single-region domain is symmetric.

3.2 Symmetric formulation for multi-region problems

In this section, we will extend the formulation (3.11) for the domain occupying multiple regions. Each region, which is homogeneous, is treated as a single-region domain, and its interfaces with other regions are considered as a portion of the ordinary boundary. Neither displacements nor tractions are prescribed on the interfaces and therefore both displacement and traction integral equations (3.1) and (3.2) are applied on the interface.

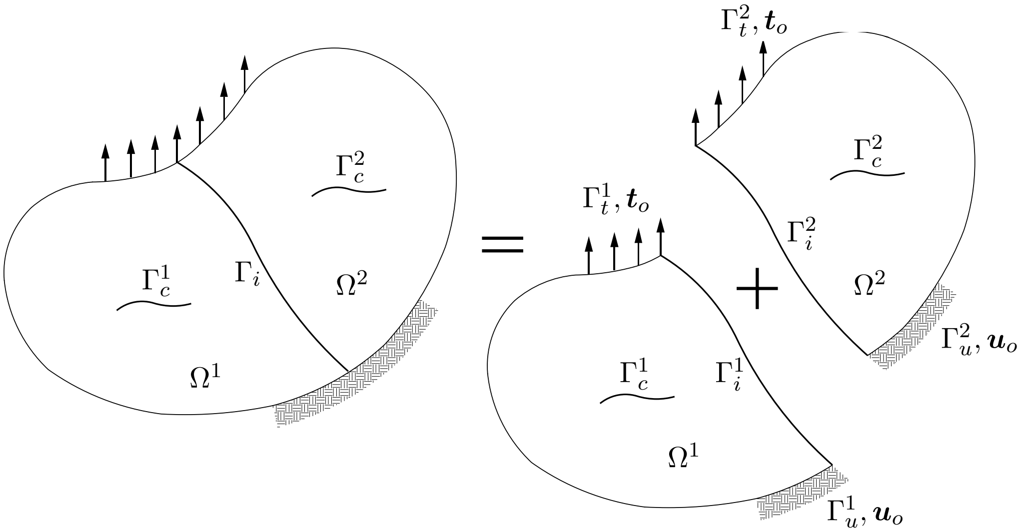

Figure 3.2: Schematic of a bounded cracked domain occupying two material regions.

For the purpose of presenting the formulation, consider a simple configuration of a domain occupying two regions Ω^1 and Ω^2 with embedded cracks $\Gamma_c^1 \in \Omega^1$ and $\Gamma_c^2 \in \Omega^2$ as shown schematically in Figure 3.2. The two domains connect to each other through an interface Γ_i where a perfectly bonded condition is assumed. Imagine sectioning the domain along the interface and consider separately each region. On the ordinary boundary Γ_o^e (where $e = \{1, 2\}$ representing for the region number) of each region, in addition to the traction-prescribed Γ_t and displacement-prescribed Γ_u, there is a new portion, denoted as Γ_i^e, which is the interface where both traction and displacement are unknown a priori. Note that the interface portions Γ_i^1 and Γ_i^2 are identical except that they have opposite normal vectors.

On each region Ω^e, we apply the displacement integral equation (3.1) for Γ_u^e (i.e. taking $\tilde{\boldsymbol{t}}^e = \boldsymbol{0}$ on $\Gamma_t^e + \Gamma_i^e$), the traction integral equation (3.2) for Γ_t^e (i.e. taking $\tilde{\boldsymbol{u}}^e = \boldsymbol{0}$ on $\Gamma_u^e + \Gamma_i^e + \Gamma_c^e$), and Γ_c^e (i.e. taking $\tilde{\boldsymbol{u}}^e = \boldsymbol{0}$ on $\Gamma_u^e + \Gamma_t^e + \Gamma_i^e$). On the interface Γ_i^e, since both traction and displacement are unknowns a priori, we apply both the displacement integral relation (3.1) (i.e. taking $\tilde{\boldsymbol{t}}^e = \boldsymbol{0}$ on $\Gamma_u^e + \Gamma_t^e$) and the traction integral relation (3.2) (i.e. taking $\tilde{\boldsymbol{u}}^e = \boldsymbol{0}$ on $\Gamma_u^e + \Gamma_t^e + \Gamma_c^e$). The results are expressed as follows

$$\begin{array}{lllllll}
\mathcal{B}_{uu}^e(\tilde{\boldsymbol{t}}^e, \boldsymbol{t}^e) & + & \bar{\mathcal{A}}_{ut}^e(\tilde{\boldsymbol{t}}^e, \boldsymbol{u}^e) & + & \bar{\mathcal{A}}_{uc}^e(\tilde{\boldsymbol{t}}^e, \Delta\boldsymbol{u}^e) & + & \bar{\mathcal{A}}_{ui}^e(\tilde{\boldsymbol{t}}^e, \boldsymbol{u}^e) \\
 & & & & & + & \mathcal{B}_{ui}^e(\tilde{\boldsymbol{t}}^e, \boldsymbol{t}^e) \quad = \quad \mathcal{R}_1^e(\tilde{\boldsymbol{t}}^e) \\[1ex]
\mathcal{A}_{tu}^e(\tilde{\boldsymbol{u}}^e, \boldsymbol{t}^e) & + & \mathcal{D}_{tt}^e(\tilde{\boldsymbol{u}}^e, \boldsymbol{u}^e) & + & \mathcal{D}_{tc}^e(\tilde{\boldsymbol{u}}^e, \Delta\boldsymbol{u}^e) & + & \mathcal{D}_{ti}^e(\tilde{\boldsymbol{u}}^e, \boldsymbol{u}^e) \\
 & & & & & + & \mathcal{A}_{ti}^e(\tilde{\boldsymbol{u}}^e, \boldsymbol{t}^e) \quad = \quad \mathcal{R}_2^e(\tilde{\boldsymbol{u}}^e) \\[1ex]
\mathcal{A}_{cu}^e(\Delta\tilde{\boldsymbol{u}}^e, \boldsymbol{t}^e) & + & \mathcal{D}_{ct}^e(\Delta\tilde{\boldsymbol{u}}^e, \boldsymbol{u}^e) & + & \mathcal{D}_{cc}^e(\Delta\tilde{\boldsymbol{u}}^e, \Delta\boldsymbol{u}^e) & + & \mathcal{D}_{ci}^e(\Delta\tilde{\boldsymbol{u}}^e, \boldsymbol{u}^e) \\
 & & & & & + & \mathcal{A}_{ci}^e(\Delta\tilde{\boldsymbol{u}}^e, \boldsymbol{t}^e) \quad = \quad \mathcal{R}_3^e(\Delta\tilde{\boldsymbol{u}}^e) \\[1ex]
\mathcal{A}_{iu}^e(\tilde{\boldsymbol{u}}^e, \boldsymbol{t}^e) & + & \mathcal{D}_{it}^e(\tilde{\boldsymbol{u}}^e, \boldsymbol{u}^e) & + & \mathcal{D}_{ic}^e(\tilde{\boldsymbol{u}}^e, \boldsymbol{u}^e) & + & \mathcal{D}_{ii}^e(\tilde{\boldsymbol{u}}^e, \boldsymbol{u}^e) \\
 & & & + & \mathcal{A}_{ii}^e(\tilde{\boldsymbol{u}}^e, \boldsymbol{t}^e) & - & \mathcal{E}_i^e(\tilde{\boldsymbol{u}}^e, \boldsymbol{t}^e) \quad = \quad \mathcal{R}_4^e(\tilde{\boldsymbol{u}}^e) \\[1ex]
\mathcal{B}_{iu}^e(\tilde{\boldsymbol{t}}^e, \boldsymbol{t}^e) & + & \bar{\mathcal{A}}_{it}^e(\tilde{\boldsymbol{t}}^e, \boldsymbol{u}^e) & + & \bar{\mathcal{A}}_{ic}^e(\tilde{\boldsymbol{t}}^e, \Delta\boldsymbol{u}^e) & + & \bar{\mathcal{A}}_{ii}^e(\tilde{\boldsymbol{t}}^e, \boldsymbol{u}^e) \\
 & & & + & \mathcal{B}_{ii}^e(\tilde{\boldsymbol{t}}^e, \boldsymbol{t}^e) & - & \mathcal{F}_i^e(\tilde{\boldsymbol{t}}^e, \boldsymbol{u}^e) \quad = \quad \mathcal{R}_5^e(\tilde{\boldsymbol{t}}^e)
\end{array} \tag{3.24}$$

where the operators $\mathcal{B}_{pq}^e$, $\mathcal{A}_{pq}^e$, $\bar{\mathcal{A}}_{pq}^e$ and $\mathcal{D}_{pq}^e$ are defined in (3.12), (3.13), (3.14) and (3.15), respectively, and the superscript e refers to the region Ω^e. Also, the operators $\mathcal{R}_1^e$, $\mathcal{R}_2^e$ and $\mathcal{R}_3^e$ are defined in (3.16), (3.17) and (3.18), respectively. The new operators $\mathcal{E}_i^e$ and $\mathcal{F}_i^e$ are defined as

$$\mathcal{E}_i^e(\tilde{\boldsymbol{u}}^e, \boldsymbol{t}^e) = \frac{1}{2}\int_{\Gamma_i^e} t_K^e \tilde{u}_K^e ds(\boldsymbol{y}) \tag{3.25}$$

$$\mathcal{F}_i^e(\tilde{\boldsymbol{t}}^e, \boldsymbol{u}^e) = \frac{1}{2}\int_{\Gamma_i^e} \tilde{t}_K^e u_K^e ds(\boldsymbol{y}) \tag{3.26}$$

and the operations $\mathcal{R}_4^e$ and $\mathcal{R}_5^e$ on the right hand side are defined as

$$\begin{aligned} \mathcal{R}_4^e(\tilde{\boldsymbol{u}}^e) &= -\mathcal{A}_{it}^e(\tilde{\boldsymbol{u}}^e, \boldsymbol{t}^e) - \mathcal{D}_{iu}^e(\tilde{\boldsymbol{u}}^e, \boldsymbol{u}^e) & (3.27)\\ \mathcal{R}_5^e(\tilde{\boldsymbol{t}}^e) &= -\mathcal{B}_{it}^e(\tilde{\boldsymbol{t}}^e, \boldsymbol{t}^e) - \bar{\mathcal{A}}_{iu}^e(\tilde{\boldsymbol{t}}^e, \boldsymbol{u}^e) & (3.28)\end{aligned}$$

Note that with the assumption of perfectly bonded interface, the displacement $\boldsymbol{u}^e$ and the traction $\boldsymbol{t}^e$ on the interface Γ_i^e of each region must satisfy the continuity condition

$$\begin{aligned} \boldsymbol{u}^1 &= \boldsymbol{u}^2 \\ \boldsymbol{t}^1 &= -\boldsymbol{t}^2 \end{aligned} \tag{3.29}$$

and the test function on Γ_i^e are chosen such that

$$\begin{aligned} \tilde{\boldsymbol{u}}^1 &= \tilde{\boldsymbol{u}}^2 \\ \tilde{\boldsymbol{t}}^1 &= -\tilde{\boldsymbol{t}}^2 \end{aligned} \tag{3.30}$$

In order to construction a symmetric formulation for the original two-region problem, first we define the data (unknowns) on the interface as

$$\begin{aligned} \boldsymbol{u} &\equiv \boldsymbol{u}^1 \\ \boldsymbol{t} &\equiv \boldsymbol{t}^1 \end{aligned} \tag{3.31}$$

then make a combination of equations (3.24) by retaining the first three equations of (3.24) for each of the region Ω^1 and Ω^2 and adding the fourth and the fifth equation of (3.24) of region Ω^1 to that of region Ω^2. Noting that

$$-\mathcal{E}^1_i(\tilde{\boldsymbol{u}}^1,\boldsymbol{t}^1)-\mathcal{E}^2_i(\tilde{\boldsymbol{u}}^2,\boldsymbol{t}^2)=0 \tag{3.32}$$

$$-\mathcal{F}^1_i(\tilde{\boldsymbol{t}}^1,\boldsymbol{u}^1)-\mathcal{F}^2_i(\tilde{\boldsymbol{t}}^2,\boldsymbol{u}^2)=0 \tag{3.33}$$

and $\mathcal{B}^e_{pq}$, $\mathcal{A}^e_{pq}$, $\bar{\mathcal{A}}^e_{pq}$ and $\mathcal{D}^e_{pq}$ are odd functions of their arguments, that is

$$\begin{array}{l}\mathcal{A}^e_{pq}(\boldsymbol{X},\boldsymbol{Y})=-\mathcal{A}^e_{pq}(-\boldsymbol{X},\boldsymbol{Y})\\ \mathcal{A}^e_{pq}(\boldsymbol{X},\boldsymbol{Y})=-\mathcal{A}^e_{pq}(\boldsymbol{X},-\boldsymbol{Y})\end{array} \tag{3.34}$$

and similarly for the other operators.

The final set of equations after combining the equations (3.24) are as follows

$$\begin{array}{cccccccc}
\mathcal{B}^1_{uu}(\tilde{\boldsymbol{t}}^1,\boldsymbol{t}^1) & + & \bar{\mathcal{A}}^1_{ut}(\tilde{\boldsymbol{t}}^1,\boldsymbol{u}^1) & + & \bar{\mathcal{A}}^1_{uc}(\tilde{\boldsymbol{t}}^1,\Delta\boldsymbol{u}^1) & + & 0 & + \\
0 & + & 0 & + & \bar{\mathcal{A}}^1_{ui}(\tilde{\boldsymbol{t}}^1,\boldsymbol{u}) & + & \mathcal{B}^1_{ui}(\tilde{\boldsymbol{t}}^1,\boldsymbol{t}) & = \\
 & & & & & & \mathcal{R}^1_1(\tilde{\boldsymbol{t}}^1) & \\
\mathcal{A}^1_{tu}(\tilde{\boldsymbol{u}}^1,\boldsymbol{t}^1) & + & \mathcal{D}^1_{tt}(\tilde{\boldsymbol{u}}^1,\boldsymbol{u}^1) & + & \mathcal{D}^1_{tc}(\tilde{\boldsymbol{u}}^1,\Delta\boldsymbol{u}^1) & + & 0 & + \\
0 & + & 0 & + & \mathcal{D}^1_{ti}(\tilde{\boldsymbol{u}}^1,\boldsymbol{u}) & + & \mathcal{A}^1_{ti}(\tilde{\boldsymbol{u}}^1,\boldsymbol{t}) & = \\
 & & & & & & \mathcal{R}^1_2(\tilde{\boldsymbol{u}}^1) & \\
\mathcal{A}^1_{cu}(\Delta\tilde{\boldsymbol{u}}^1,\boldsymbol{t}^1) & + & \mathcal{D}^1_{ct}(\Delta\tilde{\boldsymbol{u}}^1,\boldsymbol{u}^1) & + & \mathcal{D}^1_{cc}(\Delta\tilde{\boldsymbol{u}}^1,\Delta\boldsymbol{u}^1) & + & 0 & + \\
0 & + & 0 & + & \mathcal{D}^1_{ci}(\Delta\tilde{\boldsymbol{u}}^1,\boldsymbol{u}) & + & \mathcal{A}^1_{ci}(\Delta\tilde{\boldsymbol{u}}^1,\boldsymbol{t}) & = \\
 & & & & & & \mathcal{R}^1_3(\Delta\tilde{\boldsymbol{u}}^1) & \\
0 & + & 0 & + & 0 & + & \mathcal{B}^2_{uu}(\tilde{\boldsymbol{t}}^2,\boldsymbol{t}^2) & + \\
\bar{\mathcal{A}}^2_{ut}(\tilde{\boldsymbol{t}}^2,\boldsymbol{u}^2) & + & \bar{\mathcal{A}}^2_{uc}(\tilde{\boldsymbol{t}}^2,\Delta\boldsymbol{u}^2) & + & \bar{\mathcal{A}}^2_{ui}(\tilde{\boldsymbol{t}}^2,\boldsymbol{u}) & - & \mathcal{B}^2_{ui}(\tilde{\boldsymbol{t}}^2,\boldsymbol{t}) & = \\
 & & & & & & \mathcal{R}^2_1(\tilde{\boldsymbol{t}}^2) & \\
0 & + & 0 & + & 0 & + & \mathcal{A}^2_{tu}(\tilde{\boldsymbol{u}}^2,\boldsymbol{t}^2) & + \\
\mathcal{D}^2_{tt}(\tilde{\boldsymbol{u}}^2,\boldsymbol{u}^2) & + & \mathcal{D}^2_{tc}(\tilde{\boldsymbol{u}}^2,\Delta\boldsymbol{u}^2) & + & \mathcal{D}^2_{ti}(\tilde{\boldsymbol{u}}^2,\boldsymbol{u}) & - & \mathcal{A}^2_{ti}(\tilde{\boldsymbol{u}}^2,\boldsymbol{t}) & = \\
 & & & & & & \mathcal{R}^2_2(\tilde{\boldsymbol{u}}^2) & \\
0 & + & 0 & + & 0 & + & \mathcal{A}^2_{cu}(\Delta\tilde{\boldsymbol{u}}^2,\boldsymbol{t}^2) & + \\
\mathcal{D}^2_{ct}(\Delta\tilde{\boldsymbol{u}}^2,\boldsymbol{u}^2) & + & \mathcal{D}^2_{cc}(\Delta\tilde{\boldsymbol{u}}^2,\Delta\boldsymbol{u}^2) & + & \mathcal{D}^2_{ci}(\Delta\tilde{\boldsymbol{u}}^2,\boldsymbol{u}) & - & \mathcal{A}^2_{ci}(\Delta\tilde{\boldsymbol{u}}^2,\boldsymbol{t}) & = \\
 & & & & & & \mathcal{R}^2_3(\Delta\tilde{\boldsymbol{u}}^2) & \\
\mathcal{A}^1_{iu}(\tilde{\boldsymbol{u}},\boldsymbol{t}^1) & + & \mathcal{D}^1_{it}(\tilde{\boldsymbol{u}},\boldsymbol{u}^1) & + & \mathcal{D}^1_{ic}(\tilde{\boldsymbol{u}},\boldsymbol{u}^1) & + & \mathcal{A}^2_{iu}(\tilde{\boldsymbol{u}},\boldsymbol{t}^2) & + \\
\mathcal{D}^2_{it}(\tilde{\boldsymbol{u}},\boldsymbol{u}^2) & + & \mathcal{D}^2_{ic}(\tilde{\boldsymbol{u}},\boldsymbol{u}^2) & + & \mathcal{E}_{ii}(\tilde{\boldsymbol{u}},\boldsymbol{u}) & + & \mathcal{F}_{ii}(\tilde{\boldsymbol{u}},\boldsymbol{t}) & = \\
 & & & & & & \mathcal{R}_6(\tilde{\boldsymbol{u}}) & \\
\mathcal{B}^1_{iu}(\tilde{\boldsymbol{t}}^1,\boldsymbol{t}^1) & + & \bar{\mathcal{A}}^1_{it}(\tilde{\boldsymbol{t}}^1,\boldsymbol{u}^1) & + & \bar{\mathcal{A}}^1_{ic}(\tilde{\boldsymbol{t}}^1,\Delta\boldsymbol{u}^1) & + & \mathcal{B}^2_{iu}(\tilde{\boldsymbol{t}}^2,\boldsymbol{t}^2) & + \\
\bar{\mathcal{A}}^2_{it}(\tilde{\boldsymbol{t}}^2,\boldsymbol{u}^2) & + & \bar{\mathcal{A}}^2_{ic}(\tilde{\boldsymbol{t}}^2,\Delta\boldsymbol{u}^2) & + & \bar{\mathcal{F}}_{ii}(\tilde{\boldsymbol{t}},\boldsymbol{u}) & + & \mathcal{G}_{ii}(\tilde{\boldsymbol{t}},\boldsymbol{t}) & = \\
 & & & & & & \mathcal{R}_7(\tilde{\boldsymbol{t}}) &
\end{array} \tag{3.35}$$

where the new operators $\mathcal{E}_{ii}$, $\mathcal{F}_{ii}$, $\bar{\mathcal{F}}_{ii}$ and $\mathcal{G}_{ii}$ on the left hand side are defined as

$$\mathcal{E}_{ii}(\tilde{\boldsymbol{u}},\boldsymbol{u}) = \mathcal{D}^1_{ii}(\tilde{\boldsymbol{u}},\boldsymbol{u}) + \mathcal{D}^2_{ii}(\tilde{\boldsymbol{u}},\boldsymbol{u}) \tag{3.36}$$

$$\mathcal{F}_{ii}(\tilde{\boldsymbol{u}},\boldsymbol{t}) = \mathcal{A}^1_{ii}(\tilde{\boldsymbol{u}},\boldsymbol{t}) - \mathcal{A}^2_{ii}(\tilde{\boldsymbol{u}},\boldsymbol{t}) \tag{3.37}$$

$$\bar{\mathcal{F}}_{ii}(\tilde{\boldsymbol{t}},\boldsymbol{u}) = \bar{\mathcal{A}}^1_{ii}(\tilde{\boldsymbol{t}},\boldsymbol{u}) - \bar{\mathcal{A}}^2_{ii}(\tilde{\boldsymbol{t}},\boldsymbol{u}) \tag{3.38}$$

$$\mathcal{G}_{ii}(\tilde{\boldsymbol{t}},\boldsymbol{t}) = \mathcal{B}^1_{ii}(\tilde{\boldsymbol{t}},\boldsymbol{t}) + \mathcal{B}^2_{ii}(\tilde{\boldsymbol{t}},\boldsymbol{t}) \tag{3.39}$$

and the new operators $\mathcal{R}_6$ and $\mathcal{R}_7$ on the right hand side as

$$\mathcal{R}_6(\tilde{\boldsymbol{u}}) = -\mathcal{A}^1_{it}(\tilde{\boldsymbol{u}},\boldsymbol{t}^1) - \mathcal{D}^1_{iu}(\tilde{\boldsymbol{u}},\boldsymbol{u}^1) - \mathcal{A}^2_{it}(\tilde{\boldsymbol{u}},\boldsymbol{t}^2) - \mathcal{D}^2_{iu}(\tilde{\boldsymbol{u}},\boldsymbol{u}^2) \tag{3.40}$$

$$\mathcal{R}_7(\tilde{\boldsymbol{t}}) = -\mathcal{B}^1_{it}(\tilde{\boldsymbol{t}},\boldsymbol{t}^1) - \bar{\mathcal{A}}^1_{iu}(\tilde{\boldsymbol{t}},\boldsymbol{u}^1) + \mathcal{B}^2_{it}(\tilde{\boldsymbol{t}},\boldsymbol{t}^2) + \bar{\mathcal{A}}^2_{iu}(\tilde{\boldsymbol{t}},\boldsymbol{u}^2) \tag{3.41}$$

It is readily verified that

$$\mathcal{E}_{ii}(\tilde{\boldsymbol{u}},\boldsymbol{u}) = \mathcal{E}_{ii}(\boldsymbol{u},\tilde{\boldsymbol{u}}) \tag{3.42}$$

$$\mathcal{F}_{ii}(\tilde{\boldsymbol{u}},\boldsymbol{t}) = \bar{\mathcal{F}}_{ii}(\tilde{\boldsymbol{t}},\boldsymbol{u}) \tag{3.43}$$

$$\mathcal{G}_{ii}(\tilde{\boldsymbol{t}},\boldsymbol{t}) = \mathcal{G}_{ii}(\boldsymbol{t},\tilde{\boldsymbol{t}}) \tag{3.44}$$

therefore, the overall system of equations (3.35) for the two-region problems is in fact symmetric.

The symmetric formulation for the problem of two regions having embedded cracks was developed. We remark that the procedure is not restricted to this typical case but it is readily extended for problems occupying multiple regions with or without crack. However, limitation of the developed procedure is that it is only applicable for the problems that an assumption of perfectly bonded interface is made. For problems with cracks lying along or crossing the interface, further consideration would be required.

3.3 Numerical Implementation

A Galerkin technique is implemented for numerically solving the system of integral equations (3.11) and (3.35) for single-region and multi-region problems, respectively. Due to the weak singularity of all kernels, isoparametric quadratic elements are employed everywhere (except right behind the crack tips) to discretize the total boundary of the problem (i.e. the domain of integration). Special crack-tip elements are utilized behind the crack tips to properly model the asymptotic behavior of the relative displacement near the crack tip. As an important aspect of the numerical implementation, an algorithm to accurately and efficiently evaluate the weakly-singular double line integrals in (3.11) and (3.35), as well as the kernels in (3.5)-(3.7) will be discussed.

3.3.1 Formulation of discretization

The functions of displacement on regular boundary, relative displacement on crack face and traction on regular boundary as well as their associated test functions are interpolated in terms of trial and test functions as

$$\boldsymbol{u} = \boldsymbol{\Phi}^{\mathrm{T}}\boldsymbol{U} \quad , \quad \tilde{\boldsymbol{u}} = \boldsymbol{\Phi}^{\mathrm{T}}\tilde{\boldsymbol{U}} \qquad \text{on } \Gamma_t \tag{3.45}$$

$$\Delta\boldsymbol{u} = \boldsymbol{\Phi}^{\mathrm{T}}\Delta\boldsymbol{U} \quad , \quad \Delta\tilde{\boldsymbol{u}} = \boldsymbol{\Phi}^{\mathrm{T}}\Delta\tilde{\boldsymbol{U}} \qquad \text{on } \Gamma_c \tag{3.46}$$

$$\boldsymbol{t} = \boldsymbol{\Phi}^{\mathrm{T}}\boldsymbol{T} \quad , \quad \tilde{\boldsymbol{t}} = \boldsymbol{\Phi}^{\mathrm{T}}\tilde{\boldsymbol{T}} \qquad \text{on } \Gamma_u \tag{3.47}$$

where $\boldsymbol{\Phi}^{\mathrm{T}}$ denotes the transpose of $\boldsymbol{\Phi}$ which is the column vector of nodal basis functions, and $\{\boldsymbol{U}, \boldsymbol{T}, \Delta\boldsymbol{U}\}$ and $\{\tilde{\boldsymbol{U}}, \tilde{\boldsymbol{T}}, \Delta\tilde{\boldsymbol{U}}\}$ denote the column vectors of nodal quantities.

Employing the interpolation (3.45)-(3.47) for the system of integral equations (3.11), we can form a linear system of algebraic equations as follows

$$\begin{bmatrix} \boldsymbol{B}_{uu} & \bar{\boldsymbol{A}}_{ut} & \bar{\boldsymbol{A}}_{uc} \\ \boldsymbol{A}_{tu} & \boldsymbol{D}_{tt} & \boldsymbol{D}_{tc} \\ \boldsymbol{A}_{cu} & \boldsymbol{D}_{ct} & \boldsymbol{D}_{cc} \end{bmatrix} \begin{bmatrix} \boldsymbol{T} \\ \boldsymbol{U} \\ \Delta\boldsymbol{U} \end{bmatrix} = \begin{bmatrix} \boldsymbol{R}_1 \\ \boldsymbol{R}_2 \\ \boldsymbol{R}_3 \end{bmatrix} \tag{3.48}$$

where the sub-matrices $\boldsymbol{A}_{PQ}$, $\bar{\boldsymbol{A}}_{PQ}$, $\boldsymbol{B}_{PQ}$ and $\boldsymbol{D}_{PQ}$ (with $P, Q \in \{u, t, c\}$) correspond to the integral operators $\mathcal{A}_{PQ}, \bar{\mathcal{A}}_{PQ}, \mathcal{B}_{PQ}, \mathcal{D}_{PQ}$, and where the column vectors $\boldsymbol{R}_1$, $\boldsymbol{R}_2$ and $\boldsymbol{R}_3$ correspond to the integral operators $\mathcal{R}_1$, $\mathcal{R}_2$, $\mathcal{R}_3$. We note that, while these vectors can be exactly calculated from the expression of prescribed displacement and traction, they are numerically evaluated using the same interpolation procedure described in (3.45)-(3.47) for the functions of prescribed displacement and traction.

3.3.2 Special crack-tip element

For elastic media, the relative displacement in the vicinity of crack tip has square-root behavior, and is in terms of powers of ρ which differ by unity, where ρ is the distance along the crack measured in the direction tangential to the crack curve at the crack tip. Based on the idea of Li *et al* [42] for the special crack-tip element in three-dimensional isotropic elastic media, we introduce special shape functions associated with the master element shown in Fig. 3.3 as follows

$$\psi'_{(i)}(\zeta) = \frac{\sqrt{1-\zeta}}{A_{(i)}}\, \psi_{(i)}(\zeta) \quad \text{(no sum on } i\text{)} \tag{3.49}$$

where $\psi_{(i)}(\zeta)$ are standard 3-node quadratic shape functions associated with the i^{th} node, and

$$A_{(i)} = \begin{cases} \sqrt{1-\zeta_{(i)}} & \text{for } \zeta_{(i)} \neq 1 \\ 1/2 & \text{for } \zeta_{(i)} = 1 \end{cases} \tag{3.50}$$

in which $\zeta_{(i)}$ is (natural) coordinate of the i^{th} node (i.e. $\zeta_{(1)}$.

Note that the special shape functions (3.49) are established for the crack-tip element in which $\zeta = 1$ is associated with the tip node as shown in Fig. 3.3. For the case that $\zeta = -1$ is associated with the tip node, analogous expressions of (3.49) and (3.50) are employed with the replacement of $\sqrt{1-\zeta}$ by $\sqrt{1+\zeta}$.

The interpolation for relative crack-face displacement on the crack-tip element is then given by

$$\Delta \boldsymbol{u} = \sqrt{1-\zeta}\ \sum_{i=1}^{3} \frac{\boldsymbol{u}_{(i)}}{A_{(i)}} \psi_{(i)}(\zeta) \tag{3.51}$$

where $\boldsymbol{u}_{(i)}$ are nodal unknowns. Note that, for the nodes which are not associated with crack tip, $\boldsymbol{u}_{(i)}$ is the nodal value of relative crack-face displacement. However, for the node which is associated with crack tip, $\boldsymbol{u}_{(i)}$ corresponds to the *gradient* of the relative crack-face displacement (see Li *et al.* [42]); this feature will be discussed further below in the context of the stress intensity factors.

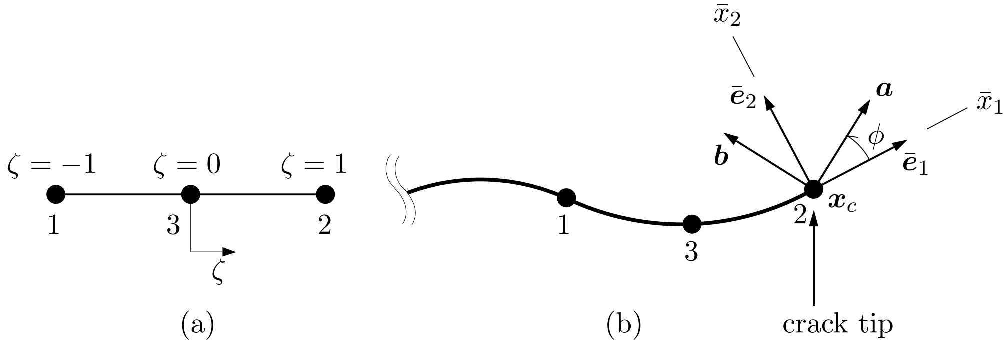

Figure 3.3: Crack-tip element: (a) Master element corresponding to crack-tip element where $\zeta = 1$ is associated with the crack tip. (b) Local coordinate system used in determining the stress intensity factors.

3.3.2.1 Determination of stress intensity factors

To begin, let us denote $\boldsymbol{x}_c$ as the (physical) global coordinates of the crack tip. At this crack tip, we define the local cartesian coordinate system $\{\bar{x}_1, \bar{x}_2\}$ with $\{\bar{\boldsymbol{e}}_1, \bar{\boldsymbol{e}}_2\}$ being the unit base vectors as shown in Fig. 3.3b, where $\bar{\boldsymbol{e}}_1$ is the tangent of the crack curve at $\boldsymbol{x}_c$, and $\bar{\boldsymbol{e}}_2$ is orthogonal to $\bar{\boldsymbol{e}}_1$. With respect to this local coordinate system $\{\bar{\boldsymbol{e}}_1, \bar{\boldsymbol{e}}_2\}$, the generalized stress intensity factors at $\boldsymbol{x}_c$ in multi-field media are the extension from the stress intensity factors for an anisotropic elastic solid (Barnett and Asaro, 1972; Xu, 2000)

$$k_I = \frac{\sqrt{2\pi}}{4} B_{IL} \lim_{\bar{x}_1 \to 0^-} \left(\frac{\Delta u_L}{\sqrt{-\bar{x}_1}} \right) \tag{3.52}$$

where

$$B_{IL} = \frac{1}{2\pi} \int_0^{2\pi} \left[(\boldsymbol{a}, \boldsymbol{a})_{IL} - (\boldsymbol{a}, \boldsymbol{b})_{IM} (\boldsymbol{b}, \boldsymbol{b})^{-1}_{MN} (\boldsymbol{b}, \boldsymbol{a})_{NL} \right] d\phi \tag{3.53}$$

where $\boldsymbol{a}$ and $\boldsymbol{b}$ are orthonormal vectors, ϕ is the angle between $\boldsymbol{a}$ and $\bar{\boldsymbol{e}}_1$ as indicated in Fig. 3.3b, and $(\boldsymbol{a}, \boldsymbol{b})_{IJ} = a_\alpha E_{\alpha IJ\beta} b_\beta$ in which $E_{\alpha IJ\beta}$ are the material constants. Note that in (3.52), the components $\Delta u_3, ..., \Delta u_N$ in the crack-tip local coordinate system are the same as that in the global coordinate system.

Forming Taylor series expansion of the relative crack-face displacement (3.51) about $\zeta = 1$ (i.e. about $\boldsymbol{x}_c$ in physical plane), we have

$$\Delta \boldsymbol{u}(\boldsymbol{x}) = \sqrt{1-\zeta} \left[\boldsymbol{u}^o(\boldsymbol{x}_c) + \mathcal{O}(1-\zeta) \right] \tag{3.54}$$

where

$$\boldsymbol{u}^o(\boldsymbol{x}_c) \equiv \sum_{i=1}^{3} \frac{\boldsymbol{u}_{(i)}}{A_{(i)}} \psi_{(i)}(1) = 2\boldsymbol{u}_{(2)} \tag{3.55}$$

To proceed, let $\boldsymbol{r}_c(\zeta) \equiv \boldsymbol{x}(\zeta) - \boldsymbol{x}_c$ be the position vector of a point $\boldsymbol{x}(\zeta)$ on the crack curve relative to the crack tip $\boldsymbol{x}_c$. Forming Taylor series expansion of this position vector about $\boldsymbol{x}_c$, with the note that $\left.\frac{\partial \boldsymbol{x}(\zeta)}{\partial \zeta}\right|_{\zeta=1} = \boldsymbol{v}_t$ where $\boldsymbol{v}_t$ is the tangential vector to the crack curve at $\boldsymbol{x}_c$, we have

$$\boldsymbol{r}_c = J\boldsymbol{e}_t(\zeta - 1) + \mathcal{O}\big((\zeta - 1)^2\big) \tag{3.56}$$

where

$$J = \|\boldsymbol{v}_t\| \quad , \quad \boldsymbol{e}_t = \frac{\boldsymbol{v}_t}{J} \tag{3.57}$$

Note that $\boldsymbol{e}_t = \bar{\boldsymbol{e}}_1$, and $\bar{x}_1 = \boldsymbol{r}_c \cdot \bar{\boldsymbol{e}}_1$, then from (3.56) we obtain the expression of $\bar{x}_1$ in the vicinity of $\boldsymbol{x}_c$ as follows

$$\bar{x}_1 = J(\zeta - 1) \tag{3.58}$$

Then based on (3.58) and (3.55), the expression of $\Delta\boldsymbol{u}(\boldsymbol{x})$ of (3.54) in the vicinity of $\boldsymbol{x}_c$ becomes

$$\Delta\boldsymbol{u}(\boldsymbol{x}) = 2\sqrt{\frac{-\bar{x}_1}{J}}\, \boldsymbol{u}_{(2)} \tag{3.59}$$

Finally, upon combining (3.52) with (3.59) we obtain

$$k_I(\boldsymbol{x}_c) = \sqrt{\frac{\pi}{2J}}\, B_{IL}\big[\boldsymbol{u}_{(2)} \cdot \bar{\boldsymbol{e}}_L\big]. \tag{3.60}$$

We remark that the unit vectors $\bar{\boldsymbol{e}}_L$ appearing in (3.60) are the unit base vectors of the (local) 'generalized' coordinate system with $\{\bar{\boldsymbol{e}}_1, \bar{\boldsymbol{e}}_2\}$ indicated in Fig. 3.3b, and $\{\bar{\boldsymbol{e}}_3, ..., \bar{\boldsymbol{e}}_N\}$ are coincident with the corresponding unit base vectors of the global coordinate system. It is obvious that the stress intensity factors are given directly in terms of the extra degrees of freedom associated with the node at the crack tip (e.g. $\boldsymbol{u}_{(2)}$).

3.3.3 Treatment of weakly-singular double line integral

The sub-matrices $\boldsymbol{A}_{PQ}$, $\bar{\boldsymbol{A}}_{PQ}$, $\boldsymbol{B}_{PQ}$ and $\boldsymbol{D}_{PQ}$ appearing in (3.48) are evaluated through double line integrations involving weakly-singular kernels. Although these integrals exist in an ordinary sense, it is necessary to have an efficient strategy to accurately evaluate them in an optimized computational time. Toward developing such a strategy, let $K^{I\alpha}_{J\beta}$ in (3.9) be decomposed into two parts as

$$K^{I\alpha}_{J\beta}(r,\theta) = \bar{K}^{I\alpha}_{J\beta} \ln r + \hat{K}^{I\alpha}_{J\beta}(\theta) \tag{3.61}$$

where

$$\begin{aligned} \bar{K}^{I\alpha}_{J\beta} &= -\frac{1}{4\pi^2} \oint_{\|\boldsymbol{z}\|=1} z_\alpha z_\beta (\boldsymbol{z},\boldsymbol{z})^{-1}_{IJ} d\boldsymbol{z} && (3.62) \\ \hat{K}^{I\alpha}_{J\beta}(\theta) &= -\frac{1}{4\pi^2} \oint_{\|\boldsymbol{z}\|=1} z_\alpha z_\beta (\boldsymbol{z},\boldsymbol{z})^{-1}_{IJ} \ln |\boldsymbol{z}\cdot\boldsymbol{e}| d\boldsymbol{z} && (3.63) \end{aligned}$$

With this decomposition of $K^{I\alpha}_{J\beta}$, all the kernels $\{U^P_J, G^P_J, C^K_J\}$ defined in (3.5) (3.6) and (3.7) are now expressed in two separate parts: one is a function of $\ln r$ and the other one is a function of the direction of $\boldsymbol{r}$ (i.e. $\boldsymbol{e}$ where $\boldsymbol{e} = \frac{\boldsymbol{r}}{r}$). Treatment of the weakly-singular double line integrals corresponding to the first part is discussed in this section. For the integration of the second part, we defer the discussion to the next section where we also present an interpolation strategy to compute these integrals in an efficient manner.

With the decomposition (3.61) of $K^{I\alpha}_{J\beta}$, the double line integrals (3.12)-(3.15) contain (weakly) singular integrals of $\ln r$ which are associated with the first term in equation (3.61). Upon applying the discretization (3.45)-(3.47), these integrals can be expressed in a common form as

$$I = \int_{\Omega_s} \int_{\Omega_f} f(\boldsymbol{y}, \boldsymbol{\xi}) \ln r \, ds(\boldsymbol{\xi}) ds(\boldsymbol{y}) \tag{3.64}$$

where Ω_s and Ω_f represent 'source element' and 'field element' as shown in Fig. 3.4, respectively.

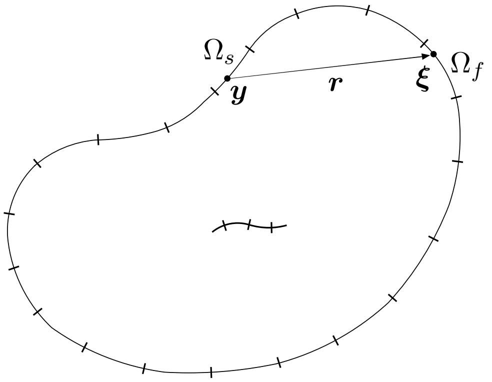

Figure 3.4: Source element Ω_s and field element Ω_f.

The expression for function $f(\boldsymbol{y}, \boldsymbol{\xi})$ in (3.64) depending on the integrand in each integral of (3.12)-(3.15). For instance, the function f used to compute one component in the submatrix $\boldsymbol{B}_{uu}$ in (3.48) will be

$$f(\boldsymbol{y}, \boldsymbol{\xi}) = -\phi_u^m(\boldsymbol{y}) \bar{U}_{J\alpha}^{P\alpha}(\boldsymbol{y} - \boldsymbol{\xi}) \phi_u^n(\boldsymbol{\xi}) \tag{3.65}$$

in which ϕ_u^m and ϕ_u^n represent the nodal basic functions associated with *node m* and *node n* on Γ_u, respectively.

Note that the integral (3.64) will be (weakly) singular when the source element Ω_s and the field element Ω_f are coincident or adjacent to each other. In this case, an effective algorithm for numerically calculating these integrals is needed. To do so, we adopt the technique developed by Parreira *et al.* [51] with some modification for the cases when either source element or field element is a crack-tip element or when both of them are crack-tip elements. As a start point, the integration domains of the integral (3.64) are transformed to [-1,1] (i.e. the integration domain of master element) as

$$I = \int_{-1}^{1}\int_{-1}^{1} f(\boldsymbol{y}(\eta), \boldsymbol{\xi}(\zeta)) \ln r \, J_f d\zeta \, J_s d\eta = \int_{-1}^{1}\int_{-1}^{1} g(\eta, \zeta) \ln r \, d\zeta d\eta \tag{3.66}$$

where J_s and J_f are jacobians of source element Ω_s and field element Ω_f, and $g(\eta, \zeta)$ is a function of η and ζ, defined as

$$g(\eta, \zeta) \equiv f(\boldsymbol{y}(\eta), \boldsymbol{\xi}(\zeta)) \, J_s \, J_f \tag{3.67}$$

Depending on the relative location (e.g. coincident or adjacent) and on the element type (e.g. regular or crack-tip) of Ω_s and Ω_f, different techniques to treat the (weakly) singular integral (3.66) are utilized as described further below.

3.3.3.1 Regular source element Ω_s is coincident with regular field element Ω_f

For this case, the function $g(\eta, \zeta)$ in (3.67) is a regular function of (η, ζ) and $\ln r$ in (3.66) is singular when $\eta = \zeta$. To proceed, I in (3.66) is decomposed into two parts (see [51]) as

$$\begin{aligned} I &= \int_{-1}^{1}\int_{-1}^{1} g(\eta, \zeta) \ln \frac{2r}{|\eta - \zeta|} \, d\zeta \, d\eta + \int_{-1}^{1}\int_{-1}^{1} g(\eta, \zeta) \ln \frac{|\eta - \zeta|}{2} \, d\zeta \, d\eta \\ &= I_1 + I_2 \end{aligned} \tag{3.68}$$

Since $\ln \frac{2r}{|\eta-\zeta|} \to \ln 2J$ as $\eta \to \zeta$ where J is the Jacobian, the first term I_1 in (3.68) is a regular integral. For this reason, standard quadratic Gaussian integration is employed to evaluate this term. However, different integration orders for η and ζ must be used in order to eliminate the divided-by-zero error. For the second term I_2 in (3.68), a geometric transformation on (η, ζ) is applied as follows (see Fig. 3.5)

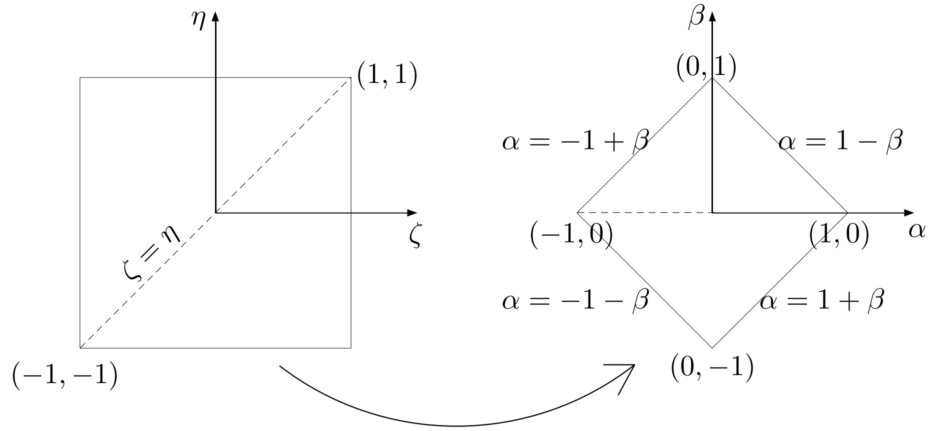

Figure 3.5: Transformation of the integration variables for coincident elements.

$$\left\{\begin{array}{lcl} \alpha & = & \frac{\eta+\zeta}{2} \\ \beta & = & \frac{\eta-\zeta}{2} \end{array}\right. \Rightarrow \left\{\begin{array}{lcl} \eta & = & \alpha+\beta \\ \zeta & = & \alpha-\beta \end{array}\right. \Rightarrow \quad d\eta d\zeta = 2d\alpha d\beta \tag{3.69}$$

With the transformation (3.69), the second term in (3.68) becomes

$$I_2 = 2\int_{-1}^{0} \ln|\beta| \int_{-1-\beta}^{1+\beta} g(\alpha,\beta)\ d\alpha\ d\beta + 2\int_{0}^{1} \ln\beta \int_{-1+\beta}^{1-\beta} g(\alpha,\beta)\ d\alpha\ d\beta \tag{3.70}$$

by changing of $\beta = -\beta$ for the first term in(3.70), I_2 becomes

$$I_2 = 2\int_{0}^{1} \ln\beta \int_{-1+\beta}^{1-\beta} \left[g(\alpha,-\beta) + g(\alpha,\beta)\right]\ d\alpha\ d\beta \tag{3.71}$$

Finally, the domain of inner integral of (3.71) is scaled up to $[-1,1]$ by changing the variable $\alpha = (1-\beta)\bar{\alpha}$, then

$$I_2 = 2\int_0^1 (1-\beta)\ln\beta \int_{-1}^{1} \big[g(\bar{\alpha},-\beta) + g(\bar{\alpha},\beta)\big]\; d\bar{\alpha}\; d\beta \tag{3.72}$$

Standard Gaussian quadrature and logarith Gaussian integration are employed to evaluate the inner integral and outer integral of (3.72), respectively.

3.3.3.2 Crack-tip source element Ω_s is coincident with crack-tip field element Ω_f

With the remark that the derivatives of the shape functions defined in (3.49) contain a singularity of $\mathcal{O}(\frac{1}{\sqrt{1-\zeta}})$, then the function $g(\eta,\zeta)$ of (3.67) is not a regular element when evaluating the submatrix $\boldsymbol{D}_{pq}$ in (3.48). This singularity exists in every pair of (Ω_s,Ω_f), even when they are far apart elements, and significantly reduces the accuracy of the results when using Gaussian integration. To overcome this barrier, we make a change of variable as

$$\zeta = 1 - \frac{1}{2}(1-\zeta')^2 \quad \Rightarrow \quad d\zeta = (1-\zeta')d\zeta' \;\text{ and }\; \frac{1}{\sqrt{1-\zeta}} = \frac{\sqrt{2}}{1-\zeta'} \tag{3.73}$$

and similarly for η.

Then the integral I of (3.66) becomes

$$\begin{aligned} I &= \int_{-1}^{1}\int_{-1}^{1} g(\eta(\eta'),\zeta(\zeta'))\ln r\,(1-\zeta')d\zeta'(1-\eta')d\eta' \\ &= \int_{-1}^{1}\int_{-1}^{1} g'(\eta',\zeta')\ln r\, d\zeta' d\eta' \end{aligned} \tag{3.74}$$

where the function $g'(\eta',\zeta') \equiv g(\eta(\eta'),\zeta(\zeta'))\ln r\,(1-\zeta')(1-\eta')$ is now a regular function of (η',ζ').

Similar to the case of coincident regular elements, I in (3.74) is decomposed into two parts as

$$I = \int_{-1}^{1}\int_{-1}^{1} g'(\eta',\zeta')\ln\frac{2r}{|\eta-\zeta|}\,d\zeta'\,d\eta' + \int_{-1}^{1}\int_{-1}^{1} g'(\eta',\zeta')\ln\frac{|\eta-\zeta|}{2}\,d\zeta'\,d\eta' \tag{3.75}$$

With regard to the equation (3.73), the integral I of (3.75) can be rewritten as

$$\begin{aligned} I &= \int_{-1}^{1}\int_{-1}^{1} g'(\eta',\zeta')\ln\frac{4r}{|\eta'-\zeta'||2-\eta'-\zeta'|}\,d\zeta'\,d\eta' \\ &+ \int_{-1}^{1}\int_{-1}^{1} g'(\eta',\zeta')\ln\frac{|\eta'-\zeta'|}{2}\,d\zeta'\,d\eta' \\ &+ \int_{-1}^{1}\int_{-1}^{1} g'(\eta',\zeta')\ln\frac{|2-\eta'-\zeta'|}{2}\,d\zeta'\,d\eta' \end{aligned} \tag{3.76}$$

The first term in (3.76) is a regular integral due to the fact that $\ln\frac{2r}{|\eta-\zeta|} \to \ln 2J$ as $\eta \to \zeta$ where J is the Jacobian, and it is evaluated using standard Gaussian integration with different integration orders for η' and ζ'. The second term in (3.76), which is singular when $\eta' = \zeta'$, is in the same form as that of the case of coincident regular elements and it is evaluated using the same technique that we described above. For the third term in (3.76), the singularity occurs when $\eta' = 1$ and $\zeta' = 1$ and it is treated by applying a transformation on (η',ζ') as (see transform (A) of Fig. 3.6)

$$\left\{\begin{array}{lcl} \alpha &=& \frac{-\eta'+\zeta'}{2} \\ \beta &=& \frac{-\eta'-\zeta'}{2} \end{array}\right. \Rightarrow \left\{\begin{array}{lcl} \eta' &=& -\alpha-\beta \\ \zeta' &=& \alpha-\beta \end{array}\right. \Rightarrow \quad d\eta' d\zeta' = -2d\alpha d\beta \tag{3.77}$$

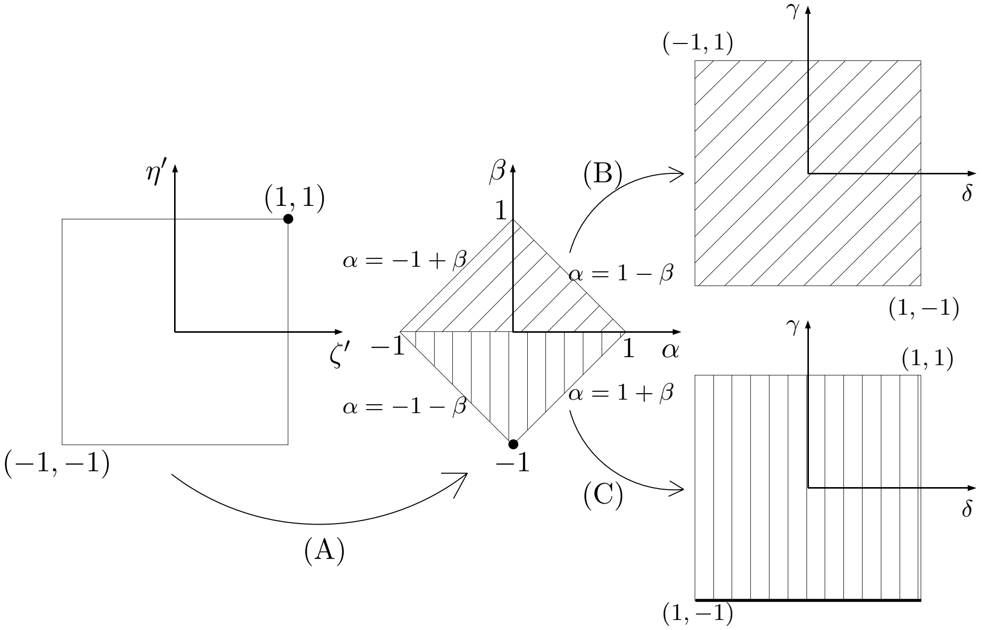

Figure 3.6: Transformation of the integration variables for crack-tip coincident elements.

Then the third term in (3.76) becomes

$$\int_{-1}^{1}\int_{-1}^{1} g'(\eta',\zeta')\ln\frac{|2-\eta'-\zeta'|}{2}\,d\zeta'\,d\eta' = 2\int_{-1}^{0}\int_{-1-\beta}^{1+\beta} g'(\alpha,\beta)\ln|1+\beta|\,d\alpha d\beta + 2\int_{0}^{1}\int_{-1+\beta}^{1-\beta} g'(\alpha,\beta)\ln|1+\beta|\,d\alpha d\beta \tag{3.78}$$

The second term in (3.78) which is a regular integral is computed by using standard Gaussian integration. To do so, the domain of integration is transformed to $[-1,1]$ as

$$\left\{\begin{array}{lcl}\delta & = & \frac{\alpha}{1-\beta}\\ \gamma & = & 2\beta-1\end{array}\right. \Rightarrow \left\{\begin{array}{lcl}\alpha & = & \frac{(1-\gamma)\delta}{2}\\ \beta & = & \frac{\gamma+1}{2}\end{array}\right. \Rightarrow \quad d\alpha d\beta = \frac{1-\gamma}{4}d\delta d\gamma \tag{3.79}$$

Then

$$2\int_0^1 \int_{-1+\beta}^{1-\beta} g'(\alpha,\beta) \ln|1+\beta| \, d\alpha d\beta \quad = \quad \frac{1}{2}\int_{-1}^{1} (1-\gamma) \ln\frac{3+\gamma}{2} \int_{-1}^{1} g'(\delta,\gamma) \, d\delta d\gamma \tag{3.80}$$

The first term in (3.78) is singular at $\beta = -1$. To treat this singularity, the domain of integration is transformed to $[-1,1]$ by applying the geometric transformation as follows

$$\left\{ \begin{array}{lcl} \delta & = & \frac{\alpha}{1+\beta} \\ \gamma & = & 2\beta+1 \end{array} \right. \quad \Rightarrow \quad \left\{ \begin{array}{lcl} \alpha & = & \frac{(1+\gamma)\delta}{2} \\ \beta & = & \frac{\gamma-1}{2} \end{array} \right. \quad \Rightarrow \quad d\alpha d\beta = \tfrac{1+\gamma}{4} d\delta d\gamma \tag{3.81}$$

Then, the first term in (3.78) becomes

$$2\int_{-1}^0 \int_{-1-\beta}^{1+\beta} g'(\alpha,\beta) \ln|1+\beta| \, d\alpha d\beta \quad = \quad \frac{1}{2}\int_{-1}^{1} (1+\gamma) \ln\frac{1+\gamma}{2} \int_{-1}^{1} g'(\delta,\gamma) \, d\delta d\gamma \tag{3.82}$$

Note that $(1+\gamma)\ln\frac{1+\gamma}{2} \to 0$ as $\gamma \to -1$, therefore the outer integral in (3.82) is regular. However, to increase the accuracy of this integral, extra scaling transformation is applied as

$$\gamma = \frac{1}{2}(1+\rho)^2 - 1 \tag{3.83}$$

then (3.82) becomes

$$2\int_{-1}^0 \int_{-1-\beta}^{1+\beta} g'(\alpha,\beta) \ln|1+\beta| \, d\alpha d\beta \quad = \quad \frac{1}{2}\int_{-1}^{1} (1+\rho)^3 \ln\frac{1+\rho}{2} \int_{-1}^{1} g'(\delta,\rho) \, d\delta d\rho \tag{3.84}$$

At this point, standard Gaussian integration can now be employed to evaluate (3.84).

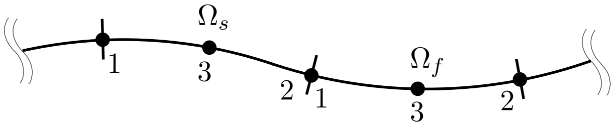

Figure 3.7: Regular source element Ω_s is adjacent to regular field element Ω_f.

3.3.3.3 Regular source element Ω_s is adjacent to regular field element Ω_f

Consider two elements Ω_s and Ω_f being adjacent to each other as shown schematically in Fig. 3.7. The common node, in this illustrated case, is the local node 2 of the source element, and the local node 1 of the field element. Regarding to this nodal connectivity, the integral (3.66) is singular at $(\eta = 1, \zeta = -1)$. To proceed, (3.66) is decomposed into two parts as

$$\begin{aligned} I &= \int_{-1}^{1}\int_{-1}^{1} g(\eta,\zeta)\ln\frac{2r}{|2-\eta+\zeta|}\,d\zeta\,d\eta + \int_{-1}^{1}\int_{-1}^{1} g(\eta,\zeta)\ln\frac{|2-\eta+\zeta|}{2}\,d\zeta\,d\eta \\ &= I_1 + I_2 \end{aligned} \tag{3.85}$$

Since $\ln\frac{2r}{2-\eta+\zeta} \to \ln 2J$ as $(\eta,\zeta)\to(1,-1)$ where J is the Jacobian, the first term I_1 in (3.85) is a regular integral. From this fact, a standard Gaussian integration is employed to numerically evaluate this term. For the second term I_2 in (3.85), a geometric transformation is applied to decompose it again into two parts as follows

$$\left\{\begin{array}{lcl} \alpha &=& \frac{\eta+\zeta}{2} \\ \beta &=& \frac{\eta-\zeta}{2} \end{array}\right. \Rightarrow \left\{\begin{array}{lcl} \eta &=& \alpha+\beta \\ \zeta &=& \alpha-\beta \end{array}\right. \Rightarrow \quad d\eta d\zeta = 2d\alpha d\beta \tag{3.86}$$

Then the integral I_2 in (3.85) becomes

$$\begin{aligned} I_2 &= 2\int_{-1}^{0} \ln(1-\beta) \int_{-1-\beta}^{1+\beta} g(\alpha,\beta)\, d\alpha\, d\beta + 2\int_{0}^{1} \ln(1-\beta) \int_{-1+\beta}^{1-\beta} g(\alpha,\beta)\, d\alpha\, d\beta \\ &= I_3 + I_4 \end{aligned} \tag{3.87}$$

Note that I_3 in (3.87) is a regular integral and it is evaluated using standard

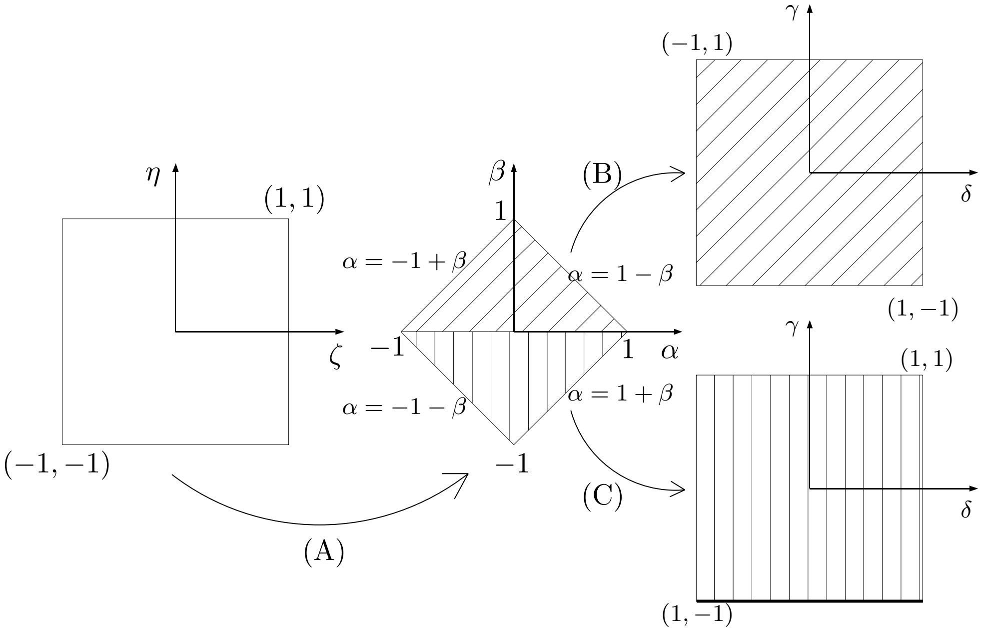

Figure 3.8: Transformation of integration variables for adjacent elements.

Gaussian integration. To do so, the domain of integration is scaled up to $[-1, 1]$ by a transformation as follows

$$\left\{ \begin{array}{lcl} \delta &=& \frac{\alpha}{1+\beta} \\ \gamma &=& 2\beta+1 \end{array} \right. \quad \Rightarrow \quad \left\{ \begin{array}{lcl} \alpha &=& \frac{(1+\gamma)\delta}{2} \\ \beta &=& \frac{\gamma-1}{2} \end{array} \right. \quad \Rightarrow \quad d\alpha d\beta = \tfrac{1+\gamma}{4} d\delta d\gamma \tag{3.88}$$

Then

$$I_3 = \frac{1}{2}\int_{-1}^{1} (1+\gamma) \ln\frac{3-\gamma}{2} \int_{-1}^{1} g(\delta,\gamma)\, d\delta d\gamma \tag{3.89}$$

For the second integral I_4 in (3.87), a geometric transformation described below is employed to treat the singularity at $\beta = 1$.

$$\left\{\begin{array}{lcl}\gamma & = & 1-\beta \\ \alpha & = & \gamma\delta\end{array}\right. \tag{3.90}$$

Then

$$I_4 = 2\int_0^1 \gamma \ln \gamma \int_{-1}^1 g(\delta,\gamma)\, d\delta d\gamma \tag{3.91}$$

Logarith Gaussian integration and standard Gaussian integration are employed to evaluate the outer integral and the inner integral of I_4, respectively.

3.3.3.4 Regular source element Ω_s is adjacent to crack-tip field element Ω_f

Consider the case of two adjacent elements Ω_s and Ω_f in which the field element Ω_f is a crack-tip element as shown in Fig. 3.9. The common node of the two elements, in this illustrated case, is the local node 2 of the source element and local node 1 of the field element. Then the crack tip is at the local node 1 of the field element. It should be noted that the treatment of singular integration described below is applied for this illustrated case, but it is also applicable, with a minor change in the algorithm, to the other case where the local node 1 of source element and local node 2 of crack-tip field element is the common node.

As discussed in the section of coincident crack-tip elements, a changing of variable (3.73) is needed to make the integrand in (3.66) become a regular function of the integration variables. For the considering case, after applying (3.73) for the

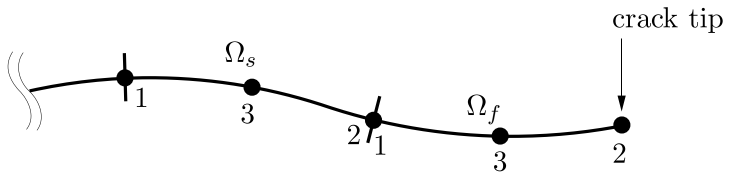

Figure 3.9: Regular source element Ω_s is adjacent to crack-tip field element Ω_f.

variable ζ, the integral I of (3.66) becomes

$$\begin{aligned} I &= \int_{-1}^{1}\int_{-1}^{1} g(\eta,\zeta(\zeta'))\ln r\,(1-\zeta')d\zeta' d\eta' \\ &= \int_{-1}^{1}\int_{-1}^{1} g'(\eta,\zeta')\ln r\,d\zeta' d\eta \end{aligned} \tag{3.92}$$

where the function $g'(\eta,\zeta') \equiv g(\eta,\zeta(\zeta'))\ln r\,(1-\zeta')$ is now a regular function of (η,ζ').

Applying a geometric transformation to the integration variables as

$$\left\{ \begin{array}{lcl} \alpha & = & \frac{\eta+\zeta'}{2} \\ \beta & = & \frac{\eta-\zeta'}{2} \end{array} \right. \Rightarrow \left\{ \begin{array}{lcl} \eta & = & \alpha+\beta \\ \zeta' & = & \alpha-\beta \end{array} \right. \Rightarrow \quad d\eta d\zeta' = 2d\alpha d\beta \tag{3.93}$$

then the integral I of (3.92) can be split into two parts as

$$\begin{aligned} I &= 2\int_{-1}^{0}\int_{-1-\beta}^{1+\beta} g'(\alpha,\beta)\ln r\,d\alpha\,d\beta + 2\int_{0}^{1}\int_{-1+\beta}^{1-\beta} g'(\alpha,\beta)\ln r\,d\alpha\,d\beta \\ &= I_1 + I_2 \end{aligned} \tag{3.94}$$

Note that the singularity of the original integral (3.92) occurs at $(\eta = 1, \zeta = -1)$, i.e. $(\eta = 1, \zeta' = -1)$. This fact makes the first integral I_1 be regular and the second one I_2 be singular. For this reason, after scaling the integration domain to $[-1, 1]$, a standard Gaussian integration is used to evaluate I_1 as

$$\left\{ \begin{array}{lcl} \delta & = & \frac{\alpha}{1+\beta} \\ \gamma & = & 2\beta + 1 \end{array} \right. \Rightarrow \left\{ \begin{array}{lcl} \alpha & = & \frac{(1+\gamma)\delta}{2} \\ \beta & = & \frac{\gamma-1}{2} \end{array} \right. \Rightarrow \quad d\alpha d\beta = \tfrac{1+\gamma}{4} d\delta d\gamma \tag{3.95}$$

$$\Rightarrow I_1 = \frac{1}{2} \int_{-1}^{1} (1+\gamma) \int_{-1}^{1} g'(\delta, \gamma) \ln r \, d\delta d\gamma \tag{3.96}$$

For the singular integration I_2, we use again a geometric transformation as follows

$$\left\{ \begin{array}{lcl} \delta & = & \frac{\alpha}{1-\beta} \\ \gamma & = & 2\beta - 1 \end{array} \right. \Rightarrow \left\{ \begin{array}{lcl} \alpha & = & \frac{(1-\gamma)\delta}{2} \\ \beta & = & \frac{\gamma+1}{2} \end{array} \right. \Rightarrow \quad d\alpha d\beta = \tfrac{1-\gamma}{4} d\delta d\gamma \tag{3.97}$$

$$\Rightarrow I_2 = \frac{1}{2} \int_{-1}^{1} (1-\gamma) \int_{-1}^{1} g'(\delta, \gamma) \ln r \, d\delta d\gamma \tag{3.98}$$

Then, to improve the accuracy for the evaluation of the integral (3.98), a coordinate transformation is applied as

$$\gamma = 1 - \frac{1}{2}(1-\rho)^2 \tag{3.99}$$

$$\Rightarrow I_2 = \frac{1}{4} \int_{-1}^{1} (1-\rho)^3 \int_{-1}^{1} g'(\delta, \rho) \ln r \, d\delta d\rho \tag{3.100}$$

Both the inner and outer integrals of (3.100) are evaluated using standard Gaussian integration.

3.3.3.5 Crack-tip source element Ω_s is adjacent to regular field element Ω_f

An illustrated configuration is shown in Fig. 3.10 where the local node 2 of the crack-tip source element is the local node 1 of the regular field element. With the notice that the crack tip is now at the local node 1, a transformation similar to (3.73) is applied for the integration variable η as follows

$$\eta = \frac{1}{2}(1+\eta')^2 - 1 \quad \Rightarrow \quad d\eta = (1+\eta')d\eta' \text{ and } \frac{1}{\sqrt{1+\zeta}} = \frac{\sqrt{2}}{1+\zeta'} \tag{3.101}$$

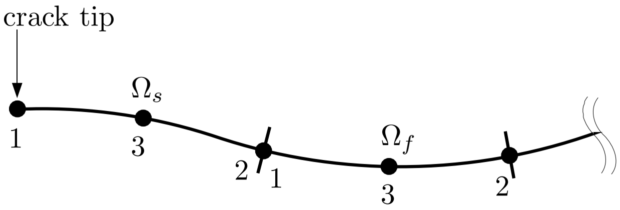

Figure 3.10: Crack-tip source element Ω_s is adjacent to regular field element Ω_f.

then the integral (3.66) becomes

$$\begin{aligned} I &= \int_{-1}^{1}\int_{-1}^{1} g(\eta(\eta'),\zeta)\ln r\, d\zeta(1+\eta')d\eta' \\ &= \int_{-1}^{1}\int_{-1}^{1} g'(\eta',\zeta)\ln r\, d\zeta d\eta' \end{aligned} \tag{3.102}$$

where the function $g'(\eta',\zeta) \equiv g(\eta(\eta'),\zeta)\ln r\,(1+\eta')$ is now a regular function of (η',ζ). Using the same technique that was applied for the previous case of regular source element adjacent to crack-tip field element, and replacing η by η' and ζ' by ζ for all equations (3.93)-(3.100), we can use standard Gaussian integration for the evaluation of the integral (3.102).

3.3.3.6 Crack-tip source element Ω_s is adjacent to crack-tip field element Ω_f

Consider an illustrated configuration shown in Fig. 3.11 where both the source element and field element are crack-tip elements. The common node of these two adjacent elements is the local node 2 of Ω_s and local node 1 of Ω_f. To regularize the integrand of (3.66), a change of variable similar to (3.73) is applied for both η

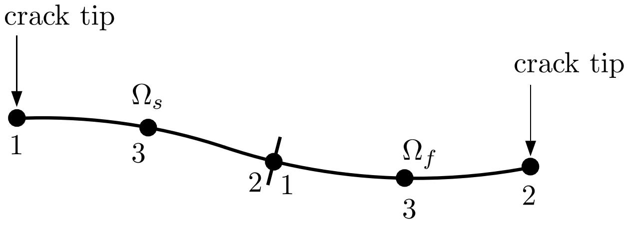

Figure 3.11: Crack-tip source element Ω_s is adjacent to crack-tip field element Ω_f.

and ζ as

$$\begin{aligned}\eta &= \frac{1}{2}(1+\eta')^2 - 1 \\ \zeta &= 1 - \frac{1}{2}(1-\zeta')^2 \end{aligned} \tag{3.103}$$

Then the integral I of (3.66) becomes

$$\begin{aligned} I &= \int_{-1}^{1}\int_{-1}^{1} g(\eta(\eta'),\zeta(\zeta'))\ln r\,(1+\zeta')d\zeta'(1+\eta')d\eta' \\ &= \int_{-1}^{1}\int_{-1}^{1} g'(\eta',\zeta')\ln r\,d\zeta' d\eta' \end{aligned} \tag{3.104}$$

where the function $g'(\eta',\zeta') \equiv g(\eta(\eta'),\zeta(\zeta'))\ln r\,(1+\zeta')(1+\eta')$ is a regular function of (η',ζ').

Again, applying the same technique described in equations (3.93)-(3.100), and replacing η by η', we can use standard Gaussian integration to evaluate the integral (3.104).

3.3.4 Treatment of weakly-singular contour integral

The kernel $\hat{K}^{I\alpha}_{J\beta}$ in (3.63) is a (weakly) singular integral of order $\mathcal{O}(\ln|\boldsymbol{z}\cdot\boldsymbol{e}|)$. Before discussing about the treatment of this singularity, let us consider about the

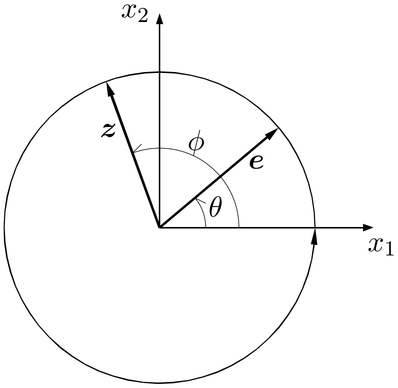

Figure 3.12: Contour in the integration of the kernels.

aspect of computational time for evaluating this integral. We note that if this line integral is computed for every pair of source point $\boldsymbol{x}$ and field point $\boldsymbol{\xi}$ (i.e. every value of $\boldsymbol{e}$), it would take an excessive amount of computational time. For this reason, we introduce an interpolation strategy to approximate these kernels to (arbitrary) specified accuracy. Since $\hat{K}^{I\alpha}_{J\beta}$ is an even function of $\boldsymbol{e}$, i.e. $\hat{K}^{I\alpha}_{J\beta}(\theta) = \hat{K}^{I\alpha}_{J\beta}(\theta + \pi)$ where θ is the angle between the unit vector $\boldsymbol{e}$ and x_1 axis as depicted in Fig. 3.12, the value of $\hat{K}^{I\alpha}_{J\beta}$ will be interpolated over $[0, \pi]$, and to do so we introduce a table of data obtained by discretizing the interval $[0, \pi]$ into sub-intervals. Let $\theta_{(i)}$ (for $i = 1, 2, ..., N_\theta$) be nodal points on $[0, \pi]$. The approximation of $\hat{K}^{I\alpha}_{J\beta}$ is then given by

$$\hat{K}^{I\alpha}_{J\beta}(\theta) \approx \sum_{i=1}^{N_\theta} \hat{K}^{I\alpha}_{J\beta}(\theta_{(i)})\varphi_i(\theta) \tag{3.105}$$

in which $\varphi_i(\theta)$ are basis functions associated with nodal points $\theta_{(i)}$, and where $\hat{K}^{I\alpha}_{J\beta}(\theta_{(i)})$ are nodal values obtained by evaluating (3.63). The intervals associated with the partitioning of the angular coordinates are taken to be uniform, standard quadratic interpolantion is employed over the resulting one-dimensional grid.

Now let us go back to the treatment for the weakly-singular integral (3.63). To do so, we introduce ϕ as the angle between the unit vector $\boldsymbol{z}$ with x_1 axis as shown in Fig. 3.12. Then the integral (3.63) is written as

$$\hat{K}^{I\alpha}_{J\beta}(\theta) = -\frac{1}{4\pi^2}\int_0^{2\pi} f^{I\alpha}_{J\beta}(\phi)\ln|\cos(\phi-\theta)|d\phi \tag{3.106}$$

where f is a function of the angle ϕ defined as

$$f^{I\alpha}_{J\beta}(\phi) = z_\alpha z_\beta(\boldsymbol{z},\boldsymbol{z})^{-1}_{IJ} \tag{3.107}$$

Note that f is an even function of $\boldsymbol{z}$, i.e.

$$f^{I\alpha}_{J\beta}(\phi) = f^{I\alpha}_{J\beta}(\phi+\pi) \tag{3.108}$$

then (3.106) becomes

$$\hat{K}^{I\alpha}_{J\beta}(\theta) = -\frac{1}{2\pi^2}\int_{-\frac{\pi}{2}+\theta}^{\frac{\pi}{2}+\theta} f^{I\alpha}_{J\beta}(\phi)\ln\cos(\phi-\theta)d\phi \tag{3.109}$$

To proceed, we introduce a change of variable as

$$t \equiv \cos(\phi-\theta) \tag{3.110}$$

with the notice that

$$\begin{aligned} d(\phi) &= d(\phi-\theta) \\ &= d(\arccos t) \\ &= \begin{cases} \frac{1}{\sqrt{1-t^2}}dt & , \quad -\frac{\pi}{2} \le \phi-\theta \le 0 \\ \frac{-1}{\sqrt{1-t^2}}dt & , \quad 0 \le \phi-\theta \le \frac{\pi}{2} \end{cases} \end{aligned} \tag{3.111}$$

then equation (3.109) becomes

$$\begin{aligned}\hat{K}^{I\alpha}_{J\beta}(\theta) &= \frac{-1}{2\pi^2}\Bigg[\int_0^1 f^{I\alpha}_{J\beta}(t)\frac{\ln t}{\sqrt{1-t^2}}dt - \int_1^0 f^{I\alpha}_{J\beta}(t)\frac{\ln t}{\sqrt{1-t^2}}dt\Bigg] \\ &= \frac{-1}{\pi^2}\int_0^1 f^{I\alpha}_{J\beta}(t)\frac{\ln t}{\sqrt{1-t^2}}dt \qquad (3.112)\end{aligned}$$

In order to treat the (weakly) singularity of the integral (3.112) we divide the integral domain $[0,1]$ into three sub-domains $[0,a]$, $[a,b]$ and $[b,1]$ where $0 < a, b < 1$ as

$$\begin{aligned}\hat{K}^{I\alpha}_{J\beta}(\theta) &= \frac{-1}{\pi^2}\Bigg[\int_0^a \frac{f^{I\alpha}_{J\beta}(t)}{\sqrt{1-t^2}}\ln t dt + \int_a^b f^{I\alpha}_{J\beta}(t)\frac{\ln t}{\sqrt{1-t^2}}dt \\ &+ \int_b^1 \frac{f^{I\alpha}_{J\beta}(t)\ln t}{\sqrt{1+t}}\frac{1}{\sqrt{1-t}}dt\Bigg] \qquad (3.113)\end{aligned}$$

The first integral in (3.113) is evaluated by utilizing logarithmic Gaussian integration (see [65]). The second integral in (3.113) is regular so that standard Gaussian integration is employed. For the third integral in (3.113), we use a 'stretching' technique to eliminate the singularity at $t = 1$ as follows.

Let

$$t = 1 - \frac{1}{2}(1-t')^2 \qquad (3.114)$$

then the third integral in (3.113) becomes a regular integral in terms of t' as

$$\int_b^1 \frac{f^{I\alpha}_{J\beta}(t)\ln t}{\sqrt{1+t}}\frac{1}{\sqrt{1-t}}dt = \sqrt{2}\int_c^1 h(t')dt' \qquad (3.115)$$

in which

$$\begin{aligned} h(t') &= \frac{f(t)\ln t}{\sqrt{1+t}}\bigg|_{t=1-\frac{1}{2}(1-t')^2} \qquad (3.116) \\ c &= 1 - \sqrt{2(1-a)} \qquad (3.117)\end{aligned}$$

Chapter 4

Numerical Results

This chapter examines several examples to illustrate the versatility and accuracy of the method for analyzing fractures in multi-field media. The media treated include elastic media, piezoelectric media and magnetoelectroelastic media. For the purpose of comparison with exact solutions and other authors, problems of isotropic elastic materials are also examined but they are treated as 'anisotropic' materials to illustrate the capability of the procedure for solving problems in general anisotropic media. Specifically, the kernels for these problems are computed by numerically integrating the general forms for anisotropic material although they can be analytically integrated (see Appendix D for closed form expression of these kernels). For problems in anisotropic media, unless it is explicitly indicated, the material coordinates are taken to be coincident with the cartesian coordinates describing the problem.

4.1 Problems in anisotropic elastic media

4.1.1 Straight crack in unbounded domain

Consider a straight crack of length $2a$ in an unbounded domain subjected to a uniform normal stress $\sigma_{22} = \sigma_o$ and a uniform shear stress $\sigma_{23} = \tau_o$ at infinity as shown schematically in Fig. 4.1. The crack is centrally located at the origin of the cartesian coordinate system and is inclined an angle of ϕ with respect to the x_1-axis. For this problem, the mixed-mode stress intensity factors are independent of material properties [5] with the analytic solution given by

$$\left\{ \begin{array}{c} K_I \\ K_{II} \end{array} \right\} = \sigma_o \sqrt{\pi a} \cos\phi \left\{ \begin{array}{c} \cos\phi \\ \sin\phi \end{array} \right\} \tag{4.1}$$

$$K_{III} = \tau_o \sqrt{\pi a} \cos\phi \tag{4.2}$$

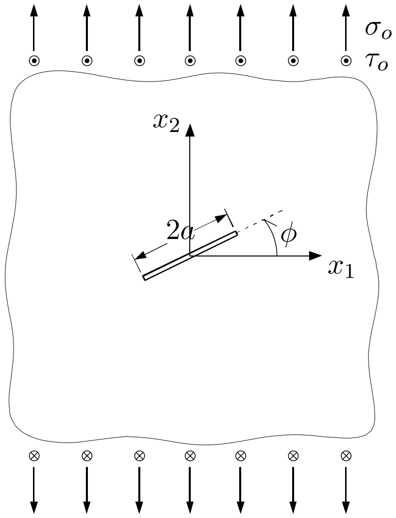

Figure 4.1: Straight crack in unbounded domain subjected to far-field uniform normal stress in x_2-direction and uniform shear stress in x_3-direction.

C_{1111}	C_{1122}	C_{1133}	C_{2222}	C_{1212}
2.130	0.825	1.013	21.000	0.587

Table 4.1: Elastic moduli ($\times 10^6$ psi) of graphite-reinforced composite employed for the analysis of problem of Fig. 4.1.

The material employed for the analysis of this problem is graphite-reinforced composite [56] with the moduli shown in Table 4.1. Note that the material is transversely isotropic with the x_2-axis being the axis of elastic symmetry. Since $x_3 = 0$ is one of the symmetric planes of the material, the out-of-plane stress intensity factor K_{III} is uncoupled from the in-plane stress intensity factors K_I and K_{II} as seen in the analytic solution (4.2).

Fig. 4.2 displays the normalized stress intensity factors $\bar{K}_{I,II} = K_{I,II}/\sigma_o\sqrt{\pi a}$ and $\bar{K}_{III} = K_{III}/\tau_o\sqrt{\pi a}$ as functions of the inclined angle. The solid lines correspond to the exact solutions (4.1) and (4.2). The numerical results are computed with a uniform mesh of 4 crack elements (i.e. the elements are divided by equidistant nodes along the crack line). All results have an error of less than 0.03%. For the particular case of the inclined angle $\phi = 45^o$, Table 4.2 shows the stress intensity factors, normalized by the exact values, obtained with several uniform meshes differing by the total number of elements. All results are very close to the exact solution (with errors of equal or less than 0.05%). However, the results do not seem to convert to the exact solution as increasing the total number of elements for the mesh. This fact results from the decreasing of the crack-tip element size when the mesh is refined, i.e the decreasing of the region where the crack-face displacements are modeled by proper interpolation functions (i.e. special shape functions of crack-tip element). To compensate for this drawback, an alternative strategy for meshing is performed such that the size of the crack-tip element is kept unchanged while the remaining mesh is refined as shown in Fig. 4.3. The computed results associated with these improved meshes are shown in Table 4.3. It can be seen that the results quickly convert to the exact solution, and this fact proves our argument/explanation.

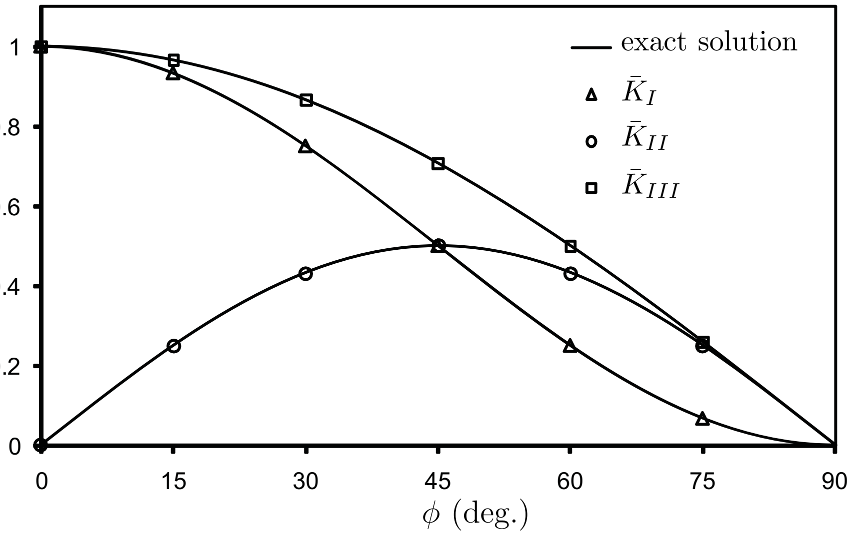

Figure 4.2: Normalized stress intensity factors for the problem of Fig. 4.1. Results are obtained with a uniform crack mesh of 4 elements. All results have an error of less than 0.03%.

# Crack Elements	K_I/K_I^{exa}	K_{II}/K_{II}^{exa}	K_{III}/K_{III}^{exa}
2	0.9983	0.9983	0.9983
4	1.0002	1.0002	1.0002
6	1.0005	1.0005	1.0004
8	1.0005	1.0005	1.0005
10	1.0005	1.0005	1.0005

Table 4.2: Stress intensity factors for the problem of Fig. 4.1 with $\phi = 45^o$. Results are normalized by exact solution.

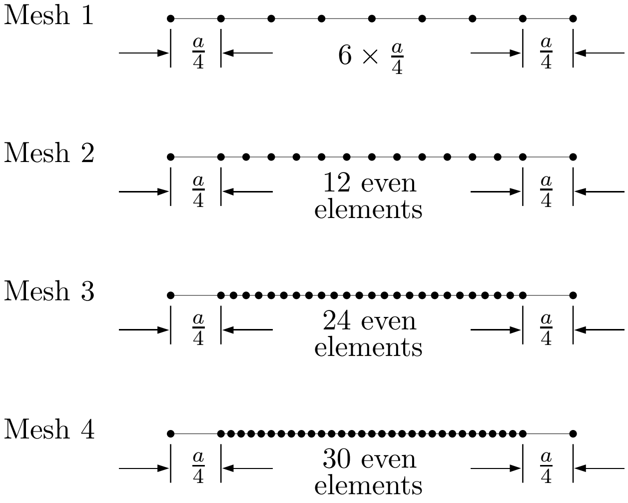

Figure 4.3: Improved mesh for straight crack in an unbounded domain.

Mesh #	K_I/K_I^{exa}	K_{II}/K_{II}^{exa}	K_{III}/K_{III}^{exa}
1	1.0005	1.0005	1.0005
2	1.0001	1.0001	1.0001
3	1.0000	1.0000	1.0000
4	1.0000	1.0000	1.0000

Table 4.3: Stress intensity factors for the problem of Fig. 4.1 with $\phi = 45^o$ utilizing the improved meshes shown in Fig. 4.3. Results are normalized by exact solution.

4.1.2 Circular arc crack in isotropic unbounded domain

A circular arc crack in an unbounded domain is examined to demonstrate the accuracy of the proposed procedure for curve cracks. The domain is subjected to a uniform normal stress $\sigma_{22} = \sigma_o$ at infinity as shown schematically in Fig. 4.4. The crack has a radius r and an opening angle 2θ. For isotropic material, the exact solutions of stress intensity factors which are independent from the material properties are given as [70]

$$\left\{ \begin{array}{c} K_I \\ K_{II} \end{array} \right\} = \frac{\sigma_o \sqrt{\pi r \sin\theta}}{2\big[1 + \big(\sin\frac{\theta}{2}\big)^2\big]} \left\{ \begin{array}{l} \cos\frac{\theta}{2}\big[2 - 4\big(\sin\frac{\theta}{2}\big)^2 - 3\big(\sin\frac{\theta}{2}\big)^4\big] \\ \sin\frac{\theta}{2}\big[4 - 2\big(\sin\frac{\theta}{2}\big)^2 - 3\big(\sin\frac{\theta}{2}\big)^4\big] \end{array} \right\} \tag{4.3}$$

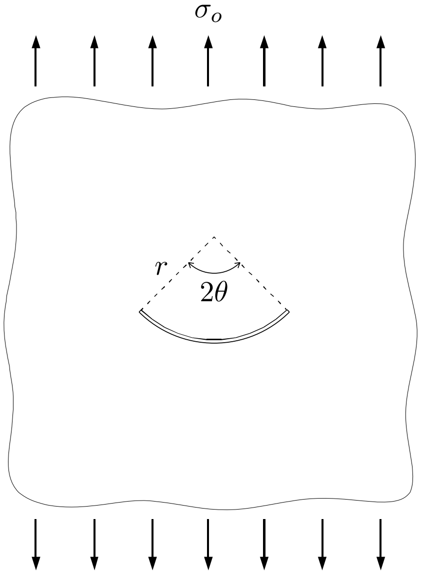

Figure 4.4: Circular arc crack in an unbounded domain subjected to far-field uniform normal stress in x_2-direction.

Table 4.4 shows the results for the case of $\theta = 45^o$ computed with various meshes. In this table, the first 3 meshes are uniform meshes (i.e. all elements have the same length). For the fourth and the fifth mesh, the projected length for horizontal direction of crack-tip element is $a/4$ where $a = r \sin\theta$ while the remaining elements have projected lengths of $a/8$ and $a/16$, respectively. Excellent convergence to the exact solution is obtained.

# Crack Elements	K_I/K_I^{exa}	K_{II}/K_{II}^{exa}
2	1.0174	0.9891
4	1.0028	0.9990
8	1.0008	1.0003
14	1.0004	0.9999
26	1.0003	0.9998

Table 4.4: Stress intensity factors for the problem of Fig. 4.4 with $\theta = 45^o$, isotropic material. Results are normalized by exact solution.

4.1.3 Straight crack in isotropic finite domain

Consider a straight crack of length $2a$ which is located at the center of a square plate as shown in Fig. 4.5(b) and (c). The crack has an inclined angle of 30^o with respect to x_1-axis and each side of the plate has a length of $4a$. An isotropic material is employed for this example. To 'mimic' the problem of a straight crack in an unbounded domain subjected to a uniaxial remote stress, the applied traction on the sides of the plate are derived from the exact stress field of the associated problem in an unbounded domain (see Fig. 4.5(a)). Since the exact solution is available for the associated problem (i.e. equations (4.1) and (4.2)), we can validate the computational procedure for the finite domain problem. Fig. 4.5 (b) & (c) schematically show the traction distribution on the boundary of plate in x_1 and x_2 directions, respectively. Note that this traction distribution is non trivial since the plate boundary is taken at a position relatively close to the crack.

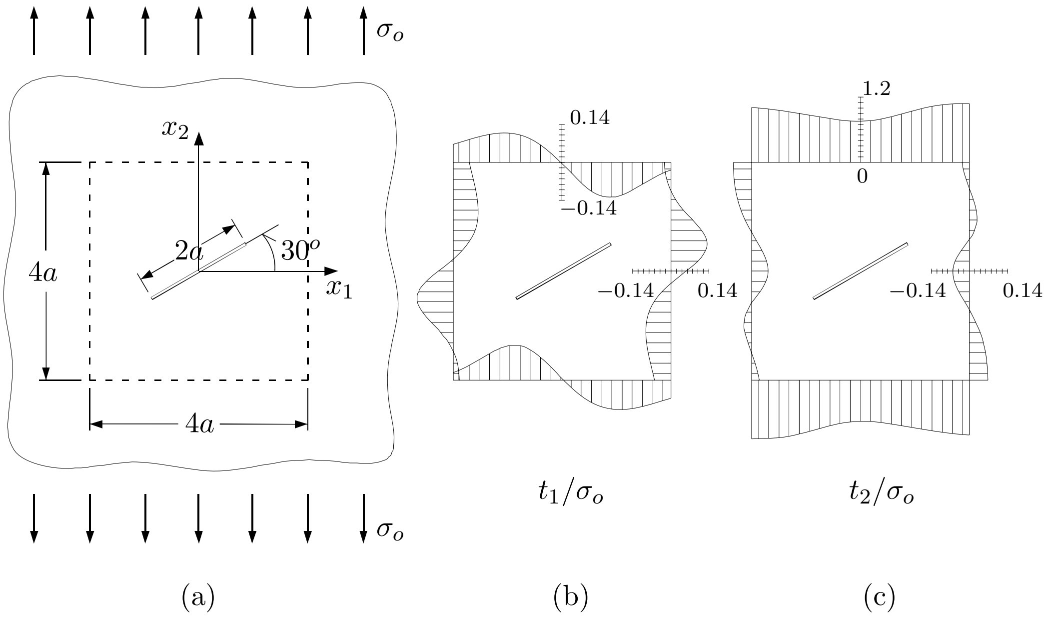

Figure 4.5: Straight crack in finite domain: (a) crack in unbounded domain with the dash line indicating the boundary of the 'mimic' problem in the finite domain; (b) and (c) applied traction derived from the exact stress field associated with the problem (a) for the 'mimic' finite domain problem.

Five meshes are adopted for the analysis. All five meshes contain 64 elements equally distributed over the boundary of the plate. For the crack, the first three meshes are uniform (i.e. all crack elements have the same length) while the last two meshes correspond to the second and the third mesh in Fig. 4.3. The stress intensity factors computed by utilizing these five meshes are presented in Table 4.5. Similar to the previous examples when the improved meshes are employed, excellent agreement with the exact solution is obtained and the results quickly convert to the exact solution.

# Crack Elements	K_I/K_I^{exa}	K_{II}/K_{II}^{exa}
2	0.9983	0.9983
4	1.0002	1.0002
8	1.0005	1.0005
14	1.0001	1.0001
26	1.0000	1.0000

Table 4.5: Stress intensity factors for the problem of Fig. 4.5. Results are normalized by exact solution.

4.1.4 Square plate with centered crack under tension

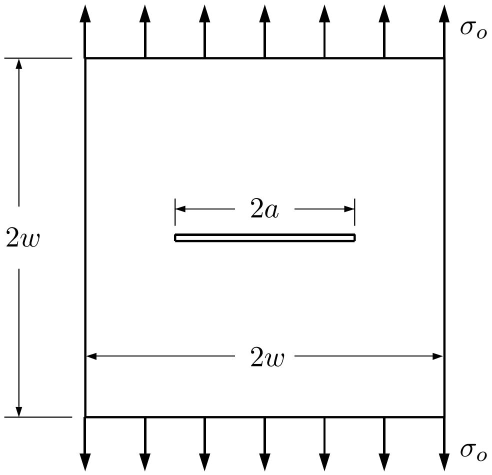

Figure 4.6: Schematic of a square plate with centered straight crack.

Consider a square plate containing a centered straight crack as shown schematically in Fig. 4.6. The crack has a length of $2a$ which is half of the plate width w.

Uniform tractions σ_o are applied in the vertical direction at the top and bottom faces of the plate. This problem was solved by Bowie and Fresse [11], and later by Banks-Sills *et al.* [4] utilizing FEM analysis. For the purpose of comparison to these authors, two orthotropic materials adopted in [4] with the properties shown in Table 4.6 are employed for the analysis. The plane stress condition is assumed for this problem.

Material	E_{11}	E_{22}	ν_{12}	μ_{12}
A	5	10	0.1	2.941
B	1	10	0.1	0.769

Table 4.6: Material properties employed for the problem of Fig. 4.6.

The normalized stress intensity factors $\bar{K}_I = K_I/\sigma_o\sqrt{\pi a}$, computed by utilizing the meshes shown in Fig. 4.7, are given in Table 4.7. For comparison, the results obtained by Bowie and Freese [11] and Banks-Sills *et al.* [4] are also presented in this table. The results of Banks-Sills *et al.* are computed by M-integral method in conjunction with an FEM analysis which are reported in their paper to have the fastest convergence among the other methods. Excellent agreements between the present results and that of both of the references are observed. We note that our results show a very fast convergence even with the material B where the anisotropy is relatively large (i.e. $E_{22}/E_{11} = 10$).

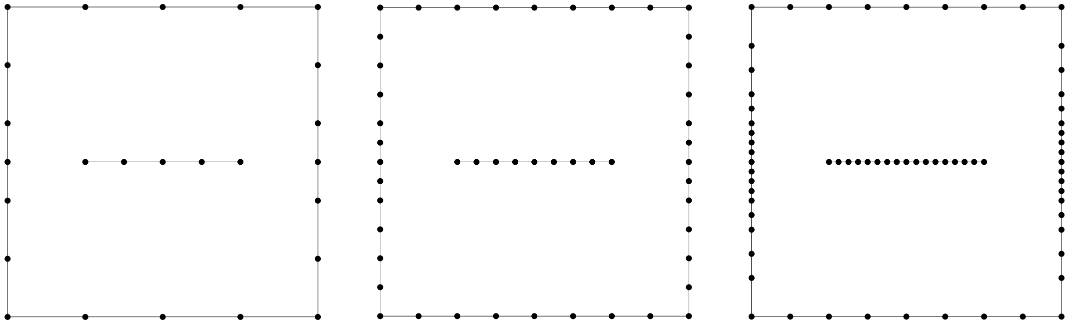

Figure 4.7: Meshes adopted for problem in Fig. 4.6.

Mesh	$\bar{K}_I = \frac{K_I}{\sigma_o\sqrt{\pi a}}$	
	Material A	Material B
1	1.455	1.843
2	1.456	1.846
3	1.456	1.846
References		
Bowie and Freese [11]	1.46	1.85
Banks-Sills *et al.* [4]	1.455	1.845

Table 4.7: Normalized stress intensity factor for the problem of Fig. 4.6.

4.1.5 Rectangular plate with double surface breaking cracks

The next example is a rectangular plate containing two surface breaking cracks under tension as shown in Fig. 4.8. This problem was examined by Atluri *et al.* [2], Boone *et al.* [10] and Banks-Sills *et al.* [4]. The dimensions of the plate are taken as $a/w = 0.8$ and $h/w = 4$, where a is the length of each crack, $2w$ and $2h$ are the width and the height of plate, respectively. An orthotropic material ([4]) with properties shown in Table 4.8 is employed for this problem. The material coordinates denoted as $\bar{x}_1$ and $\bar{\mathrm{x}}_2$ differ by an angle of 45^o with respect to the Cartesian coordinates describing the geometry of problem. Plane stress condition is assumed.

E_{11} (psi)	E_{22} (psi)	ν_{12}	μ_{12} (psi)
25×10^6	1.75×10^6	0.27	0.77×10^6

Table 4.8: Material properties expressed in material coordinates employed for the problem of Fig. 4.8.

Four meshes shown in Fig. 4.9 are employed for this analysis. The mixed-mode stress intensity factors computed by the meshes are displayed in Table 4.9. Results obtained from the above-mentioned authors are also shown in Table 4.9 where the results of Atluri *et al.* and Boone *et al.* are graphic results and the results of Banks-Sills *et al.* are obtained by utilizing the finest mesh. It can be seen that there is a good agreement between our results and that from [4] in which the authors utilized several meshes with increasing refinements to improve their results.

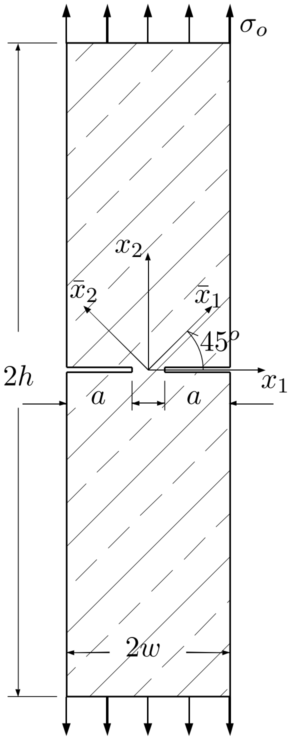

Figure 4.8: Schematic of a rectangular plate containing double edged cracks.

Mesh #	$\bar{K}_I$	K_{II}/K_I
1	1.6730	0.0638
2	1.6792	0.0665
3	1.6802	0.0670
4	1.6804	0.0670
References		
Atluri *et al.* [2]	1.59	0.09
Boone *et al.* [10]	1.60	0.09
Banks-Sills *et al.* [4]	1.679	0.0667

Table 4.9: Normalized stress intensity factors for the problem of Fig. 4.8.

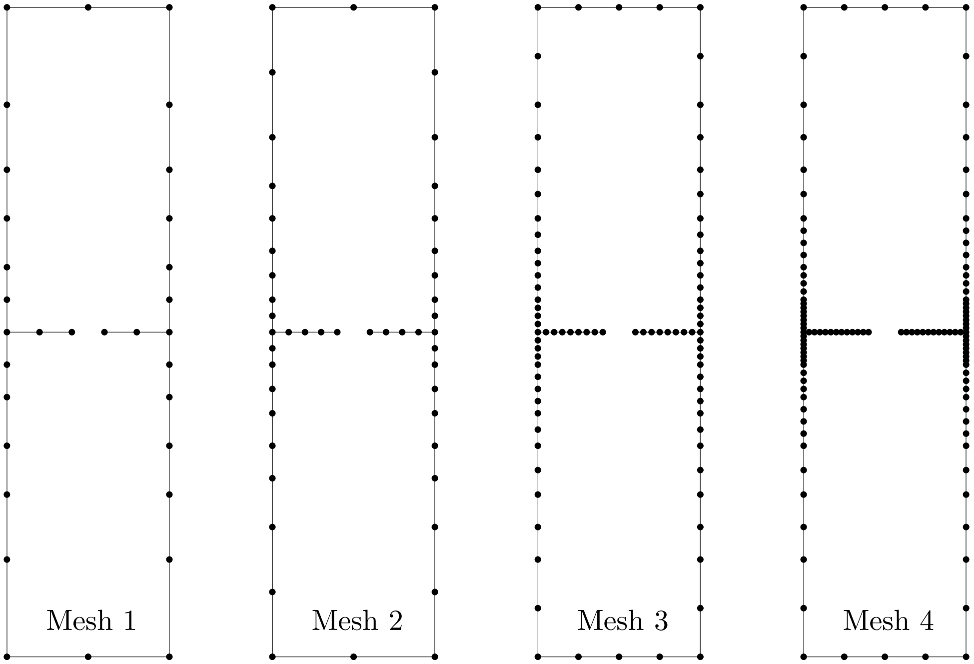

Figure 4.9: Meshes employed for analysis of problem of Fig. 4.8.

4.1.6 Isotropic plate with doubly cracked hole

We now examine the problem of a plate with a doubly-cracked hole as shown in Fig. 4.10(a). The domain of this problem is a multiply connected domain with inner boundary subjected to a pure traction. For this type of problems, the SGBEM experiences a singularity in the coefficient matrix that results in an undetermined solution. A special treatment which is shown in Appendix E is employed for this problem. The dimensions of the plate are $h/w = a/r = 1$ and $2(r + a) = w$. For the purpose of comparison with Chang and Mear [14], an isotropic material is employed for this problem. The stress intensity factors are independent with the Poisson's ratio as well as the plane stress/strain conditions.

The three meshes shown in Fig. 4.11 are employed for the analysis to obtain

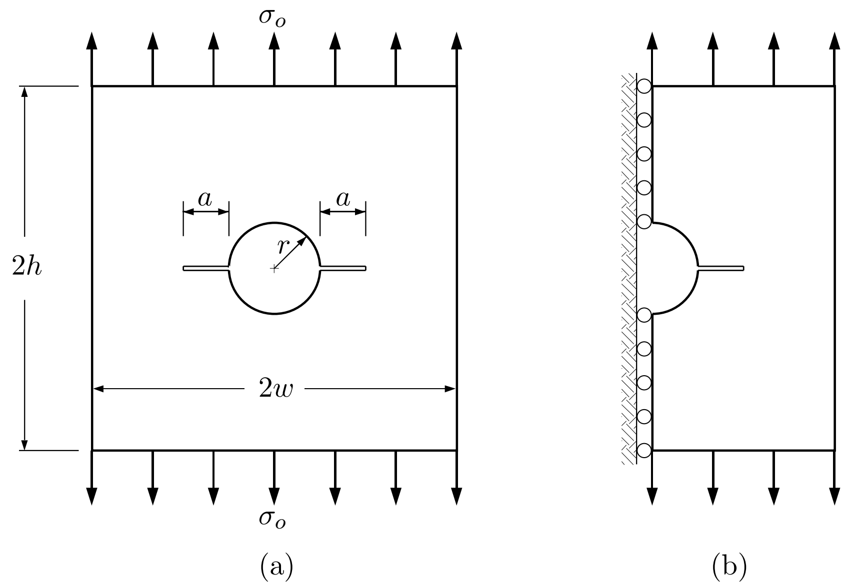

(a) (b)

Figure 4.10: Schematic of a square plate with doubly-cracked hole: (a) description of the problem; (b) boundary conditions for the simplified problem due to the symmetry of the original problem with respect to the x_2-axis.

the stress intensity factor K_I. The results of $K_I/\sigma_o\sqrt{\pi(r+a)}$ are displayed in Table 4.10. For comparison, the result obtained by Chang and Mear [14] is also shown in this table. Excellent agreement with the reference can be seen.

To illustrate that the developed procedure can solve problems having a portion of boundary subjected to both traction and displacement, this problem is resolved utilizing the boundary conditions that represent the symmetric plane $x_1 = 0$ as shown in Fig. 4.10(b). The result computed by employing the mesh shown in Fig. 4.12 is $K_I/\sigma_o\sqrt{\pi(r+a)} = 1.5640$ which well agrees with the results obtained earlier by analyzing the whole plate.

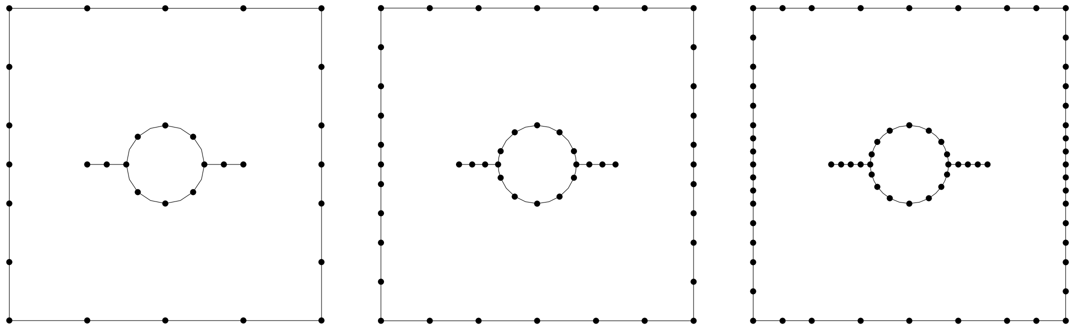

Figure 4.11: Meshes adopted for the analysis of the problem in Fig. 4.10.

Mesh #	$K_I/\sigma_o\sqrt{\pi(r+a)}$
1	1.5644
2	1.5639
3	1.5637
Chang and Mear [14]	1.5627

Table 4.10: Stress intensity factors for the problem of Fig. 4.10.

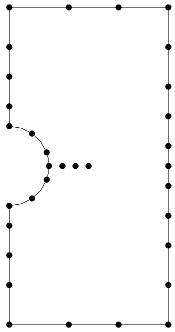

Figure 4.12: Mesh adopted for problem in Fig. 4.10(b). The stress intensity factor computed for this mesh is $K_I/\sigma_o\sqrt{\pi(r+a)} = 1.5640$.

4.1.7 Crack in layered medium

As the last example in this section, we examine a sandwiched plate containing surface breaking crack located in the middle of the plate as shown schematically in Fig. 4.13. For the purpose of comparison, the dimensions and the materials of the plate are taken to be the same as that employed in [14]. These dimensions are $a/w = 0.5$ and $3h/w = 1$. The two materials constituting the plate are isotropy with $\mu_1/\mu_2 = 0.5$ and $\nu_1 = \nu_2 = 0.25$, where the subindices 1 and 2 refer to the material (1) and material (2) as shown in Fig. 4.13. Note that the mode I stress intensity factor depends on the value of Poisson's ratio.

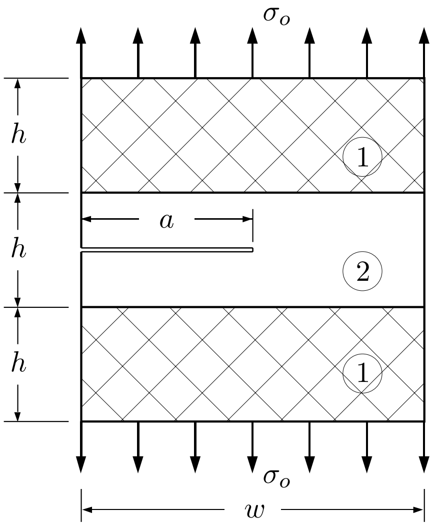

Figure 4.13: Schematic of a sandwiched plate with an edge crack.

The three meshes shown in Fig. 4.14 are employed for the analysis of the problem. The results are displayed in Table 4.11 for the normalized stress intensity factor $K_I/\sigma_o\sqrt{\pi a}$. For comparison, the result obtained by Chang and Mear [14] is also presented in this table. Good agreement between the computed results and that of the reference [14] can be seen.

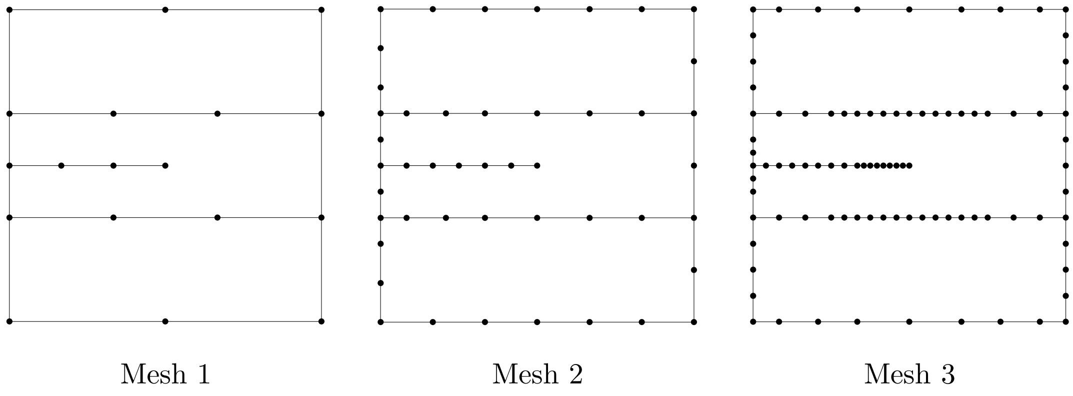

Figure 4.14: Meshes adopted for the analysis of the problem in Fig. 4.13.

Mesh #	$K_I/\sigma_o\sqrt{\pi a}$
1	2.6821
2	2.6850
3	2.6841
Chang and Mear [14]	2.6892

Table 4.11: Normalized mode I stress intensity factor for the problem of Fig. 4.13.

4.2 Problems in piezoelectric media

4.2.1 Straight crack in unbounded domain

Consider again the problem of a straight crack of length $2a$ in an unbounded domain which is now a piezoelectric medium. The crack makes an inclined angle of ϕ with respect to the x_1-axis and is subjected to either a uniaxial far-field stress $\sigma_{22} = \sigma_o$ or a far-field electric displacement D_o in x_2-direction as shown schematically in Fig. 4.15. A transversely isotropic material PZT-4 [50] is employed for this problem. This material has the x_2-axis being the symmetric axis and the properties displayed in Table 4.12.

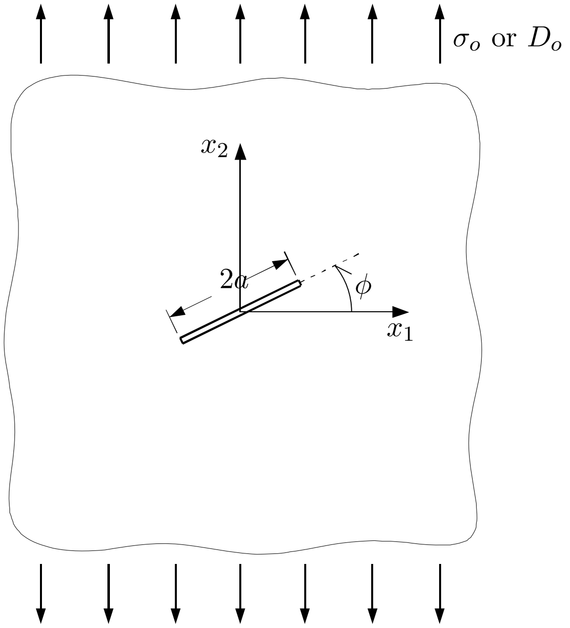

Figure 4.15: Straight crack in unbounded piezoelectric domain subjected to either uniaxial mechanical stress or electric displacement in x_2-direction at infinity.

As can be seen in Table 4.12, the elastic moduli, the piezoelectric coefficients

Elastic moduli (10^9 N/m^2)				
C_{1111}	C_{1122}	C_{1133}	C_{2222}	C_{2323}
139	74.3	77.8	115	25.6
Piezoelectric coefficients (10^1 C/m^2)				
e_{211}	e_{222}	e_{112}		
-0.52	1.51	1.27		
Dielectric permittivity (10^{-9} C/Vm)				
κ_{11}	κ_{22}			
6.461	5.620			

Table 4.12: Material properties for lead zicronate titanate PZT-4 employed for the problem of Fig. 4.15.

and the dielectric permittivity constants are of the order of 10^{11} N/m^2, 10^1 C/m^2 and 10^{-9} C/Vm, respectively. The wide difference in magnitude of these constants will result in truncation errors when a double precision format is utilized to represent real numbers in computers. For this reason, a normalization of these constants should be applied to avoid these errors. We apply the normalization proposed by Denda *et al.* [21] in which a dimensional quantity q is normalized by its reference value q_n to have a non-dimensional quantity $\bar{q} = q/q_n$. From four independent reference values for the strain $\epsilon_n = 10^{-3}$, the stress $\sigma_n = 10^8$ N/m^2, the electric field $E_n = 10^7$ V/m and the electric displacement $D_n = 10^{-2}$ C/m^2, the reference values for other quantities are determined from the constitutive relations stated in Chapter 2 (i.e. equations (2.5) and (2.6)) so that the normalized governing equations of the problem are unchanged.

For this problem, the generalized stress intensity factors (i.e. stress intensity factors and electric displacement intensity factor) are uncoupled. This means that the far-field elastic stress induces only the stress intensity factors and the far-field electric displacement induces only the electric displacement intensity factor. Fig. 4.16 displays the normalized stress intensity factors $\bar{K}_{I,II} = K_{I,II}/\sigma_o\sqrt{\pi a}$ when the crack is subjected to the elastic stress σ_o, and the normalized electric displacement intensity factor $\bar{K}_{IV} = K_{IV}/D_o\sqrt{\pi a}$ when the crack is subjected to electric displacement D_o. These results are computed with a uniform mesh containing 4 elements for the crack. The numerical results are compared with the exact solution obtained by Pak [49] and Suo *et al.* [68]. There is excellent agreement between the numerical results and the exact solutions (all results have an error less than 0.03%).

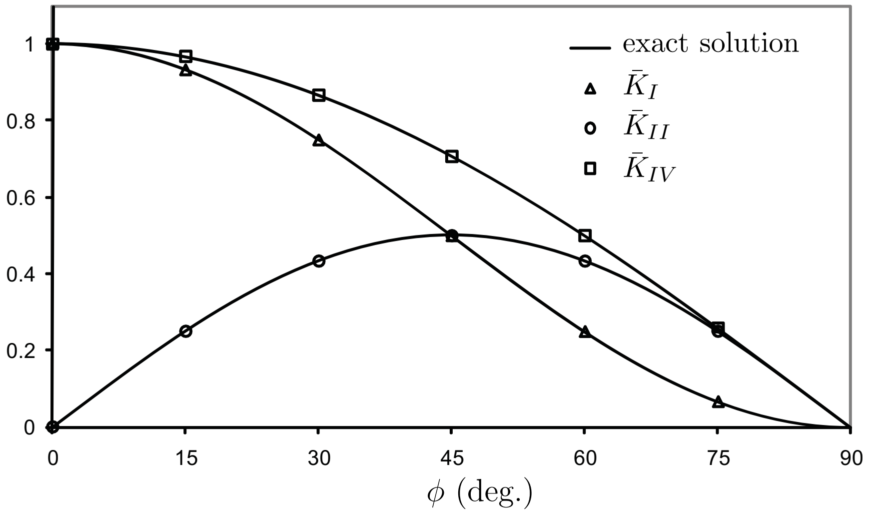

Figure 4.16: Normalized stress and electric displacement intensity factors for the problem in Fig. 4.15.

4.2.2 Two collinear cracks in unbounded domain

Consider a pair of collinear cracks having the same length of $2a$ in an unbounded piezoelectric domain subjected to either far-field elastic stress $\sigma_{22} = \sigma_o$ or far-field electric displacement D_o in x_2-direction as shown schematically in Fig. 4.17. The distance between the two crack centers is $2L$. A PZT-4 material [50] with properties shown in Table 4.12 is employed for the analysis of this example.

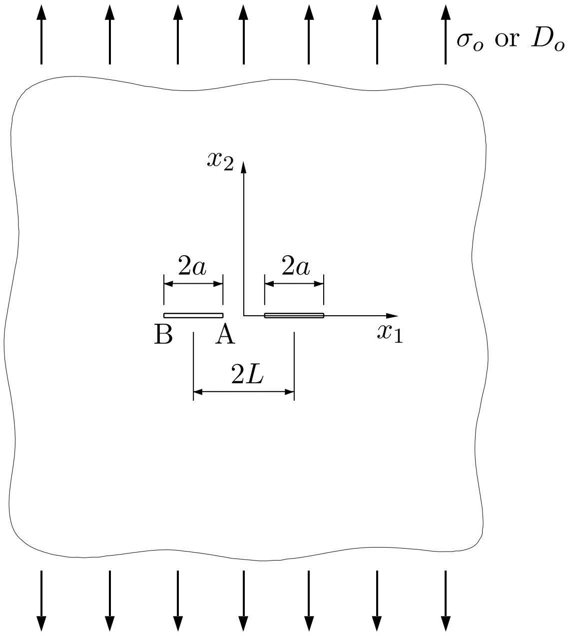

Figure 4.17: Schematic of collinear cracks in unbounded piezoelectric domain

This problem has an exact solution for isotropic elastic material obtained by Erdogan [23]. For anisotropic elastic material, Denda [20] numerically verified that the stress intensity factors are uncoupled and do not depend on the material properties. Subsequently, Liew [43] numerically showed that the generalized stress intensity factors are still uncoupled and independent of the material constants for piezoelectric material. Our results, which are shown in Table 4.13, again verify the uncoupling of the generalized stress intensity factors (i.e. far-field elastic stress induces only stress intensity factor and far-field electric displacement induces only electric induction intensity factor). These results are compared with the exact solution of the corresponding problem in an isotropic elastic medium given by Erdogan [23]. In table 4.13, the generalized stress intensity factors are normalized by the exact solution, for different values of a/L. The second column of the table shows the number of elements utilized for crack in order to obtain results with less than 0.2% error.

a/L	# elements/crack	$\frac{K_I}{K_I^{exa}}(A)$	$\frac{K_I}{K_I^{exa}}(B)$	$\frac{K_{IV}}{K_{IV}^{exa}}(A)$	$\frac{K_{IV}}{K_{IV}^{exa}}(B)$
0.1	2	0.9983	0.9983	0.9983	0.9983
0.3	2	0.9983	0.9983	0.9983	0.9983
0.5	2	0.9981	0.9982	0.9981	0.9982
0.7	4	0.9998	1.0002	0.9998	1.0002
0.9	8	0.9982	1.0005	0.9982	1.0005

Table 4.13: Stress and electric displacement intensity factors for the problem of Fig. 4.17.

4.2.3 Rectangular plate with a central inclined crack

As the last example in this section, we examine the problem of a rectangular plate with a central inclined crack subjected to either uniform tension σ_o or electric displacement D_o in x_2-direction as shown schematically in Fig. 4.18. The crack has a length of $2a$ and makes an inclined angle of 45^o with respect to the x_1-direction. The dimensions of the problem are taken as $a/w = 0.2$ and $h/w = 2$, which are the same as those used by Pan [50] for the purpose of comparison, where $2h$ and $2w$ are the height and the width of plate, respectively. The material employed for the analysis of this problem is PZT-4 with the properties displayed in Table 4.12.

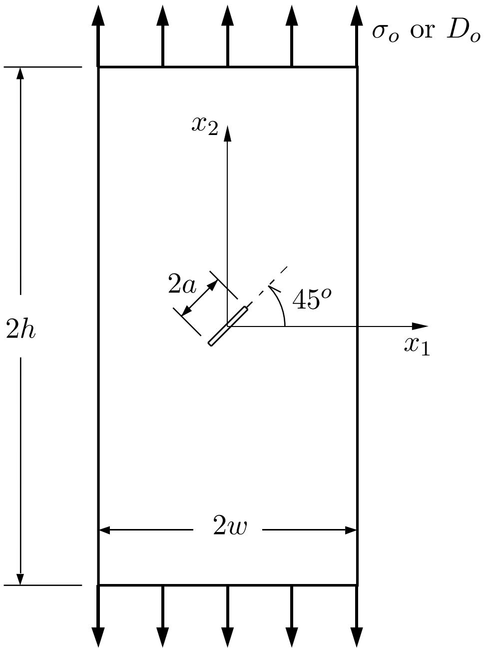

Figure 4.18: Schematic of a rectangular plate with a central inclined crack.

The three meshes shown in Fig. 4.19 are employed for the analysis. The computed generalized stress intensity factors together with the results obtain from referenced authors are presented in Table 4.14. For the case of tension σ_o being applied, the electric displacement intensity factor is normalized by D^* which is a nominal electric displacement in the unit of Cm^{-2} and its magnitude is equal to that of σ_o in the unit of Nm^{-2}. Similarly, for the case of electric displacement D_o

being applied, the stress intensity factors are normalized by σ^* which is a nominal stress in the unit of Nm^{-2} and its magnitude is equal to that of D_o in the unit of Cm^{-2}.

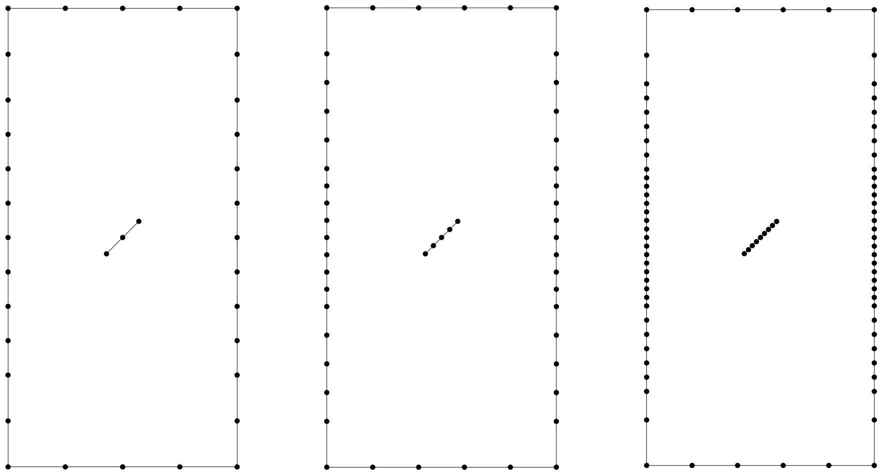
Mesh 1

Mesh 2

Mesh 3

Figure 4.19: Meshes employed for the analysis of the problem in Fig. 4.18.

4.3 Problems in magnetoelectroelastic media

4.3.1 Straight crack in unbounded domain

The problem of a straight crack in an unbounded domain, which has exact solution, is examined in this section to illustrate the accuracy of the developed procedure for magnetoelectroelastic medium. The crack makes an inclined angle of ϕ with respect to x_1-direction and is subjected to an elastic stress $\sigma_{22} = \sigma_o$ or an electric displacement D_o or a magnetic induction B_o in x_2-direction at infinity as shown schematically in Fig. 4.20. The material employed for this example is $\mathrm{BaTiO_3{-}CoFe_2O_4}$ [30] with the properties shown in Table 4.15 and the polling axis

Mesh	Elastic tension is applied			Electric displacement is applied		
	$\frac{K_I}{\sigma_o\sqrt{\pi a}}$	$\frac{K_{II}}{\sigma_o\sqrt{\pi a}}$	$\frac{K_{IV}}{D^*\sqrt{\pi a}}$	$\frac{K_I}{\sigma^*\sqrt{\pi a}}$	$\frac{K_{II}}{\sigma^*\sqrt{\pi a}}$	$\frac{K_{IV}}{D_o\sqrt{\pi a}}$
1	0.5211	0.5063	2.9493×10^{-12}	-1.3773×10^{6}	1.6310×10^{5}	0.71533
2	0.5220	0.5073	2.9529×10^{-12}	-1.3786×10^{6}	1.6280×10^{5}	0.71670
3	0.5222	0.5075	2.9535×10^{-12}	-1.3788×10^{6}	1.6300×10^{5}	0.71689
References						
Liew *et al.* [43]	0.5219	0.5072	2.9518×10^{-12}	-1.3779×10^{6}	1.6312×10^{5}	0.71654
Pan [50]	0.5303	0.5151	2.97×10^{-12}	-1.417×10^{6}	1.692×10^{5}	0.72785

Table 4.14: Stress and electric displacement intensity factors for the problem of Fig. 4.18.

along the x_2-direction.

Similar to the case of piezoelectric material, a normalization for the material constants of a magnetoelectroelastic material is essential to prevent truncation error. Based on the idea proposed by Denda *et al.* [21] for a piezoelectric material, we introduce six independent reference values for the strain $\epsilon_n = 10^{-3}$, the stress $\sigma_n = 10^8\,\mathrm{N/m^2}$, the electric field $E_n = 10^8\,\mathrm{V/m}$, the electric displacement $D_n = 10^{-3}\,\mathrm{C/m^2}$, the magnetic field $H_n = 10^7\,\mathrm{A/m}$ and the magnetic induction $B_n = 10^{-2}\,\mathrm{N/Am}$. The reference values of other quantities are then determined via the constitutive relations (2.14)-(2.16) so that the normalized governing equations of the problem are unchanged.

A uniform mesh with 4 elements for the crack is utilized for the analysis.

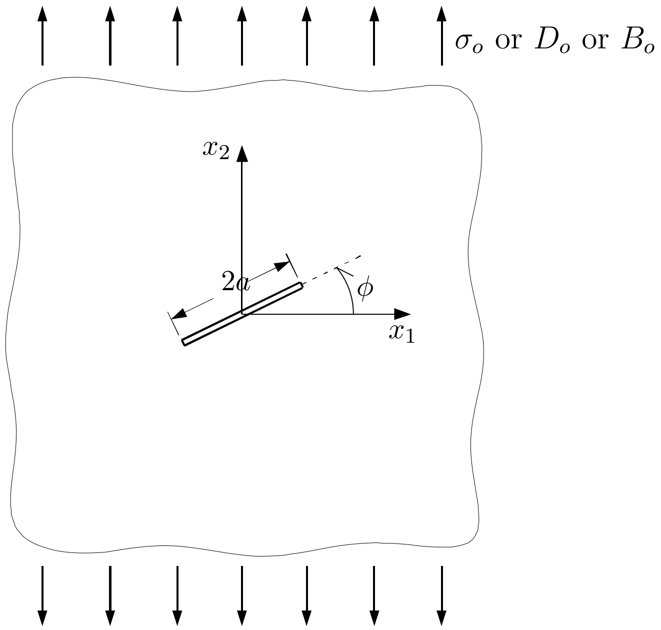

Figure 4.20: Straight crack in unbounded magnetoelectroelastic domain.

Elastic moduli (10^9 N/m^2)							
C_{1111}	C_{1122}	C_{1133}	C_{2222}	C_{2323}			
226	124	125	216	44			
Piezoelectric constants (C/m^2)					Piezomagnetic constants (N/Am)		
e_{211}	e_{222}	e_{112}			h_{211}	h_{222}	h_{112}
-2.2	9.3	5.8			290.2	350	275
Dielectric permittivity (10^{-9} C/Vm)			Electromagnetic constants (10^{-12} Ns/VC)			Magnetic permeability (10^{-6} Ns^2/C^2)	
κ_{11}	κ_{22}		β_{11}	β_{22}		γ_{11}	γ_{22}
5.64	6.35		5.367	2737.5		297	83.5

Table 4.15: Material properties for $BaTiO_3{-}CoFe_2O_4$ with x_2 being the polling direction.

Fig. 4.21 shows the generalized stress intensity factors for the three cases of loading in which the solid lines correspond to the exact solutions given by Gao *et al.* [26]. The results are uncoupled, i.e. applied stress σ_o induces only stress intensity factors K_I and K_{II}, applied electric displacement D_o induces only electric displacement intensity factor K_{IV}, and applied magnetic induction B_o induces only magnetic induction intensity factor K_V. Compared to the exact solutions, all the numerical results have an error of less than 0.03% when utilizing a mesh of 4 elements.

4.3.2 Two parallel cracks in unbounded domain

Consider next the problem of two parallel cracks in an unbounded magnetoelectroelastic domain. The cracks are along the x_1-direction and subjected to various combinations of far-field elastic stress $\sigma_{22} = \sigma_o$ (in unit of Nm^{-2}), electric displacement $D_o = 10^{-8}\sigma_o\,\mathrm{C/N}$ and magnetic induction $B_o = 10^{-6}\sigma_o\,\mathrm{m/A}$ acting in the x_2-direction as shown schematically in Fig. 4.22. Each crack has a length of $2a$ and the vertical distance between the two cracks is $1.2a$. The material is $\mathrm{BaTiO_3{-}CoFe_2O_4}$ [30] with the properties shown in Table 4.15.

Employing a uniform mesh with 4 elements for each crack, the stress intensity factor K_I and magnetic induction intensity factor K_V at crack tip A are computed. The results are displayed in Tables 4.16 and 4.17 together with the results obtained by Tian and Gabbert which were graphically presented in [71] for comparison. Good agreement between the two results is seen.

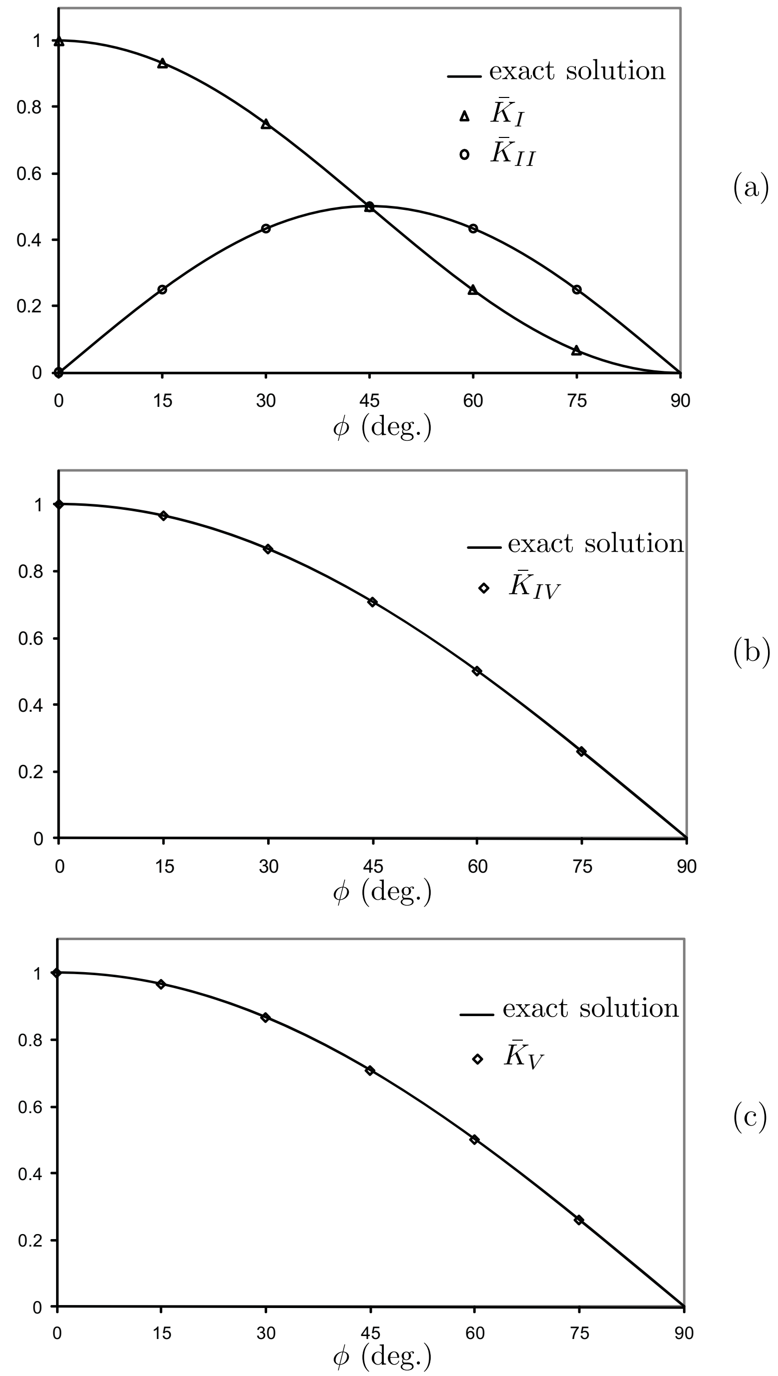

Figure 4.21: Results for problem in Fig. 4.20: (a) Stress intensity factors when σ_o is applied; (b) Electric displacement intensity factor when D_o is applied; (c) Magnetic induction intensity factor when B_o is applied.

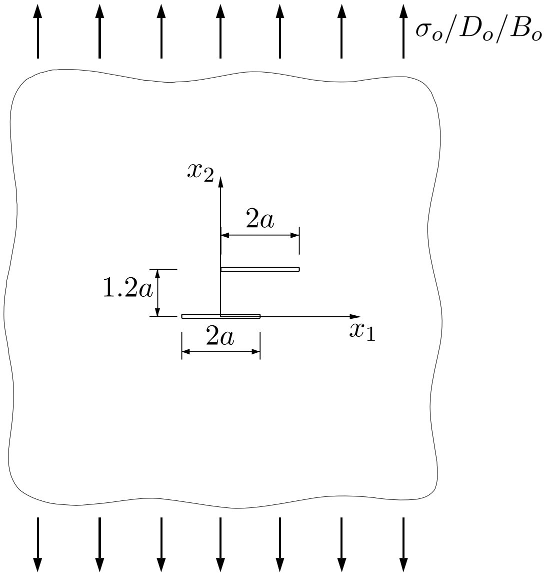

Figure 4.22: Two parallel cracks in unbounded magnetoelectroelastic medium.

Loading	present	Tian and and Gabbert [71]
σ_o	0.6989	0.701
σ_o and B_o	0.5691	0.574
σ_o and $(-B_o)$	0.8287	0.828
σ_o and D_o	0.5738	0.576
σ_o and D_o and B_o	0.4440	0.450
σ_o and D_o and $(-B_o)$	0.7036	0.705

Table 4.16: Normalized stress intensity factor $K_I/\sigma_o\sqrt{\pi a}$ for the problem in Fig. 4.22.

Loading	present	Tian and and Gabbert [71]
σ_o	-0.0002	0.
σ_o and B_o	0.9315	0.934
σ_o and $(-B_o)$	-0.9320	-0.926
σ_o and D_o	-0.0011	0.
σ_o and D_o and B_o	0.9307	-
σ_o and D_o and $(-B_o)$	-0.9328	-

Table 4.17: Normalized magnetic induction intensity factor $K_V/B_o\sqrt{\pi a}$ for the problem in Fig. 4.22.

4.3.3 Edge cracked plate under tension

As the final example in this section, consider a rectangular plate with an edged crack located at mid-height of the plate as shown in Fig. 4.23. The dimensions of the plate are taken as $a/w = 0.4$ and $h/w = 1.2$ where a, w, h are the length of crack, the width and the height of plate, respectively. The plate is subjected to a uniform tension σ_o acting in x_2-direction on the top and bottom faces. The material is $\mathrm{BaTiO_3{-}CoFe_2O_4}$ [30] with the properties shown in Table 4.15.

The meshes shown in Fig. 4.24 are employed for the analysis. The normalized stress intensity factor $K_I/\sigma_o\sqrt{\pi a}$ is displayed in Table 4.18 together with the value obtained by Sladek *et al.* [64] for comparison. Also in the table, the values of normalized electric displacement intensity factor $K_{IV}/D^*\sqrt{\pi a}$ and the magnetic induction intensity factor $K_V/B^*\sqrt{\pi a}$ are presented where D^* and B^* are nominal electric displacement and magnetic induction. The units of D^* and B^* are $\mathrm{Cm^{-2}}$ and $\mathrm{N(Am)^{-1}}$, respectively, and their magnitudes are equal to that of σ_o.

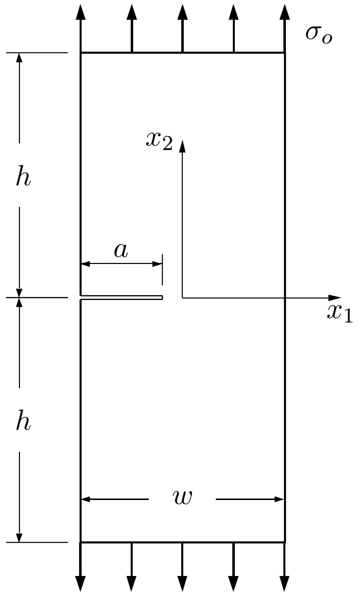

Figure 4.23: Schematic of a plate with an edged crack subjected to uniform tension.

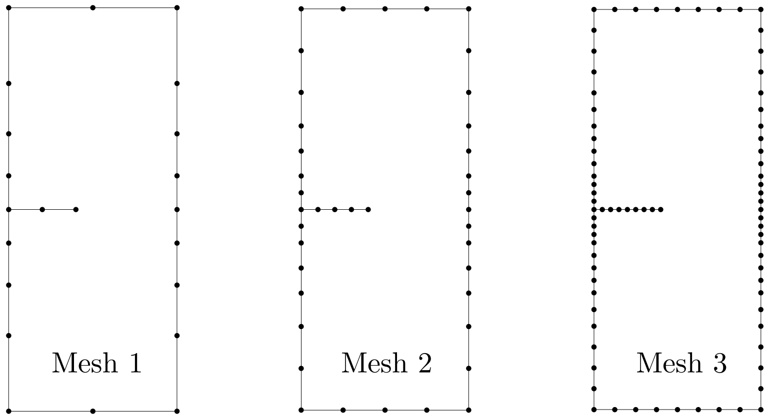

Figure 4.24: Meshes employed for analysis of the problem in Fig. 4.23.

Mesh	$K_I/\sigma_o\sqrt{\pi a}$	$K_{IV}/D^*\sqrt{\pi a}$ $(\times 10^{-11})$	$K_V/B^*\sqrt{\pi a}$ $(\times 10^{-10})$
1	2.1088	7.7793	21.9760
2	2.1072	7.7661	21.9475
3	2.1071	7.7652	21.9453
Reference			
Sladek *et al.* [64]	2.105	-	-

Table 4.18: Normalized stress, electric displacement and magnetic induction intensity factors for the problem of Fig. 4.23.

Chapter 5

T-stress Calculation for Elastic Media

As briefly stated in the introduction chapter, T-stress has a significant effect on the problems of crack growth and crack stability. Over the last 40 years, many methods have been developed to calculate T-stress for a variety of cracked geometries and loadings. Most of the numerical methods utilized path-independent contour integrals based on Eshelby theorem in conjunction with an FEM solution (e.g. Cardew *et al.* [12], Kfouri [36], Chen *et al.* [15], Sladek *et al.* [63], Nakamura and Parks [48]) or a BEM solution (Sutradhar and Paulino [69], Kim and Paulino [37]). Although this method uses the path-independent contour integrals to avoid the crack-tip neighborhood singular stress field and thereby provide accurate results, it is laborious to implement into the existing FEM/BEM code. Utilizing second order weight functions and a reciprocal work integral, Sham [61] presented another method to compute T-stress through an FEM analysis (see also Wang [80], [81]). Similar to the contour-integral method, this method requires much computational efforts to implement in an FEM code.

A distinct category of numerical methods is to compute T-stress directly from the numerical solutions. Larsson and Carlsson [39] presented a 'boundary layer' method in which T-stress, in pure mode-I problems, can be computed by subtracting the tangential stress (i.e. the normal stress acting in the tangential direction of the crack face) of the boundary layer model from that of the actual model (see also Leevers [40]). Yang and Ravi-Chandar [87] developed a method called 'stress difference' in which they employed a boundary element procedure to compute the difference $(\sigma_{11} - \sigma_{22})$ (where $\{1, 2\}$ refers to the crack-tip local coordinate system) at a point in front of the crack tip to obtain T-stress. By doing this, the errors, which vary in the same manner when calculating σ_{11} and σ_{22}, may be eliminated. However, the development of Yang and Ravi-Chandar [87] was just for isotropic material. Instead of employing the stress components in front of the crack tip, Al-Ani and Hancock [1] utilized the displacement on one crack face to compute T-stress. Although this method has an advantage that the T-stress is computed without having to calculate stress intensity factors, it is only applicable to pure mode-I loading (see also Henry and Luxmoore [34]). Ayatollahi *et al.* [3] generally indicated that T-stress can be calculated from either the stresses at various positions around the crack tip or the crack-face displacements for a mixed mode I/II loading. However, this method is again only for isotropic material and it employs the FEM for the analysis. Hence, the accuracy of the results depends on the mesh refinement and the application of a quarter-point crack-tip element.

The number of studies for T-stress calculation in anisotropic material is much less than its isotropic counterpart. Gao and Chiu [28] employed a perturbation method to derive (approximate) closed-form solutions for T-stress of slightly curved and kink cracks in an orthotropic unbounded domain. Yang and Yuan [89] presented explicit expressions for T-stress in 2D anisotropic media by developing a system of singular integral equations based on Stroh formalism. These authors also derived the analytical expressions for the asymptotic stress and displacement fields including the constant terms (e.g. T-stress) and higher-order terms for an anisotropic cracked body. T-stress is then obtained via either J-integral or Betti's reciprocal theorem methods (Yang and Yuan [88]). However, there were no numerical implementation or results presented in this paper. Su and Sun [66] employed an eigenfunction expansion approach to derive the analytical displacement field around crack tip for 2D orthotropic media which was then employed, in conjunction with a 'fractal' FEM, to compute T-stress (Su and Sun [67]). Kim and Paulino [38] utilized an M-integral method to compute T-stress for functionally graded orthotropic material through an FEM analysis. Shah *et al.* [60] also utilized an M-integral method but with a BEM analysis for the computation of T-stress in 2D orthotropic media. To overcome the difficulty when evaluating the displacement and stress at interior points in the neighborhood of crack tips (i.e. 'boundary' of the domain) for M-integral calculation, they applied the technique proposed by Richardson and Cruse [55]. However, this method did not clearly show the satisfaction of the smoothness requirement for crack-face displacements.

This chapter presents a numerical procedure for the determination of T-stress at crack tips in a 2D anisotropic elastic medium. It presents two approaches for calculating the derivatives of displacement at the crack tip. For the purpose of verifying the accuracy of the proposed method, several examples will be analyzed, and the computed results will be compared with analytical solutions and with other authors in literature.

5.1 Asymptotic crack-tip field

Consider the usual setting of a semi-infinite (two-dimensional) crack which lies along the negative x_1-axis as shown schematically in Fig. 5.1 and, for purpose of discussion, restrict attention to mode-I loading of a traction-free crack. Let $\{r, \theta\}$ be a polar coordinate system with origin at the crack tip. The asymptotic crack tip displacements are expressed, for isotropic material (e.g. Yang and Ravi-Chandar [87]) as

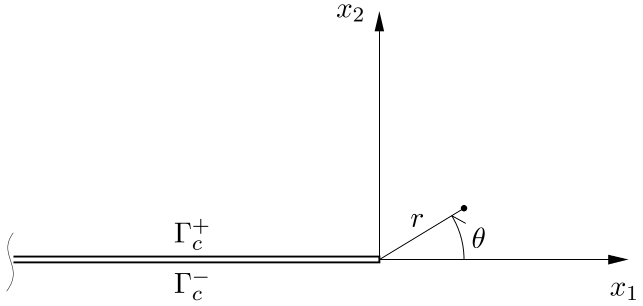

Figure 5.1: Schematic of a semi-infinite crack.

$$\begin{aligned} u_1 &= K_I\sqrt{\frac{r}{2\pi}}\Big(\frac{1+\nu}{E}\Big)\cos(\theta/2)\big[\kappa-1+2\sin^2(\theta/2)\big] \\ &+ \frac{1-\nu^2}{E}Tr\cos\theta + \mathcal{O}(r^{3/2}) \qquad (5.1) \\ u_2 &= K_I\sqrt{\frac{r}{2\pi}}\Big(\frac{1+\nu}{E}\Big)\sin(\theta/2)\big[\kappa+1-2\cos^2(\theta/2)\big] \\ &- \frac{\nu+\nu^2}{E}Tr\sin\theta + \mathcal{O}(r^{3/2}) \qquad (5.2) \end{aligned}$$

where E and ν are Young's modulus and Poisson's ratio of the material, respectively; K_I and T are the stress intensity factor and T-stress, respectively, and

$$\kappa = \begin{cases} 3-4\nu & \text{for plane strain} \\ \frac{3-\nu}{1+\nu} & \text{for plane stress} \end{cases} \qquad (5.3)$$

and for anisotropic material (e.g. Kim and Paulino [38]) as

$$\begin{aligned} u_1 &= K_I\sqrt{\frac{r}{2\pi}}\mathcal{R}\Big[\frac{1}{\mu_1-\mu_2}\big(\mu_1 p_2\sqrt{\cos\theta+\mu_2\sin\theta}-\mu_2 p_1\sqrt{\cos\theta+\mu_1\sin\theta}\big)\Big] \\ &+ S_{11}Tr\cos\theta+\mathcal{O}(r^{3/2}) \qquad (5.4) \\ u_2 &= K_I\sqrt{\frac{r}{2\pi}}\mathcal{R}\Big[\frac{1}{\mu_1-\mu_2}\big(\mu_1 q_2\sqrt{\cos\theta+\mu_2\sin\theta}-\mu_2 q_1\sqrt{\cos\theta+\mu_1\sin\theta}\big)\Big] \\ &+ S_{12}Tr\sin\theta+\mathcal{O}(r^{3/2}) \qquad (5.5) \end{aligned}$$

where $\mathcal{R}$ denotes the real part of a complex function; p_k and q_k $(k=1,2)$ are given by

$$p_k = S_{11}\mu_k^2+S_{12}-S_{16}\mu_k \qquad (5.6)$$

$$q_k = S_{12}\mu_k+\frac{S_{22}}{\mu_k}-S_{26} \qquad (5.7)$$

in which μ_1 and μ_2 are the two roots (with positive imaginary parts) of the characteristic equations

$$S_{11}\mu^4-2S_{16}\mu^3+(2S_{12}+S_{66})\mu^2-2S_{26}\mu+S_{22}=0 \qquad (5.8)$$

where S_{ij} denote the contracted compliances of the material for plane stress condition (the indices are taken such that 23 → 4, 31 → 5, 12 → 6). For plane strain condition, S_{ij} are replaced by $S'_{ij}=S_{ij}-\frac{S_{i3}S_{j3}}{S_{33}}$.

Let $u_i^+(\boldsymbol{x})$ and $u_i^-(\boldsymbol{x})$ denote the displacement of the 'upper' and 'lower' crack faces, i.e. Γ_c^+ and Γ_c^- respectively, and define $\Delta u_i \equiv u_i^+ - u_i^-$ and $\Sigma u_i \equiv u_i^+ + u_i^-$. The expressions of asymptotic displacements (5.1) and (5.2) or (5.4) and (5.5) lead to

$$\Delta u_1 = 0 \qquad (5.9)$$

$$\Delta u_2 = \alpha K_I r^{1/2}+\mathcal{O}(r^{3/2}) \qquad (5.10)$$

and

$$\begin{aligned}\Sigma u_1 &= u_1^o + \beta T r + \mathcal{O}(r^2) && (5.11)\\ \Sigma u_2 &= u_2^o + \omega^o r && (5.12)\end{aligned}$$

in which $\{u_1^o, u_2^o\}$ correspond to a (possible) rigid body displacement of the crack tip, ω^o represents a (possible) rigid body rotation of the crack about the crack tip, $\{\alpha, \beta\}$ are known constants relating to the material properties. For instance, with isotropic material, the constants $\{\alpha, \beta\}$ are given as

$$\alpha = \frac{1+\nu}{E\sqrt{2\pi}} \tag{5.13}$$

$$\beta = \frac{\nu^2 - 1}{E} \tag{5.14}$$

We remark that Δu_i involves only fractional powers of r and that Σu_i involves only integral powers of r; this observation is important in the development to follow.

5.2 Integral relations for 2D cracks

The integral equation for the sum of crack-face displacements of an isolated crack, which was established in Chapter 2 for multi-field media (see equation (2.32)), is restated here for elastic media as

$$\frac{1}{2}\Sigma u_p(\boldsymbol{y}) = \int_{\Gamma_c} G_j^p(\boldsymbol{\xi} - \boldsymbol{y})\, D\Delta u_j(\boldsymbol{\xi})\, ds(\boldsymbol{\xi}) - \int_{\Gamma_c} H_{\alpha j}^p(\boldsymbol{\xi} - \boldsymbol{y})\, n_\alpha(\boldsymbol{\xi})\, \Delta u_j(\boldsymbol{\xi})\, ds(\boldsymbol{\xi}) \tag{5.15}$$

in which G_j^p is a weakly-singular kernel defined in (2.59), $H_{\alpha j}^p$ is defined in (2.26), and Γ_c is a unique representation for the crack face.

As mentioned in Chapter 2, the equation (5.15) is not of interest for obtaining stress intensity factors but it is used for the determination of T-stress that will be discussed further below. For the crack problems in finite domain, by utilizing the same process that described in Chapter 2 for isolated crack, but now begin with Somigliana's identity for finite domain (2.81), we can obtain the integral equation for the sum of crack-face displacement as follows

$$\begin{aligned} \frac{1}{2}\Sigma u_p(\boldsymbol{y}) &= \int_{\Gamma_o} U_j^p(\boldsymbol{\xi}-\boldsymbol{y})\, t_j(\boldsymbol{\xi})\, ds(\boldsymbol{\xi}) \\ &+ \int_{\Gamma} \left[G_j^p(\boldsymbol{\xi}-\boldsymbol{y})\, Dv_j(\boldsymbol{\xi}) - H_{\alpha j}^p(\boldsymbol{\xi}-\boldsymbol{y})\, n_\alpha(\boldsymbol{\xi})\, v_j(\boldsymbol{\xi}) \right] ds(\boldsymbol{\xi}) \end{aligned} \tag{5.16}$$

where U_j^p is the displacement fundamental solution defined in (2.48), Γ_o denotes the ordinary boundary, Γ denotes the total boundary of the domain (i.e. $\Gamma = \Gamma_o + \Gamma_c$), and

$$v_j(\boldsymbol{y}) = \begin{cases} u_j(\boldsymbol{y}) & , \quad \boldsymbol{y} \in \Gamma_o \\ \Delta u_j(\boldsymbol{y}) & , \quad \boldsymbol{y} \in \Gamma_c \end{cases} \tag{5.17}$$

5.3 T-stress determination: the first approach

It is important to note that Σu_p is in the form of an integral power series. While the equation (5.16) allows Σu_p to be directly determined at the crack tip (and anywhere on the crack face) from the (known) data on the entire boundary of the problem, it is likely best to 'enforce' a power series-type representation for Σu_p. To do so, we propose to interpolate Σu_p using standard quadratic elements and enforce (5.16) in a weak sense, that is multiply both sides of (5.16) by a test function (from the same place in which Σu_p is interpolated) and integrate the result over a domain Γ_w on the crack face (i.e. $\Gamma_w \in \Gamma_c$). Then the weak-form integral equation of Σu_p

is given as

$$
\begin{aligned}
\frac{1}{2}\int_{\Gamma_w} \Sigma u_p(\boldsymbol{y})\,\tilde{t}_p(\boldsymbol{y})\,ds(\boldsymbol{y}) &= \int_{\Gamma_w} \tilde{t}_p(\boldsymbol{y}) \int_{\Gamma_o} U_j^p\, t_j(\boldsymbol{\xi})\,ds(\boldsymbol{\xi})\,ds(\boldsymbol{y}) \\
&+ \int_{\Gamma_w} \tilde{t}_p(\boldsymbol{y}) \int_{\Gamma} \left[G_j^p\, Dv_j(\boldsymbol{\xi}) - H_{\alpha j}^p\, n_\alpha(\boldsymbol{\xi})\, v_j(\boldsymbol{\xi})\right] ds(\boldsymbol{\xi})\,ds(\boldsymbol{y})
\end{aligned}
\tag{5.18}
$$

where $\tilde{t}_p$ is a continuous test function on Γ_w.

Note that we really only need to calculate Σu_p over the crack-tip element so that the strains at crack tip (i.g. derivatives of Σu_p) can be numerically obtained from Σu_p. In this case, the domain Γ_w is the crack-tip element associated with the crack tip where T-stress is calculated. However, as a 'smoothing process', the domain Γ_w can be taken as the whole crack face (i.e. $\Gamma_w = \Gamma_c$) and, in this case, the values of Σu_p are calculated at every interpolation points (i.e. nodes) over the crack face. Both cases (Γ_w=crack-tip element and $\Gamma_w = \Gamma_c$ which are distinguished by Case A and Case B, respectively) will be investigated through the numerical examples presented in the next section to compare the accuracy of each of them.

The numerical implementation for solving the integral equation (5.18) is summarized as follows. Σu_p and $\tilde{t}_p$ are interpolated over Γ_w in terms of trial and test functions as

$$
\mathbf{\Sigma u} = \mathbf{\Phi}^{\mathrm{T}}\mathbf{\Sigma U} \tag{5.19}
$$

$$
\tilde{\boldsymbol{t}} = \mathbf{\Phi}^{\mathrm{T}}\tilde{\boldsymbol{T}} \tag{5.20}
$$

where $\mathbf{\Phi}^{\mathrm{T}}$ denotes the transpose of $\mathbf{\Phi}$ which is the column vector of nodal basis functions, and $\{\mathbf{\Sigma U}, \tilde{\boldsymbol{T}}\}$ denotes the column vectors of nodal quantities.

Employing the interpolations (5.19) and (5.20) for the integral equation (5.18), a linear system of algebra equations for the unknown nodal quantities $\mathbf{\Sigma U}$ is obtained upon utilizing the arbitrariness of the test function $\tilde{\boldsymbol{t}}$ as follows

$$\boldsymbol{K}\ \mathbf{\Sigma U} = \boldsymbol{P} \tag{5.21}$$

where the coefficient matrix $\boldsymbol{K}$ and the right-hand-side vector $\boldsymbol{P}$ are defined as

$$\boldsymbol{K} = \frac{1}{2}\int_{\Gamma_w} \mathbf{\Phi}(\boldsymbol{y})\ \mathbf{\Phi}^{\mathrm{T}}(\boldsymbol{y})\ ds(\boldsymbol{y}) \tag{5.22}$$

$$\boldsymbol{P} = \int_{\Gamma_w} \mathbf{\Phi}(\boldsymbol{y})\ \boldsymbol{F}(\boldsymbol{y})\ ds(\boldsymbol{y}) \tag{5.23}$$

in which

$$F_p(\boldsymbol{y}) = \int_{\Gamma_o} U^p_j\, t_j(\boldsymbol{\xi})\, ds(\boldsymbol{\xi}) + \int_{\Gamma} \big[G^p_j\, Dv_j(\boldsymbol{\xi}) - H^p_{\alpha j} n_\alpha(\boldsymbol{\xi}) v_j(\boldsymbol{\xi})\big]\, ds(\boldsymbol{\xi}) \tag{5.24}$$

With regard to the local coordinate system with the origin at crack tip as shown in Fig. 5.2, the strain components at crack tip are determined from the solution of (5.21) as

$$\bar{\epsilon}_{11} = \frac{\partial}{\partial \bar{x}_1}\big[\frac{1}{2}\Sigma\bar{u}_1(\bar{x}_1 = 0)\big] \tag{5.25}$$

$$\bar{\epsilon}_{33} = \frac{\partial}{\partial \bar{x}_3}\big[\frac{1}{2}\Sigma\bar{u}_3(\bar{x}_1 = 0)\big] \tag{5.26}$$

$$\bar{\epsilon}_{13} = \frac{1}{2}\frac{\partial}{\partial \bar{x}_1}\big[\frac{1}{2}\Sigma\bar{u}_3(\bar{x}_1 = 0)\big] \tag{5.27}$$

The stresses $\{\bar{\sigma}_{11}, \bar{\sigma}_{33}, \bar{\sigma}_{13}\}$ are readily obtained from the constitutive relation and the applied traction on the crack face.

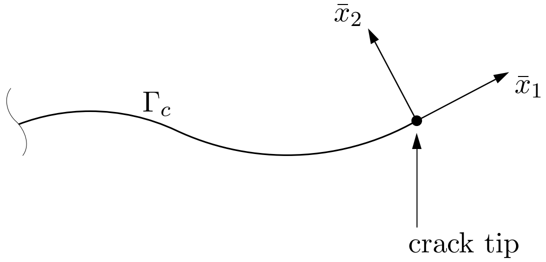

Figure 5.2: Crack-tip local coordinate system.

5.4 T-stress determination: The second approach

To avoid taking the numerical differentiation when determining the strains at crack tip as shown in the equations (5.25)-(5.27), another approach for T-stress calculation is proposed in which the derivatives of the crack-face displacement at crack tip are obtained directly from an integral equation. To begin, let us define

$$\Pi_p(\boldsymbol{y}) \equiv \frac{\partial}{\partial s}\left[\frac{1}{2}\Sigma u_p(\boldsymbol{y})\right] \tag{5.28}$$

where s is the arc length along the crack curve Γ_c.

Then the weak-form integral equation of $\boldsymbol{\Pi}$ is formed by multiplying (5.28) with a test function $\tilde{\boldsymbol{t}}$ and integrating the result over the domain Γ_w, then the final form is given, after integrating by parts, as follows

$$\begin{aligned}\int_{\Gamma_w} \Pi_p(\boldsymbol{y})\tilde{t}_p(\boldsymbol{y})\,ds(\boldsymbol{y}) \quad &= \quad \frac{1}{2}\Sigma u_p(\boldsymbol{y}_b)\tilde{t}_p(\boldsymbol{y}_b) - \int_{\Gamma_w} D\tilde{t}_p(\boldsymbol{y})\int_{\Gamma_o} U_l^p t_l(\boldsymbol{\xi})\,ds(\boldsymbol{\xi})ds(\boldsymbol{y}) \\ &- \quad \int_{\Gamma_w} D\tilde{t}_p(\boldsymbol{y})\int_{\Gamma}\left[G_l^p Dv_l(\boldsymbol{\xi}) - H_{\alpha l}^p n_\alpha v_l(\boldsymbol{\xi})\right] ds(\boldsymbol{\xi})ds(\boldsymbol{y})\end{aligned} \tag{5.29}$$

where the first term in (5.29) is evaluated at $\boldsymbol{y}_b$ which is the 'boundary' of Γ_w, i.e. the crack tip and the other end of the domain Γ_w, and $D = \frac{\partial}{\partial s}$ is the derivative with respect to the arc length of crack curve Γ_c.

Utilizing the same approximation (5.19) and (5.20) for $\mathbf{\Pi}$ and $\tilde{\boldsymbol{t}}$ respectively, the final system of linear equations for solving the nodal value of $\mathbf{\Pi}$ is as

$$\boldsymbol{M}\ \mathbf{\Pi_n} = \boldsymbol{Q} \tag{5.30}$$

where $\mathbf{\Pi_n}$ denotes the column vector of nodal values of $\mathbf{\Pi}$, the coefficient matrix $\boldsymbol{M}$ and the right hand side vector $\boldsymbol{Q}$ are defined as

$$\boldsymbol{M} = \int_{\Gamma_c} \mathbf{\Phi}(\boldsymbol{y})\ \mathbf{\Phi}^{\mathrm{T}}(\boldsymbol{y})\ ds(\boldsymbol{y}) \tag{5.31}$$

$$\boldsymbol{Q} = \int_{\Gamma_c} D\mathbf{\Phi}(\boldsymbol{y})\ \boldsymbol{F}(\boldsymbol{y})\ ds(\boldsymbol{y}) + \frac{1}{2}\mathbf{\Phi}(\boldsymbol{y}_b)\mathbf{\Sigma}\mathbf{u}(\boldsymbol{y}_b) \tag{5.32}$$

in which $\boldsymbol{F}$ is defined in (5.24).

The T-stress in then obtained from the strains and the applied traction on crack faces at the crack tip via constitutive relation.

5.5 Numerical examples

To illustrate the accuracy and versatility of the proposed procedure for T-stress calculation, several example problems are considered. Both isotropic and anisotropic material are employed for the examples. The purpose of using isotropic material is to compare the results with available exact solution and with the results from other authors. All isotropic materials are treated as 'anisotropic' materials to demonstrate and to verify the capability of the method for general anisotropic material, i.e. the kernels are forced to be numerically evaluated even though they can be analytically obtained (see Appendix D).

5.5.1 Straight crack in unbounded domain

Consider a straight crack in unbounded domain subjected to uniaxial far-field stress $\sigma_{22} = \sigma_o$ as shown schematically in Fig. 5.3. The crack is inclined an angle ϕ with respect to the x_1-direction.

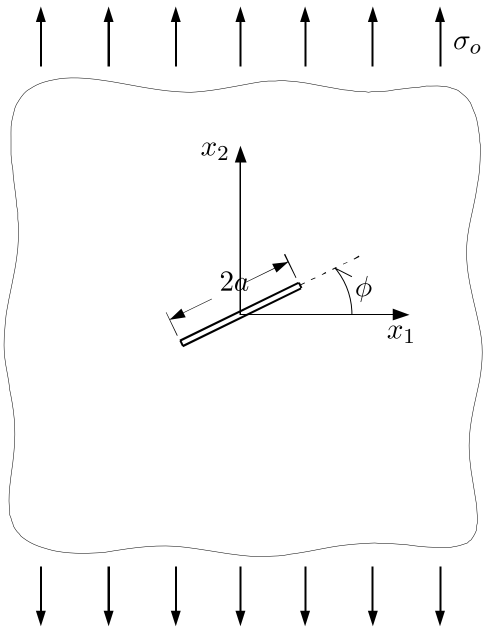

Figure 5.3: Schematic of a straight crack in unbounded domain.

An orthotropic material, with the constants shown in Table 5.1, is employed for the analysis of this problem. The exact solution is available for the particular case when $\phi = 0^{\text{o}}$ (e.g. Gao and Chiu [28]) which is given, for plane stress condition, by

$$T = -\sigma_o \sqrt{E_{11}/E_{22}} \tag{5.33}$$

E_{11} (psi)	E_{22} (psi)	ν_{12}	μ_{12} (psi)
25×10^6	1.75×10^6	0.27	0.77×10^6

Table 5.1: Properties of an orthotropic material employed for the analysis of the problem in Fig. 5.3.

Table 5.2 shows the numerical result of T-stress for the case of $\phi = 0^o$, normalized by the exact solution (5.33), obtained with different meshes of the crack. In the table, the first 3 rows correspond to uniform meshes (i.e. all elements have the same length) while the last 3 rows correspond to non-uniform meshes in which the two crack-tip elements have a length of $a/4$ for each, and the remaining elements (i.e. elements in between two crack-tip elements) have a length of $a/8$, $a/16$ and $a/20$ respectively (see Fig. 4.3 in Chapter 4). It can been seen that the results for both approaches quickly covert to the exact solution for the non-uniform meshes. This convergence behavior was already observed and explained in the case of stress intensity factor calculation in Chapter 4. It is also showed that the results obtained by the first approach is better for case A than that for case B, and the accuracy of case A of the first approach is nearly the same as that of the second approach.

For other values of the inclined angle ϕ, the exact solution for the case of

# Crack Elements	T/T^{exa}		
	1^{st} approach		2^{nd} approach
	Case A	Case B	
2	1.0019	1.0012	0.9963
4	0.9993	0.9978	1.0008
8	0.9983	0.9940	1.0022
14	0.9997	0.9991	1.0004
26	1.0000	0.9999	1.0000
32	1.0000	1.0000	1.0000

Table 5.2: Stress intensity factors for the problem of Fig. 5.3 for $\phi = 0^o$ using the orthotropic material with constants shown in Table 5.1. Results are normalized by exact solution.

isotropic material is independent of Poisson's ratio and is given as

$$T = -\sigma_o \cos 2\phi \tag{5.34}$$

Fig. 5.4 displays the normalized T-stress T/σ_o as a function of the inclined angle ϕ for isotropic material. The solid line corresponds to the exact solution (5.34), and the numerical results are computed with a uniform mesh of 4 elements by the second approach. All results have error of less than 0.2%.

5.5.2 Straight crack in finite domain

To validate the computational procedure of T-stress for finite domain, we consider again the problem of a straight crack in finite domain which 'mimics' the crack in unbounded domain that was discussed in Chapter 4 when calculating stress intensity factors. For convenience, the schematic of the problem and the applied

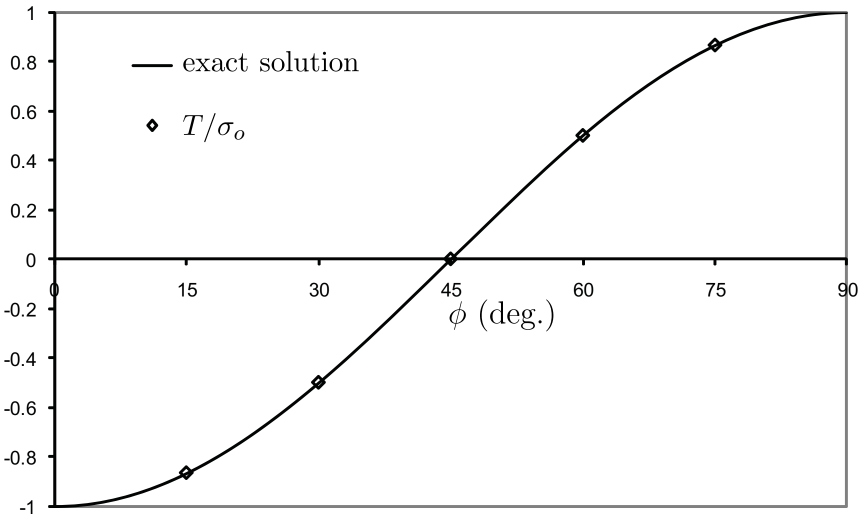

Figure 5.4: Normalized T-stress for the problem of Fig. 5.3 computed by the second approach with a uniform mesh of 4 elements and using an isotropic material. All results have error $< 0.2\%$.

traction on boundary which is derived from the exact stress field of the associated problem in unbounded domain are showed again here in Fig. 5.5. The exact solution of T-stress for this problem is displayed in (5.34). We now consider the case of $\phi = 30^o$ where ϕ is the inclined angle of the crack with respect to x_1-axis.

Five meshes are employed for the convergence study. To accurately model the applied traction which is non-trivial as shown in Fig. 5.5, all five meshes use 64 elements for the regular boundary. For the crack, the first three meshes employ a uniform mesh (i.e. all elements have the same length), and the last two meshes have the region in between the crack-tip elements be refined as mentioned before. Results of T-stress calculation utilizing these five meshes are shown in Table 5.3 in which the T-stress is normalized by the exact solution. Again, it can be seen that the fast

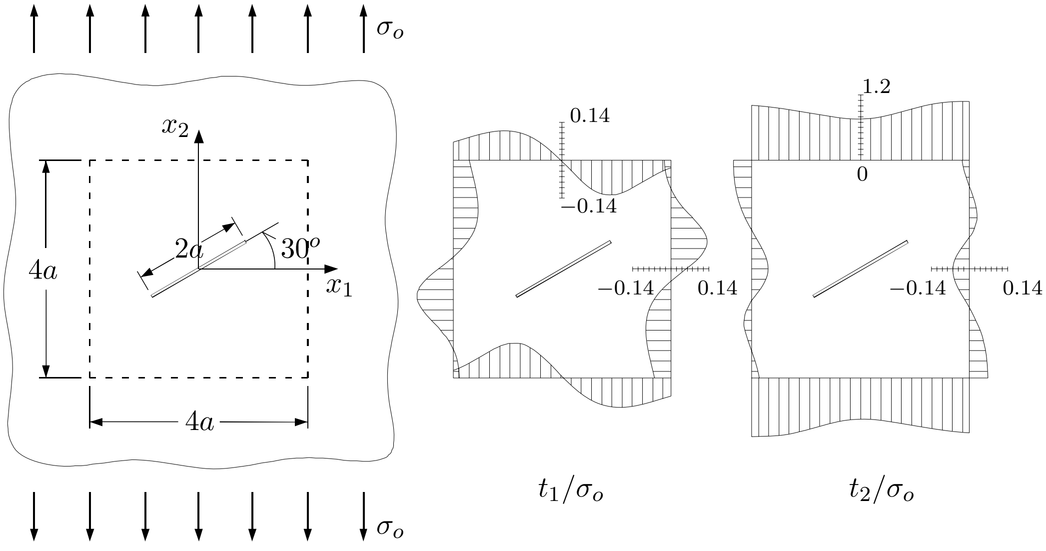

(a) (b) (c)

Figure 5.5: Straight crack in finite domain: (a) crack in unbounded domain with the dash line indicating the boundary of the 'mimic' problem in finite domain; (b) and (c) applied traction derived from the exact stress field associated with the problem (a) for the 'mimic' finite domain problem.

convergence to the exact solution occurs when using the non-uniform meshes for both approaches. The accuracy of each approach is observed to be the same as that of the isolated crack problem.

5.5.3 Single edge notched specimen

Consider a specimen with a surface breaking crack under uniform tension on the top and bottom faces as shown in Fig. 5.6. The dimensions of specimen are chosen as $a/w = 0.4$ and $h/w = 1$, where a is the crack length, w and h are the width and half of the height of specimen, respectively. An isotropic material is employed for the analysis of this problem. Both stress intensity factor and T-stress are independent with the Poisson's ratio of the material as well as the conditions

# Crack Elements	T/T^{exa}		
	1^{st} approach		2^{nd} approach
	Case A	Case B	
2	1.0018	1.0012	0.9966
4	0.9994	0.9980	1.0007
8	0.9985	0.9945	1.0021
14	0.9997	0.9992	1.0003
26	1.0000	0.9999	1.0000

Table 5.3: Stress intensity factors for the problem of Fig. 5.5, isotropic material. Results are normalized by exact solution.

of plane stress or plane strain [87]. The numerical results, computed by the first approach (case A) utilizing the meshes shown in Fig. 5.7, are presented in Table 5.4. The results are compared with Yang and Ravi-Chandar [87] and Kfouri [36] for both normalized stress intensity factor and T-stress. Good agreements with these authors are observed.

Mesh #	$\frac{K_I}{\sigma_o\sqrt{\pi a}}$	$\frac{T}{\sigma_o}$
1	2.1139	-0.5746
2	2.1138	-0.5694
3	2.1130	-0.5718
Yang and Ravi-Chandar [87]	2.134	-0.5676
Kfouri [36]	-	-0.5515

Table 5.4: Normalized stress intensity factor and T-stress for the problem of Fig. 5.6, isotropic material, computed by the first approach (case A).

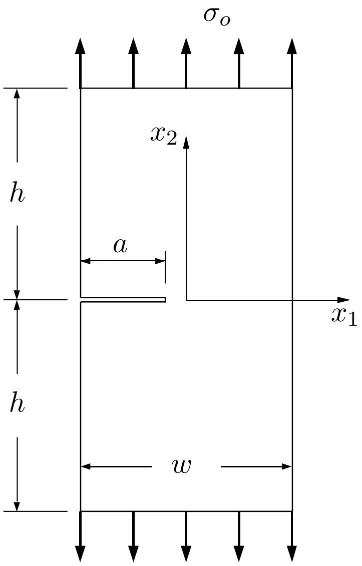

Figure 5.6: Specimen with single edged crack under uniform tension.

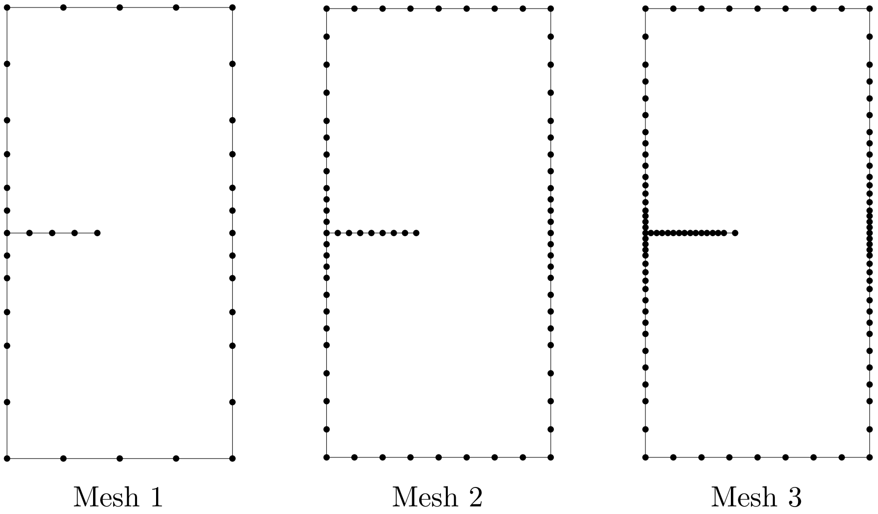

Figure 5.7: Meshes employed for the analysis of the problem in Fig. 5.6.

5.5.4 Double edge cracked panel

As the last example, a long plate with double surface breaking cracks under uniform tension as shown schematically in Fig. 5.8 is considered. The cracks are inclined an angle of 45^o with respect to x_1-axis and have a length of a for each. The width and the height of plate are $2w$ and $2h$, respectively. The dimensions of plate are taken as $a/w = 0.5$ and $h/w = 5$. An orthotropic material, with the constants displayed in Table 5.5, is employed for the analysis of the problem. The condition of plane stress is assumed.

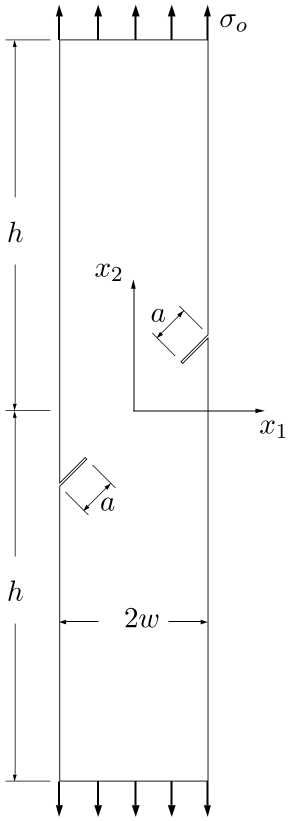

Figure 5.8: Specimen with double edged crack under uniform tension.

E_{11} (GPa)	E_{22} (GPa)	ν_{12}	μ_{12} (GPa)
345	516	0.131	173

Table 5.5: Properties of an orthotropic material employed for the analysis of the problem of Fig. 5.8.

Fig. 5.9 shows the meshes employed for the analysis of this problem in which mesh 3 has the same mesh on the boundary as that of mesh 2 but the mesh on crack is refined in the region behind the tip element. Results of the normalized T-stress are displayed in Table 5.6. The result obtained by Shah *et al.* [60] is also shown for comparison. A difference between the two results of 4.3% is observed. Note that the result from Shah *et al.* is graphically presented in [60].

Mesh #	$\frac{T}{\sigma_o}$
1	0.3013
2	0.2984
3	0.2972
Shah *et al.* [60]	0.285

Table 5.6: Normalized T-stress for the problem of Fig. 5.8.

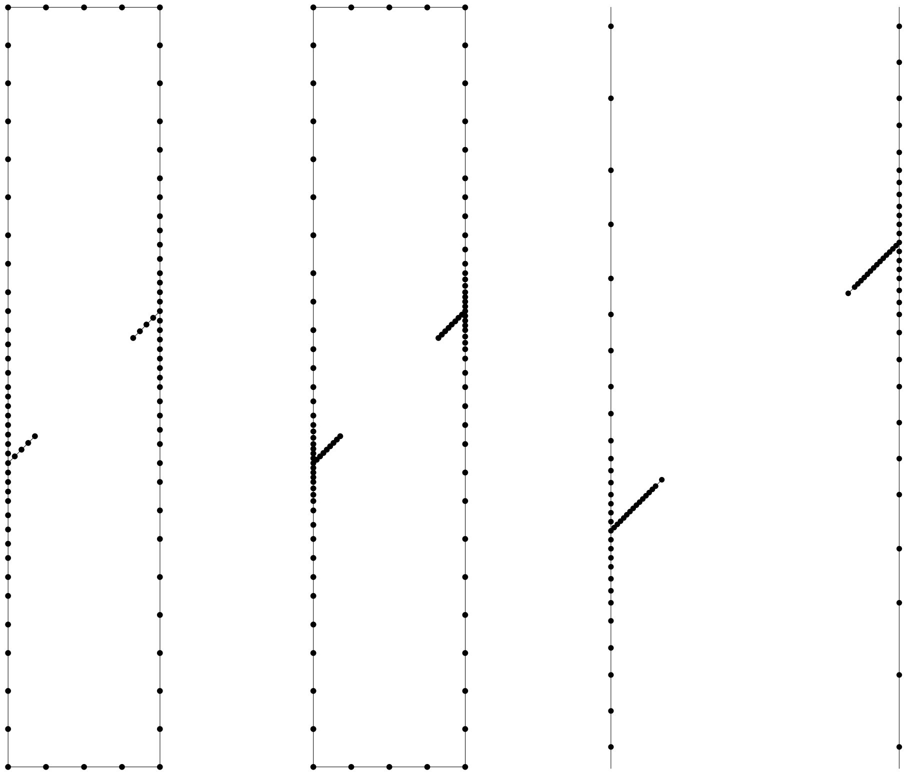

Mesh 1 Mesh 2 Mesh 3

Figure 5.9: Meshes employed for the analysis of the problem in Fig. 5.8.

Chapter 6

Conclusions

A computational procedure based upon the Symmetric Galerkin Boundary Element Method (SGBEM) has been developed for fracture analysis of two-dimensional multi-field media. The important feature of the method is that all the kernels appearing in the final forms of integral equations are weakly-singular of order $\mathcal{O}(\ln r)$ which is suitable for numerical integration and for utilization of standard C^o element. In addition, a crack-tip element is developed with special shape functions to properly model the relative crack-face displacements in the vicinity of the crack tip. Also, extra degrees of freedom are incorporated to the crack-tip element so that the generalized stress intensity factors are obtained directly from the solution of the governing discretized system of equations. To extend the capability of the method to model inhomogeneous domain, a procedure for modeling multiple-region problems is also developed. The procedure is based upon a suitable application of the integral equations (for both displacement and traction) on the interfaces so that the symmetry of the global coefficient matrix is assured. Hence, the efficiency of the Symmetric Galerkin method is preserved.

The accuracy and versatility of the developed method are illustrated through various example problems including cracks in unbounded domains and cracks in finite domains with various boundary conditions and loadings. An example of a crack in a multiple region domain was also considered. Highly accurate results for generalized stress intensity factors are obtained.

To fulfill the capacity of the developed procedure for fracture analysis using 2-parameter model, a technique to compute T-stress in anisotropic two-dimensional cracked media has been developed. The efficiency of the technique is that T-stress is simply obtained from the summation of crack-face displacements which are computed from the boundary data (displacement and traction) through a (weakly-singular) integral relation. The technique is applicable for mixed-mode fractures in general two-dimensional anisotropic domains. Example problems have been considered to demonstrate the accuracy of the method and excellent agreement with analytical solutions and other authors in literature were found.

As one of the significant applications of the developed procedure, the modeling of crack evolution in a multi-field media can be investigated. This application is quite simple to implement in two-dimensional context by either adding new elements or stretching the crack-tip element during the propagation. However, a proper criterion for crack growth initiation in general anisotropic elastic media (and especially in multi-field media) has not been clearly identified. The developed computational tool is well suited to verify experimental models in finding a crack growth criterion. In addition, with the ability to provide T-stress, the current procedure is ideal for the investigation of fracture and/or crack propagation using a 2-parameter model which takes into account both stress intensity factors and T-stress.

Appendices

Appendix A

Somiglina's identity

Consider a homogeneous finite two-dimensional domain Ω as shown schematically in Fig. A.1. The boundary Γ of the domain composes of two parts: Γ_t on which traction is prescribed and Γ_u on which displacement is prescribed (i.e. $\Gamma = \Gamma_t + \Gamma_u$). In the absence of body force, the displacement u_K satisfies the governing equilibrium equation as

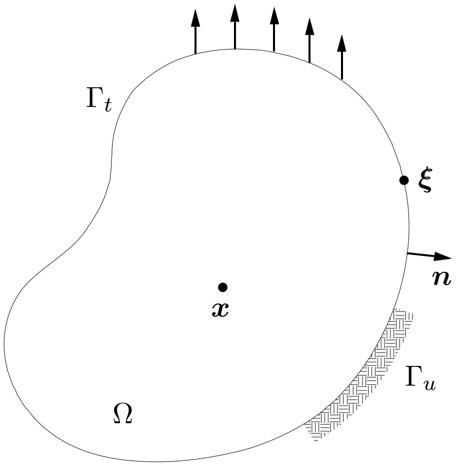

Figure A.1: Schematic of homogeneous finite domain under general boundary conditions.

$$E_{\alpha IJ\beta} \frac{\partial^2}{\partial \xi_\alpha \partial \xi_\beta} u_J(\boldsymbol{\xi}) \quad = \quad 0 \tag{A.1}$$

where $\boldsymbol{\xi} \in \Omega$ and $E_{\alpha IJ\beta}$ are material constants.

To proceed, multiply equation (A.1) with the fundamental solution defined by equation (2.47) in Chapter 2 and integrate over the domain Ω, one obtains

$$\int_{\Omega} E_{\alpha IJ\beta} \frac{\partial^2 u_J(\boldsymbol{\xi})}{\partial \xi_\alpha \partial \xi_\beta} U_I^P(\boldsymbol{\xi}-\boldsymbol{x}) dA(\boldsymbol{\xi}) \quad = \quad 0 \tag{A.2}$$

where $\boldsymbol{x}$ is the source point of the fundamental solution. Integrating by parts twice, equation (A.2) becomes

$$\begin{aligned} -\int_{\Omega} E_{\alpha IJ\beta} u_J(\boldsymbol{\xi}) \frac{\partial^2 U_I^P(\boldsymbol{\xi}-\boldsymbol{x})}{\partial \xi_\alpha \partial \xi_\beta} dA(\boldsymbol{\xi}) &= \int_{\Gamma} E_{\alpha IJ\beta} \frac{\partial u_J(\boldsymbol{\xi})}{\partial \xi_\beta} U_I^P(\boldsymbol{\xi}-\boldsymbol{x}) n_\alpha(\boldsymbol{\xi}) ds(\boldsymbol{\xi}) \\ &- \int_{\Gamma} E_{\alpha IJ\beta} u_J(\boldsymbol{\xi}) \frac{\partial U_I^P(\boldsymbol{\xi}-\boldsymbol{x})}{\partial \xi_\alpha} n_\beta(\boldsymbol{\xi}) ds(\boldsymbol{\xi}) \end{aligned} \tag{A.3}$$

where $\boldsymbol{n}$ is the normal to the boundary Γ at the point $\boldsymbol{\xi}$. Utilizing the equilibrium equation of fundamental solution

$$E_{\alpha IJ\beta} \frac{\partial^2 U_I^P(\boldsymbol{\xi}-\boldsymbol{x})}{\partial \xi_\alpha \partial \xi_\beta} = \frac{\partial S_{\beta J}^P(\boldsymbol{\xi}-\boldsymbol{x})}{\partial \xi_\beta} = -\delta_{JP} \delta(\boldsymbol{\xi}-\boldsymbol{x}) \tag{A.4}$$

where $S_{\beta J}^P$ denotes the fundamental solution for stress (i.e. $S_{\beta J}^P = E_{\beta JI\alpha} \frac{\partial U_I^P}{\partial \xi_\alpha}$), $\delta(\boldsymbol{\xi}-\boldsymbol{x})$ is the Dirac delta function, and the symmetric property of the material constants is employed.

Utilizing equation (A.3) for the left-hand side of equation (A.3), one obtains an integral equation for the displacement at a source point $\boldsymbol{x} \in \Omega$ in terms of the data on boundary, i.e. the well-known Somigliana's identity, as

$$u_P(\boldsymbol{x}) \quad = \quad \int_{\Gamma} U_I^P(\boldsymbol{\xi}-\boldsymbol{x}) t_I(\boldsymbol{\xi}) ds(\boldsymbol{\xi}) - \int_{\Gamma} S_{\beta J}^P(\boldsymbol{\xi}-\boldsymbol{x}) n_\beta(\boldsymbol{\xi}) u_J(\boldsymbol{\xi}) ds(\boldsymbol{\xi}) \tag{A.5}$$

Appendix B

Radon Transform

A brief summary of definition and properties of the Radon transform that relates to our development is presented here. More details of the Radon transform can be found in [19].

B.1 Definition

Let $f(\boldsymbol{\xi})$ is a function defined on a domain $\Omega \in \mathbb{R}^2$. The Radon transform of f is the line integral of f along any line L in the plane provided the integral exists, i.e.

$$\hat{f} = \mathcal{R}f = \int_L f(\boldsymbol{\xi})ds \tag{B.1}$$

where ds is an increment of the length along L.

If the line L is defined by a unit vector $\boldsymbol{z}$ which is perpendicular to the line L and a scalar p which is the distance from the origin of the coordinate system to the line L as shown in Fig. B.1, then the definition (B.1) can be re-expressed as

$$\hat{f}(p, \boldsymbol{z}) = \mathcal{R}f(\boldsymbol{\xi}) = \int_{\mathbb{R}^2} f(\boldsymbol{\xi})\delta(p - \boldsymbol{z} \cdot \boldsymbol{\xi})dS \tag{B.2}$$

where $\delta(p - \boldsymbol{z} \cdot \boldsymbol{\xi})$ is the 2D Dirac delta function ‘centered’ at the line $p = \boldsymbol{z} \cdot \boldsymbol{x}$, dS represents for the infinitesimal area, and the surface integral is taken over the whole plane $\mathbb{R}^2$.

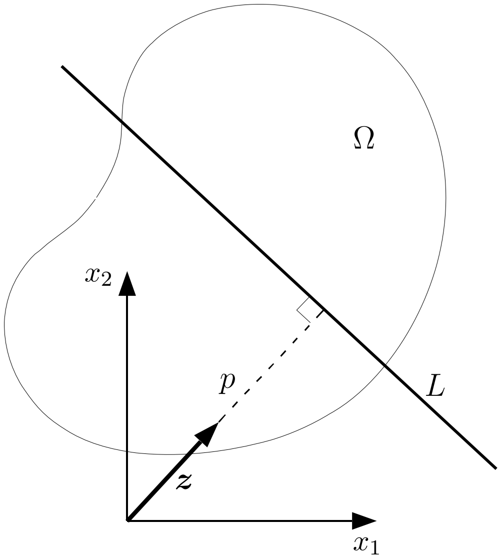

Figure B.1: Line L and its parameters utilized in the definition (B.2) for Radon transform.

B.2 Shifting property

Consider a function $f(\boldsymbol{\xi} - \boldsymbol{x})$ where $\boldsymbol{\xi} - \boldsymbol{x}$ is a vector pointing from a fixed point $\boldsymbol{x}$ to a point $\boldsymbol{\xi}$ in the domain Ω. The Radon transform of this function is given by

$$\begin{aligned} \mathcal{R}f(\boldsymbol{\xi} - \boldsymbol{x}) &= \int_{\mathbb{R}^2} f(\boldsymbol{\xi} - \boldsymbol{x})\delta(p - \boldsymbol{z} \cdot \boldsymbol{\xi}) dS \\ &= \int_{\mathbb{R}^2} f(\boldsymbol{\xi} - \boldsymbol{x})\delta\Big[(p - \boldsymbol{z} \cdot \boldsymbol{x}) - \boldsymbol{z} \cdot (\boldsymbol{\xi} - \boldsymbol{x})\Big] dS \\ &= \hat{f}(p - \boldsymbol{z} \cdot \boldsymbol{x}, \boldsymbol{z}) \end{aligned} \tag{B.3}$$

B.3 Inversion formula

The inversion of a function $\hat{f}(p, \boldsymbol{z})$ defined in (B.2) is given by Deans [19] as

$$f(\boldsymbol{\xi}) = \frac{1}{4\pi^2} \oint_{\|\boldsymbol{z}\|=1} \int_{-\infty}^{\infty} \frac{\partial^2 \hat{f}(p, \boldsymbol{z})}{\partial p^2} \ln |p - \boldsymbol{z} \cdot \boldsymbol{\xi}| \, dp \, d\boldsymbol{z} \tag{B.4}$$

where the integral $\oint_{\|\boldsymbol{z}\|=1}(\cdot)\,d\boldsymbol{z}$ denotes the contour integral over a unit circle, i.e., with $\boldsymbol{z} = (\cos\phi, \sin\phi)$, then $\oint_{\|\boldsymbol{z}\|=1}(\cdot)d\boldsymbol{z} = \int_0^{2\pi}(\cdot)\,d\phi$.

Utilizing the shifting property (B.3), equation (B.4) becomes

$$f(\boldsymbol{\xi} - \boldsymbol{x}) = \frac{1}{4\pi^2}\oint_{\|\boldsymbol{z}\|=1}\int_{-\infty}^{\infty}\frac{\partial^2 \hat{f}(p - \boldsymbol{z}\cdot\boldsymbol{x}, \boldsymbol{z})}{\partial p^2}\ln|p - \boldsymbol{z}\cdot\boldsymbol{\xi}|\,dp\,d\boldsymbol{z} \tag{B.5}$$

For a particular case where the function $\partial^2\hat{f}(p - \boldsymbol{z}\cdot\boldsymbol{x}, \boldsymbol{z})/\partial p^2$ is in the form of

$$\frac{\partial^2 \hat{f}(p - \boldsymbol{z}\cdot\boldsymbol{x}, \boldsymbol{z})}{\partial p^2} = g(\boldsymbol{z})\delta(p - \boldsymbol{z}\cdot\boldsymbol{x}) \tag{B.6}$$

where $g(\boldsymbol{z})$ is a well-defined function of $\boldsymbol{z}$ (i.e. $g(\boldsymbol{z})$ is independent of p), then the inversion formula (B.5) can be expressed in a simple form as

$$f(\boldsymbol{\xi} - \boldsymbol{x}) = \frac{1}{4\pi^2}\oint_{\|\boldsymbol{z}\|=1} g(\boldsymbol{z})\ln|\boldsymbol{z}\cdot(\boldsymbol{\xi} - \boldsymbol{x})|\,d\boldsymbol{z} \tag{B.7}$$

B.4 Transform of Dirac delta function

The Radon transform of a 2D Dirac delta function centered at $\boldsymbol{x}$ is a Dirac delta function in the transformed space and is given as

$$\mathcal{R}\delta(\boldsymbol{\xi} - \boldsymbol{x}) = \delta(p - \boldsymbol{z}\cdot\boldsymbol{x}) \tag{B.8}$$

B.5 Transform of derivative

The Radon transform of derivative of a function $f(\boldsymbol{\xi})$ with respect to $\boldsymbol{\xi}$ is given as

$$\mathcal{R}\left(\frac{\partial f(\boldsymbol{\xi})}{\partial \xi_k}\right) = z_k\frac{\partial \hat{f}(p, \boldsymbol{z})}{\partial p} \tag{B.9}$$

Appendix C

Proof that $H^P_{\alpha J} n_\alpha$ =O(1)

The expression the kernel $H^P_{\alpha J}$ derived in Chapter 2 is restated here as

$$H^P_{\alpha J}(\boldsymbol{\xi} - \boldsymbol{y}) = \delta_{JP} \frac{\partial}{\partial \xi_\alpha} (\frac{-\ln r}{2\pi}) = -\delta_{JP} \frac{\xi_\alpha - y_\alpha}{2\pi r^2} \tag{C.1}$$

where $r = \|\boldsymbol{\xi} - \boldsymbol{y}\|$ is the distance from source point $\boldsymbol{y}$ to field point $\boldsymbol{\xi}$.

This section will prove that the multiplication of the kernel $H^P_{\alpha J}$ with the normal (to the considered curve Γ) at either the source point $\boldsymbol{y}$ or the field point $\boldsymbol{\xi}$ is of order $\mathcal{O}(1)$ as $r \to 0$. The proof here is based on the work derived by Xiao [84] for three-dimensional case.

C.1 Kernel $H^P_{\alpha J}(\boldsymbol{\xi} - \boldsymbol{y}) n_\alpha(\boldsymbol{y}) = -\delta_{JP} \frac{\boldsymbol{r} \cdot \boldsymbol{n}(\boldsymbol{y})}{2\pi r^2}$

A point $\boldsymbol{y}$ is on a (locally smooth) curve Γ. At point $\boldsymbol{y}$, introduce the coordinate system (ξ_1, ξ_2) such that ξ_2 is directed along the opposite direction of the normal $\boldsymbol{n}(\boldsymbol{y})$ of the curve Γ at source point $\boldsymbol{y}$ as shown in Fig. C.1. In the vicinity of $\boldsymbol{y}$, Γ can be represented as

$$\xi_2 = f(\xi_1) \tag{C.2}$$

where f is a function to define the curve Γ. Then

$$\boldsymbol{n}(\boldsymbol{y}) \cdot \boldsymbol{r} = -\xi_2 = -f(\xi_1) \tag{C.3}$$

To proceed, a Taylor expansion of f about the source point $\boldsymbol{y}$ is given as

$$f(\xi_1) = \frac{1}{2} f''(0) \xi_1^2 + \mathcal{O}(\xi_1^3) \tag{C.4}$$

where we used the fact of $f'(0) = 0$ since the normal vector $\boldsymbol{n}(\boldsymbol{y})$ is in the direction of ξ_2-axis.

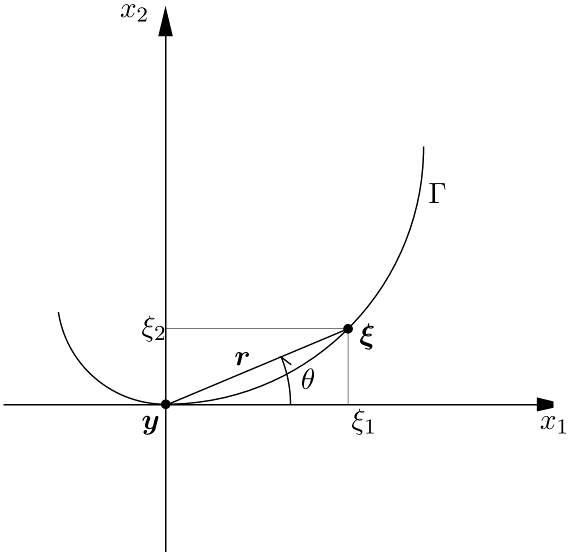

Figure C.1: Local coordinate system employed for the proof.

Note that $\xi_1 = r \cos\theta$, then equation (C.4) becomes

$$f(\xi_1) = \frac{1}{2} f''(0) r^2 \cos^2\theta + \mathcal{O}(r^3) \tag{C.5}$$

The combination of equations (C.3) and (C.5) leads to the results of

$$\frac{\boldsymbol{n}(\boldsymbol{y}) \cdot \boldsymbol{r}}{r^2} = \mathcal{O}(1) \text{ as } r \to 0 \tag{C.6}$$

C.2 Kernel $H^P_{\alpha J}(\boldsymbol{\xi}-\boldsymbol{y})n_\alpha(\boldsymbol{\xi}) - \delta_{JP}\frac{\boldsymbol{r}\cdot\boldsymbol{n}(\boldsymbol{\xi})}{2\pi r^2}$

With the expression for Γ given by equation (C.2), the components of normal vector $\boldsymbol{n}$ at the field point $\boldsymbol{\xi}$ are as follows

$$\boldsymbol{n} = \frac{1}{\sqrt{\big(f'(\xi_1)\big)^2+1}}\big(f'(\xi_1), -1\big) \tag{C.7}$$

We then have

$$\boldsymbol{n}(\boldsymbol{\xi})\cdot\boldsymbol{r} = \frac{1}{\sqrt{\big(f'(\xi_1)\big)^2+1}}\big(f'(\xi_1)\xi_1 - \xi_2\big) \tag{C.8}$$

Forming Taylor expansion of $f'(t) = f'(\xi_1)$ about $\boldsymbol{y}$, we have

$$f'(\xi_1) = f''(0)\xi_1 + \mathcal{O}(\xi_1^2) \tag{C.9}$$

Combining equations (C.4), (C.8) and (C.9), we have

$$\begin{aligned}\boldsymbol{n}(\boldsymbol{\xi})\cdot\boldsymbol{r} &= \frac{1}{\sqrt{\big(f''(0)\big)^2\xi_1^2+1+\mathcal{O}(\xi_1^3)}}\big(\frac{1}{2}f''(0)\xi_1^2+\mathcal{O}(\xi_1^3)\big)\\ &= \frac{1}{2}f''(0)\xi_1^2+\mathcal{O}(\xi_1^3) \text{ as } r\to 0\end{aligned} \tag{C.10}$$

Similarly to the previous case, with the note of $\xi_1 = r\cos\theta$, equation (C.10) leads to

$$\frac{\boldsymbol{n}(\boldsymbol{\xi})\cdot\boldsymbol{r}}{r^2} = \mathcal{O}(1) \text{ as } r\to 0 \tag{C.11}$$

Appendix D

Closed form expressions of the kernels for isotropic material

The (weakly-singular) kernels that were derived in Chapter 2 are applicable for multi-field media. This appendix will show that these kernels are reduced to simpler forms, which were obtained by other authors in literature, when applying for isotropic elastic material.

D.1 Expressions of the kernels for general anisotropic elasticity

Summary of the kernels for anisotropic elastic material are given as

$$U_j^p(\boldsymbol{\xi}-\boldsymbol{y}) = K_{j\alpha}^{p\alpha} \tag{D.1}$$

$$G_j^p(\boldsymbol{\xi}-\boldsymbol{y}) = \epsilon_{\zeta\alpha} C_{\zeta jk\beta}\, K_{k\beta}^{p\alpha} \tag{D.2}$$

$$C_j^k(\boldsymbol{\xi}-\boldsymbol{y}) = \big(C_{\eta kp\beta} C_{\eta jm\gamma} - \frac{1}{3} C_{\eta jk\eta} C_{\beta pm\gamma}\big)\, K_{m\gamma}^{p\beta} \tag{D.3}$$

where $C_{\zeta JK\beta}$ are the elastic moduli of the material, and

$$K_{j\beta}^{i\alpha} = -\frac{1}{4\pi^2} \oint_{\|\boldsymbol{z}\|=1} (\boldsymbol{z},\boldsymbol{z})_{ij}^{-1}\, z_\alpha z_\beta \big(\ln r + \ln|\boldsymbol{z}\cdot\boldsymbol{e}|\big)\, d\boldsymbol{z} \tag{D.4}$$

in which $r = ||\boldsymbol{\xi}-\boldsymbol{y}||$, $(\boldsymbol{z},\boldsymbol{z})_{ij} = z_\alpha C_{\alpha ij\beta} z_\beta$ and the contour integral is to be evaluated over a unit circle $\|\boldsymbol{z}\| = 1$.

D.2 Closed form expression for $(\boldsymbol{z},\boldsymbol{z})^{-1}_{ij}$

For isotropic material, the elastic moduli $C_{\zeta jk\beta}$ are given as

$$C_{ijkl} = \lambda\delta_{ij}\delta_{kl} + \mu(\delta_{ik}\delta_{jl} + \delta_{il}\delta_{jk}) \tag{D.5}$$

where $\{\lambda, \mu\}$ are the Lame's constants which are determined from the Young's modulus E and the Poisson's ratio ν as

$$\lambda = \frac{E\nu}{(1+\nu)(1-2\nu)} \tag{D.6}$$

$$\mu = \frac{E}{2(1+\nu)} \tag{D.7}$$

Then the matrix $(\boldsymbol{z},\boldsymbol{z})_{ij}$ are obtained as

$$(\boldsymbol{z},\boldsymbol{z}) = \begin{bmatrix} (\lambda+2\mu)z_1^2 + \mu z_2^2 & (\lambda+\mu)z_1 z_2 & 0 \\ (\lambda+\mu)z_1 z_2 & \mu z_1^2 + (\lambda+\mu)z_2^2 & 0 \\ 0 & 0 & \mu \end{bmatrix} \tag{D.8}$$

The inversion of $(\boldsymbol{z},\boldsymbol{z})$ is ready to obtained as

$$(\boldsymbol{z},\boldsymbol{z})^{-1} = \frac{1+\nu}{E(1-\nu)} \begin{bmatrix} 1-2\nu+z_2^2 & -z_1 z_2 & 0 \\ -z_1 z_2 & 1-2\nu+z_1^2 & 0 \\ 0 & 0 & 2(1-\nu) \end{bmatrix} \tag{D.9}$$

D.3 Some useful integrals

1. For $n \in \{1, 2, \ldots, N\}$

$$\int_{-\pi/2}^{\pi/2} \cos(2n\phi)\ln(\cos(\phi))d\phi = \frac{(-1)^{n+1}\pi}{2n} \tag{D.10}$$

$$\int_{-\pi/2}^{\pi/2} \sin(2n\phi)\ln(\cos(\phi))d\phi = 0 \tag{D.11}$$

2. For an angular function $f(\phi)$ defined on $[0, 2\pi]$ which is an even function with respect to the variable ϕ such that $f(\phi) = f(\phi + \pi)$, the following integral holds with any value of θ

$$\int_0^{2\pi} f(\phi) \ln|\cos(\phi - \theta)| d\phi = 2 \int_{-\frac{\pi}{2}+\theta}^{\frac{\pi}{2}+\theta} f(\phi) \ln\big(cos(\phi - \theta)\big) d\phi \tag{D.12}$$

Equation (D.12) is simply proved by changing the variable $\psi = \phi - \theta$, with the note that $f(\psi) = f(\psi + \pi)$.

With any two unit vectors $\boldsymbol{z}$ and $\boldsymbol{e}$ having direction cosines ϕ and θ respectively, as shown in Fig. D.1, the following results are the direct application of the equation (D.12)

$$\oint_{\|\boldsymbol{z}\|=1} \ln|\boldsymbol{z} \cdot \boldsymbol{e}|, d\boldsymbol{z} = -2\pi \ln 2 \tag{D.13}$$

$$\oint_{\|\boldsymbol{z}\|=1} \cos^2\phi \ln|\boldsymbol{z} \cdot \boldsymbol{e}|, d\boldsymbol{z} = -\frac{\pi}{2}(2\ln 2 - \cos 2\theta) \tag{D.14}$$

$$\oint_{\|\boldsymbol{z}\|=1} \sin^2\phi \ln|\boldsymbol{z} \cdot \boldsymbol{e}|, d\boldsymbol{z} = -\frac{\pi}{2}(2\ln 2 + \cos 2\theta) \tag{D.15}$$

$$\oint_{\|\boldsymbol{z}\|=1} \cos\phi \sin\phi \ln|\boldsymbol{z} \cdot \boldsymbol{e}|, d\boldsymbol{z} = \frac{\pi}{2}\sin 2\theta \tag{D.16}$$

$$\oint_{\|\boldsymbol{z}\|=1} \cos^2\phi \sin^2\phi \ln|\boldsymbol{z} \cdot \boldsymbol{e}|, d\boldsymbol{z} = -\frac{\pi}{16}(4\ln 2 - \cos 4\theta) \tag{D.17}$$

$$\oint_{\|\boldsymbol{z}\|=1} \cos^4\phi \ln|\boldsymbol{z} \cdot \boldsymbol{e}|, d\boldsymbol{z} = -\frac{\pi}{16}(12\ln 2 - 8\cos 2\theta + \cos 4\theta) \tag{D.18}$$

$$\oint_{\|\boldsymbol{z}\|=1} \sin^4\phi \ln|\boldsymbol{z} \cdot \boldsymbol{e}|, d\boldsymbol{z} = -\frac{\pi}{16}(12\ln 2 + 8\cos 2\theta + \cos 4\theta) \tag{D.19}$$

$$\oint_{\|\boldsymbol{z}\|=1} \cos^3\phi \sin\phi \ln|\boldsymbol{z} \cdot \boldsymbol{e}|, d\boldsymbol{z} = \frac{\pi}{16}(4\sin 2\theta - \sin 4\theta) \tag{D.20}$$

$$\oint_{\|\boldsymbol{z}\|=1} \sin^3\phi \cos\phi \ln|\boldsymbol{z} \cdot \boldsymbol{e}|, d\boldsymbol{z} = \frac{\pi}{16}(4\sin 2\theta + \sin 4\theta) \tag{D.21}$$

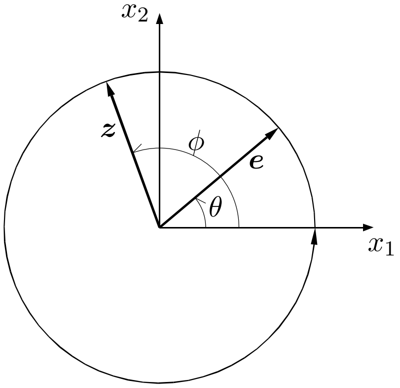

Figure D.1: Schematic of unit vectors $\boldsymbol{z}$ and $\boldsymbol{e}$ appearing in the useful integrals.

D.4 Reduction of the kernel U_j^p

Utilizing the expressions of matrix $(\boldsymbol{z},\boldsymbol{z})^{-1}$ shown in equation (D.9) and the integrals shown in equations (D.10)-(D.21), the solution of kernel U_j^p for isotropic material are derived as follows

$$\begin{aligned} U_\beta^\alpha(\boldsymbol{\xi}-\boldsymbol{y}) &= \frac{1+\nu}{4\pi E(1-\nu)}\big[(4\nu-3)\ln\big(\frac{r}{2}\big)\delta_{\alpha\beta}-\frac{\delta_{\alpha\beta}}{2}+\frac{\partial r}{\partial \xi_\alpha}\frac{\partial r}{\partial \xi_\beta}\big] && \text{(D.22)} \\ U_3^3(\boldsymbol{\xi}-\boldsymbol{y}) &= -\frac{1+\nu}{\pi E}\ln\big(\frac{r}{2}\big) && \text{(D.23)} \end{aligned}$$

We note that the results of U_β^α in (D.22) differ with that existing in the literature [32] for plane strain problem by just a constant which represents for a rigid body motion of the displacement fundamental solution.

D.5 Reduction of the kernel G_j^p

Again, utilizing the results of (D.9) for the matrix $(\boldsymbol{z},\boldsymbol{z})^{-1}$ and the integrals (D.10)-(D.21), the solution of kernel G_j^p for isotropic material is obtained after some calculation and simplification as follows

$$G^\alpha_\beta(\boldsymbol{\xi}-\boldsymbol{y}) \quad = \quad -\frac{1}{4\pi(1-\nu)}\big[(1-2\nu)\epsilon_{\alpha\beta}\ln\big(\frac{r}{2}\big)+\frac{\epsilon_{\alpha\beta}}{2}+\epsilon_{\beta\gamma}\frac{\partial r}{\partial \xi_\alpha}\frac{\partial r}{\partial \xi_\gamma}\big] \tag{D.24}$$

where $\epsilon_{\alpha\beta}$ is 2D permutation symbol (i.e. $\epsilon_{11}=\epsilon_{22}=0, \epsilon_{12}=-\epsilon_{21}=1$).

For the purpose of discussion, relation between the result (D.24) with the result obtained by Ghosh *et al.* [32] will be pointed out here in what follows. Ghosh *et al.* calculated a quantity R_{ij} such that

$$R_{\alpha\beta}(\boldsymbol{\xi}-\boldsymbol{y}) = \frac{\partial}{\partial s}T_{\alpha\beta}(\boldsymbol{\xi}-\boldsymbol{y}) \tag{D.25}$$

where s is the arc length and $T_{\alpha\beta}$ relates to the fundamental stress $S^\alpha_{\zeta\beta}$ as

$$T_{\alpha\beta}(\boldsymbol{\xi}-\boldsymbol{y}) = S^\alpha_{\zeta\beta}(\boldsymbol{\xi}-\boldsymbol{y})n_\zeta(\boldsymbol{\xi}) \tag{D.26}$$

We remind here that the stress fundamental solution $S^\alpha_{\zeta\beta}$ relates to the kernel G^α_β through a decomposition that was mentioned in Chapter 2 as

$$S^\alpha_{\zeta\beta}(\boldsymbol{\xi}-\boldsymbol{y}) = \epsilon_{\zeta\gamma}\frac{\partial}{\partial \xi_\gamma}G^\alpha_\beta(\boldsymbol{\xi}-\boldsymbol{y}) + \delta_{\alpha\beta}\frac{\partial}{\partial \xi_\zeta}\big(\frac{-\ln r}{2\pi}\big) \tag{D.27}$$

Combining (D.25), (D.26) and (D.27) to obtain a relation between $R_{\alpha\beta}$ presented in [32] and our kernel G^α_β as follows

$$\epsilon_{\zeta\gamma}\frac{\partial R_{\alpha\beta}}{\partial \xi_\gamma}n_\zeta = \big(\epsilon_{\zeta\gamma}\frac{\partial G^\alpha_\beta}{\partial \xi_\gamma} - \frac{\delta_{\alpha\beta}}{2\pi r}\frac{\partial r}{\partial \xi_\zeta}\big)n_\zeta \tag{D.28}$$

where the expression of the derivative with respect to arc length $\frac{\partial}{\partial s}=\epsilon_{\zeta\gamma}\frac{\partial}{\partial \xi_\gamma}n_\zeta$ was used. Upon utilizing the arbitrariness of normal vector $\boldsymbol{n}$, the final relation between $R_{\alpha\beta}$ and G^α_β is given as

$$\epsilon_{\zeta\gamma}\frac{\partial R_{\alpha\beta}}{\partial \xi_\gamma} = \epsilon_{\zeta\gamma}\frac{\partial G^\alpha_\beta}{\partial \xi_\gamma} - \frac{\delta_{\alpha\beta}}{2\pi r}\frac{\partial r}{\partial \xi_\zeta} \tag{D.29}$$

Note that θ is the cosine direction of the vector $\boldsymbol{r} = \boldsymbol{\xi} - \boldsymbol{y}$, i.e. $\tan\theta = \frac{\xi_2 - y_2}{\xi_1 - y_1}$, then it is readily to have the following results

$$\frac{\partial \theta}{\partial \xi_1} = \frac{y_2 - \xi_2}{r^2} = -\frac{1}{r}\frac{\partial r}{\partial \xi_2} \tag{D.30}$$

$$\frac{\partial \theta}{\partial \xi_2} = \frac{\xi_1 - y_1}{r^2} = \frac{1}{r}\frac{\partial r}{\partial \xi_1} \tag{D.31}$$

or, writing equations (D.30) and (D.31) in index form, we have the result as

$$\frac{1}{r}\frac{\partial r}{\partial \xi_\zeta} = \epsilon_{\zeta\gamma}\frac{\partial \theta}{\partial \xi_\gamma} \tag{D.32}$$

Utilizing equation (D.32), equation (D.29) becomes

$$\epsilon_{\zeta\gamma}\frac{\partial R_{\alpha\beta}}{\partial \xi_\gamma} = \epsilon_{\zeta\gamma}\frac{\partial G^\alpha_\beta}{\partial \xi_\gamma} - \frac{\delta_{\alpha\beta}}{2\pi}\epsilon_{\zeta\gamma}\frac{\partial \theta}{\partial \xi_\gamma} \tag{D.33}$$

then, a particular solution of (D.33) is ready to obtained as

$$\begin{aligned} R_{\alpha\beta} &= G^\alpha_\beta - \frac{\delta_{\alpha\beta}}{2\pi}\theta \\ &= -\frac{1}{4\pi(1-\nu)}\big[(1-2\nu)\epsilon_{\alpha\beta}\ln\big(\frac{r}{2}\big) + \frac{\epsilon_{\alpha\beta}}{2} + \epsilon_{\beta\gamma}\frac{\partial r}{\partial \xi_\alpha}\frac{\partial r}{\partial \xi_\gamma}\big] - \frac{\delta_{\alpha\beta}}{2\pi}\theta \end{aligned} \tag{D.34}$$

The result (D.34) differs with that obtained by Ghosh *et al.* [32] by only a constant.

D.6 Reduction of kernel C^k_j

Utilizing the results of (D.9) for the matrix $(\boldsymbol{z}, \boldsymbol{z})^{-1}$ and the useful integrals (D.10)-(D.21), the solution of kernel G^p_j for isotropic material is obtained after a lengthy calculation which is not presented here for simplicity. The final results are as follows

$$
\begin{aligned}
C^{\alpha}_{\beta}(\boldsymbol{\xi}-\boldsymbol{y}) &= \frac{E}{4\pi(1-\nu^2)}\big[\ln\big(\frac{r}{2}\big)\delta_{\alpha\beta}+\frac{\delta_{\alpha\beta}}{2}-\frac{\partial r}{\partial \xi_\alpha}\frac{\partial r}{\partial \xi_\beta}\big] && \text{(D.35)}\\
C^{3}_{3}(\boldsymbol{\xi}-\boldsymbol{y}) &= \frac{E}{4\pi(1+\nu)}\ln\big(\frac{r}{2}\big) && \text{(D.36)}
\end{aligned}
$$

in which the result of C^{α}_{β} differs with that obtained by Frangi and Novati [24] (for plane strain problem) only by a constant.

Appendix E

Multiply connected domain

E.1 Basic integral relations

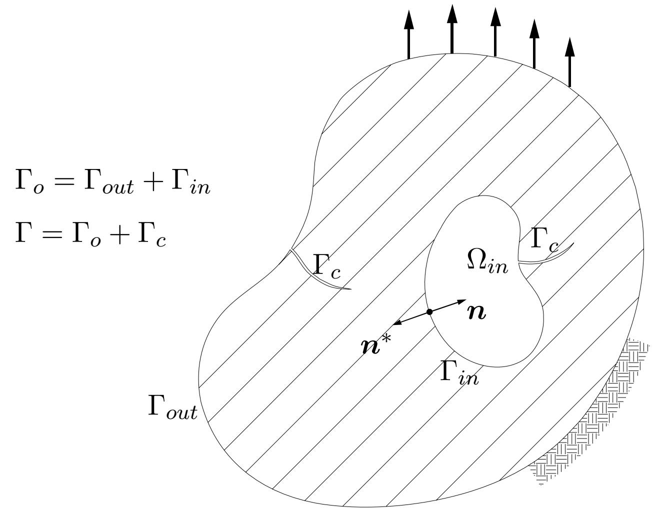

Figure E.1: Multiple-connected domain with inner boundary subjected to pure traction.

Consider a homogeneous multiply connected domain containing embedded and/or edge cracks as shown schematically in Fig. E.1. The ordinary boundary of the domain Γ_o is composed from two parts: the outer boundary denoted by Γ_{out} and the inner boundary denoted by Γ_{in} which is subjected to pure traction. For this domain, the displacement at a point $\boldsymbol{y} \in \Gamma_{out}$ is determined from equation (2.84) as

$$\begin{aligned}\frac{1}{2}u_P(\boldsymbol{y}) &= \int_{\Gamma_o} U_J^P(\boldsymbol{\xi}-\boldsymbol{y})t_J(\boldsymbol{\xi})ds(\boldsymbol{\xi}) + \int_{\Gamma} G_J^P(\boldsymbol{\xi}-\boldsymbol{y})Dv_J(\boldsymbol{\xi})ds(\boldsymbol{\xi}) \\ &- \int_{\Gamma} n_\alpha(\boldsymbol{\xi})H_{\alpha J}^P(\boldsymbol{\xi}-\boldsymbol{y})v_J(\boldsymbol{\xi})ds(\boldsymbol{\xi}) \end{aligned} \tag{E.1}$$

and the traction at any point $\boldsymbol{y} \in \Gamma$ is determined from equation (2.86) as

$$\begin{aligned} c(\boldsymbol{y})t_K(\boldsymbol{y}) &= D\int_{\Gamma_o} G_K^J(\boldsymbol{\xi}-\boldsymbol{y})t_J(\boldsymbol{\xi})ds(\boldsymbol{\xi}) - \int_{\Gamma_o} n_\alpha(\boldsymbol{y})H_{\alpha K}^J(\boldsymbol{\xi}-\boldsymbol{y})t_J(\boldsymbol{\xi})ds(\boldsymbol{\xi}) \\ &+ D\int_{\Gamma} C_J^K(\boldsymbol{\xi}-\boldsymbol{y})\,Dv_J(\boldsymbol{\xi})ds(\boldsymbol{\xi}) \end{aligned} \tag{E.2}$$

where $c = 1/2$ for $\boldsymbol{y} \in \Gamma_o$ and $c = 1$ for $\boldsymbol{y} \in \Gamma_c$, $D = \frac{\partial}{\partial s} = \epsilon_{\alpha\beta}\frac{\partial}{\partial \xi_\beta}n_\alpha$ is the derivative with respect to the arc length s, Γ is the total boundary (i.e. $\Gamma = \Gamma_o + \Gamma_c$), and

$$v_J(\boldsymbol{\xi}) = \begin{cases} u_J(\boldsymbol{\xi}) & , \quad \boldsymbol{\xi} \in \Gamma_o \\ \Delta u_J(\boldsymbol{\xi}) & , \quad \boldsymbol{\xi} \in \Gamma_c \end{cases} \tag{E.3}$$

The two integral equations (E.1) and (E.2) are then employed to form the associated weak-form boundary integral equations for displacement and traction which are the basis for a discretization process for solving nodal quantities as discussed in detail in Chapter 3. However, for a multiply connected domain which has an inner boundary subjected to pure traction, the governing system of equations resulting from the discretization process will be singular unless additional constraints are made on the inner boundary which is discussed in the next section.

E.2 Undetermined solution for multiply-connected domain

With reference to Fig. E.1, introduce Ω_{in} as a 'fictitious' region bounded by Γ_{in} which occupies the same material as the that of the original problem. Suppose that the region Ω_{in} is prescribed by a rigid body motion $\hat{u}$ (including translation and rotation, if any). For this region, since the rigid body motion does not induce any traction on the boundary, then by applying equation (E.1) for a point $\boldsymbol{y} \in \Gamma_{out}$, we have

$$0 = \int_{\Gamma_{in}} G_J^P(\boldsymbol{\xi} - \boldsymbol{y}) D\hat{u}_J(\boldsymbol{\xi}) ds(\boldsymbol{\xi}) - \int_{\Gamma_{in}} n_\alpha^*(\boldsymbol{\xi}) H_{\alpha J}^P(\boldsymbol{\xi} - \boldsymbol{y}) \hat{u}_J(\boldsymbol{\xi}) ds(\boldsymbol{\xi}) \tag{E.4}$$

and applying equation (E.2) for a point $\boldsymbol{y} \in \Gamma$, we have

$$0 = D \int_{\Gamma_{in}} C_J^K(\boldsymbol{\xi} - \boldsymbol{y})\, D\hat{u}_J(\boldsymbol{\xi})\, ds(\boldsymbol{\xi}) \tag{E.5}$$

where $\boldsymbol{n}^*$ is the normal vector at $\boldsymbol{\xi} \in \Gamma_{in}$ which directs 'outward' the region Ω_{in} (i.e. 'inward' the material of the original problem).

Adding equation (E.4) to equation (E.1) and equation (E.5) to equation (E.2), with the note that $\boldsymbol{n}^*(\boldsymbol{\xi}) = -\boldsymbol{n}(\boldsymbol{\xi})$ for any $\boldsymbol{\xi} \in \Gamma_{in}$, we have the following results for displacement and traction integral equations

$$\begin{aligned} \frac{1}{2} u_P(\boldsymbol{y}) &= \int_{\Gamma_o} U_J^P t_J(\boldsymbol{\xi}) ds(\boldsymbol{\xi}) + \int_{\Gamma - \Gamma_{in}} G_J^P D v_J(\boldsymbol{\xi}) ds(\boldsymbol{\xi}) \\ &- \int_{\Gamma - \Gamma_{in}} n_\alpha(\boldsymbol{\xi}) H_{\alpha J}^P v_J(\boldsymbol{\xi}) ds(\boldsymbol{\xi}) + \int_{\Gamma_{in}} G_J^P D\big[u_J(\boldsymbol{\xi}) - \hat{u}_J(\boldsymbol{\xi})\big] ds(\boldsymbol{\xi}) \\ &- \int_{\Gamma_{in}} n_\alpha(\boldsymbol{\xi}) H_{\alpha J}^P \big[u_J(\boldsymbol{\xi}) - \hat{u}_J(\boldsymbol{\xi})\big] ds(\boldsymbol{\xi}) \qquad \text{for } \boldsymbol{y} \in \Gamma_{out} \end{aligned} \tag{E.6}$$

$$\begin{aligned} c(\boldsymbol{y}) t_K(\boldsymbol{y}) &= D \int_{\Gamma_o} G_K^J\, t_J(\boldsymbol{\xi}) ds(\boldsymbol{\xi}) - \int_{\Gamma_o} n_\alpha(\boldsymbol{y}) H_{\alpha K}^J\, t_J(\boldsymbol{\xi}) ds(\boldsymbol{\xi}) \\ &+ D \int_{\Gamma - \Gamma_{in}} C_J^K\, D v_J(\boldsymbol{\xi})\, ds(\boldsymbol{\xi}) + D \int_{\Gamma_{in}} C_J^K\, D\big[u_J(\boldsymbol{\xi}) - \hat{u}_J(\boldsymbol{\xi})\big]\, ds(\boldsymbol{\xi}) \\ &\qquad \text{for } \boldsymbol{y} \in \Gamma \end{aligned} \tag{E.7}$$

Equations (E.6) and (E.7) shows that the basic integral equations for a multiple-connected domain subjected to pure traction is still valid with adding any rigid body motion to the real displacement for all points on the inner boundary. This fact results in the undetermined solution of the original discretized governing system of equations.

E.3 Treatment for multiply-connected domain

The non-uniqueness of the solution for multiply connected domain in SGBEM was recognized by Frangi and Novati [24] and a method was proposed to overcome this problem. However, this paper only mentioned about the problems under pure traction loading for both outer and inner boundaries. Perez-Gavilan and Aliabadi [53] [52]) reviewed the source of problem and proved that the non-uniqueness of the solution also appears in problems with arbitrary boundary conditions for the outer boundary. We found that our proof presented in the previous section is of similar to that presented by Perez-Gavilan and Aliabadi. For the treatment, we use the method proposed by Frangi and Novati [24] which is extended for the problems under general boundary conditions for the outer boundary.

To treat this problem, we add supplemental constraints to the inner boundary Γ_{in} to 'suppress' the rigid body motion of Ω_{in}. This procedure is actually adding a rigid body motion $\hat{\boldsymbol{u}}$ to Ω_{in} of the original problem and the nodal quantities on inner boundary Γ_{in} from the solution of the governing discretized equations are now $(\boldsymbol{u} - \hat{\boldsymbol{u}})$ instead of the real displacement $\boldsymbol{u}$. Once the rigid body motion $\hat{\boldsymbol{u}}$ is determined, the real displacement on the inner boundary of the original problem will then be obtained.

To determine $\hat{\boldsymbol{u}}$, we use the displacement integral equation (E.1) for two configurations: one is the inner domain Ω_{in} and the other one is the original problem. With $\boldsymbol{x} \in \Omega_{in}$, these equations are as follows

$$\hat{u}_P(\boldsymbol{x}) = \int_{\Gamma_{in}} G_J^P(\boldsymbol{\xi} - \boldsymbol{x})\, D\hat{u}_J(\boldsymbol{\xi})\, ds(\boldsymbol{\xi}) - \int_{\Gamma_{in}} H_{\alpha J}^P(\boldsymbol{\xi} - \boldsymbol{x})\, n_\alpha^*(\boldsymbol{\xi})\, \hat{u}_J(\boldsymbol{\xi})\, ds(\boldsymbol{\xi}) \tag{E.8}$$

$$\begin{aligned} 0 &= \int_{\Gamma_o} U_J^P(\boldsymbol{\xi} - \boldsymbol{x})\, t_J(\boldsymbol{\xi})\, ds(\boldsymbol{\xi}) + \int_{\Gamma} G_J^P(\boldsymbol{\xi} - \boldsymbol{x})\, Dv_J(\boldsymbol{\xi})\, ds(\boldsymbol{\xi}) \\ &- \int_{\Gamma} H_{\alpha J}^P(\boldsymbol{\xi} - \boldsymbol{x})\, n_\alpha(\boldsymbol{\xi})\, v_J(\boldsymbol{\xi})\, ds(\boldsymbol{\xi}) \end{aligned} \tag{E.9}$$

Adding equation (E.8) to equation (E.9), with the note that $\boldsymbol{n}^*(\boldsymbol{\xi}) = -\boldsymbol{n}(\boldsymbol{\xi})$, leads to the following equation for determining $\hat{\boldsymbol{u}}(\boldsymbol{x})$

$$\begin{aligned} \hat{u}_P(\boldsymbol{x}) &= \int_{\Gamma_o} U_J^P t_J(\boldsymbol{\xi})\, ds(\boldsymbol{\xi}) + \int_{\Gamma - \Gamma_{in}} G_J^P\, Dv_J(\boldsymbol{\xi})\, ds(\boldsymbol{\xi}) \\ &- \int_{\Gamma - \Gamma_{in}} H_{\alpha J}^P\, n_\alpha(\boldsymbol{\xi})\, v_J(\boldsymbol{\xi})\, ds(\boldsymbol{\xi}) + \int_{\Gamma_{in}} G_J^P\, D\big[u_J(\boldsymbol{\xi}) - \hat{u}_J(\boldsymbol{\xi})\big]\, ds(\boldsymbol{\xi}) \\ &- \int_{\Gamma_{in}} H_{\alpha J}^P\, n_\alpha(\boldsymbol{\xi})\, \big[u_J(\boldsymbol{\xi}) - \hat{u}_J(\boldsymbol{\xi})\big]\, ds(\boldsymbol{\xi}) \end{aligned} \tag{E.10}$$

Equation (E.10) are used to determine rigid body motions at two points $\boldsymbol{x}^{(1)}$ and $\boldsymbol{x}^{(2)}$ inside the domain Ω_{in}, then the rigid body displacement and rotation are readily to obtained.

E.4 Numerical examples

To verify the proposed treatment for problem of multiply connected domain with inner boundary subjected to pure traction, some examples with existing exact solution are considered.

E.4.1 Hollow square plate under uniaxial tension

To verify the treatment for multiply-connected domain under self-equilibrated traction applied on the boundary, consider a hollow square plate under uniaxial tension σ_o applied on the edges of the plate on both outer and inner boundary as shown in Fig. E.2(a). The outer edge and the inner edge of the plate have a length of $2a$ and a, respectively. An isotropic material with Young's modulus E and Poisson's ratio ν is used for the problem. The condition of plane strain is assumed. For this problem, the exact stress field in entire plate is $\sigma_{ij} = \delta_{i2}\delta_{j2}\sigma_o$. With the constraints on the outer boundary to remove the rigid body motion of the plate as shown in Fig. E.2(b) and the origin of the coordinate system being at the center of the plate, the exact solution for the displacement field is given as

$$u_1 = -\frac{\sigma_o}{E}\nu(1+\nu)(x_1+a) \tag{E.11}$$

$$u_2 = \frac{\sigma_o}{E}(1-\nu^2)(x_2+a) \tag{E.12}$$

Fig. E.2(b) also shows the supplemental constraints used for 'suppressing' the rigid body motion of the inner boundary. A mesh shown in Fig. E.2(c) is used for the analysis. Numerical results of the displacements at the corners A and B (see Fig. E.2(b)) normalized by the exact solution are shown in Table E.1.

E.4.2 Axis-symmetric holed plate

Consider a holed plate subjected to an internal pressure σ_o and fixed at the outer boundary as shown schematically in Fig.E.3(a). For an isotropic material with Young modulus E and Poisson's ration ν and a condition of plane strain, the exact

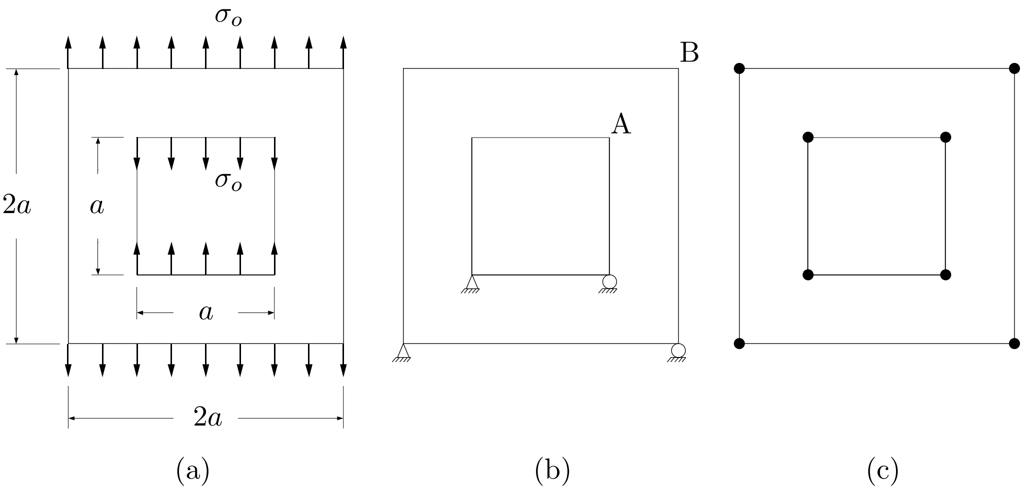

(a) (b) (c)

Figure E.2: Hollow square plate under uniaxial tension: (a) schematic of the problem; (b) constraints on outer boundary to remove rigid body motion of the plate and supplemental constraints on inner boundary to 'suppress' the rigid body motion of the inner boundary; (c) mesh used for the analysis.

Displacement at A		Displacement at B	
$\frac{u_1}{u_1^{exa}}$	$\frac{u_2}{u_2^{exa}}$	$\frac{u_1}{u_1^{exa}}$	$\frac{u_2}{u_2^{exa}}$
1.0003	1.0004	1.0005	1.0005

Table E.1: Displacements at A and B for the problem of Fig. E.2. Results are normalized by the exact solution.

solution for radial displacement of any point on the inner boundary is given as

$$u_r(a) = -\frac{3\sigma_o}{E}\frac{(1+\nu)(1-2\nu)}{8\nu-5}a \tag{E.13}$$

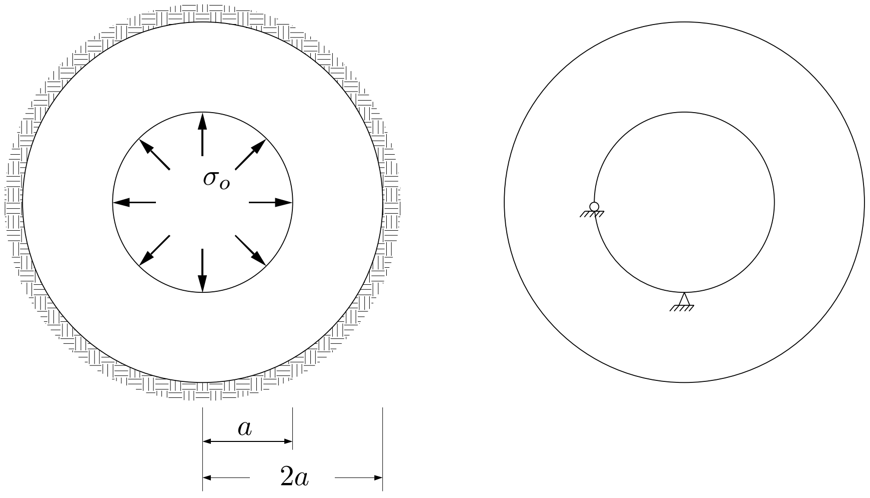

(a) (b)

Figure E.3: A holed plate subjected to inner pressure: (a) schematic of the problem; (b) supplemental constraints employed to ‘suppress’ the rigid body motion of the inner boundary.

Three constraints are added to the inner boundary as shown in Fig. E.3(b). The three meshes shown in Fig. E.4 are used for the analysis, and the corresponding results are shown in Table E.2. Excellent agreement with the exact solution are seen even with the very coarse mesh (mesh 1).

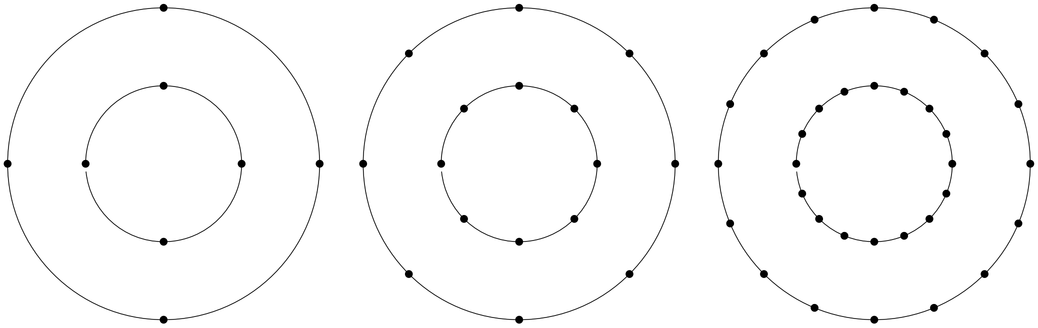

Figure E.4: Meshes employed for the analysis of the problem in Fig. E.3.

Mesh #	$\frac{u(a)}{u^{exact}}$
1	0.9918
2	0.9998
3	1.0000

Table E.2: Radial displacement of a point on the hole boundary for the problem of Fig. E.3.

Appendix F

Problems corresponding to the case of $N = 1$

Two examples for the types of problems corresponding to the case of $N = 1$ in the governing equations (2.1) and (2.2) stated in Chapter 2 are the problem of steady-state Darcy's flow in porous media and the problem of heat conduction. Specifically, for the problem of Darcy's flow in porous media, the 'stress' vector $\sigma_{\alpha 1}$ denotes the fluid flux v_α, the scalar 'displacement' u_1 denotes the fluid pressure p and the second-order tensor of material constants $E_{\alpha 11 \beta}$ denotes the permeability tensor $\kappa_{\alpha\beta}$. Then the governing equations (2.1) and (2.2) for a domain of no distributed source are rewritten as

$$\frac{\partial}{\partial x_\alpha} v_\alpha(\boldsymbol{x}) = 0 \tag{F.1}$$

$$v_\alpha(\boldsymbol{x}) = -\frac{\kappa_{\alpha\beta}}{\mu} \frac{\partial}{\partial x_\beta} p(\boldsymbol{x}) \tag{F.2}$$

Next, for the problem of heat conduction in anisotropic material, $\sigma_{\alpha 1}$ denotes the heat flux q_α, u_1 denotes the temperature T, and $E_{\alpha 11 \beta}$ denotes the Fourier constants $k_{\alpha\beta}$. Then the equations (2.1) and (2.2) are rewritten as

$$\frac{\partial}{\partial x_\alpha} q_\alpha(\boldsymbol{x}) = 0 \tag{F.3}$$

$$q_\alpha(\boldsymbol{x}) = -k_{\alpha\beta} \frac{\partial}{\partial x_\beta} T(\boldsymbol{x}) \tag{F.4}$$

Bibliography

[1] A. M. Al-Ani and J. W . Hancock. J-dominance of short cracks in tension and bending. *J. Mech. Phys. Solids*, 39:23–43, 1991.

[2] S. N. Atluri, A. S. Kobayashi, and M. Nakagaki. A finite-element program for fracture mechanics analysis of composite material. *Fracture mechanics of composites, ASTM-STP, G.P. Sendeckyj, editor; American Society for Testing and Materials*, 593:86–98, 1975.

[3] M.R. Ayatollahi, M.J. Pavier, and D.J. Smith. Determination of T-stress from finite element analysis for mode I and mixed mode I/II loading. *Internat. J. Fracture*, 91:283–298, 1998.

[4] L. Banks-Sills, I. Hershkovitz, P. A. Wawrzynek, R. Eliasi, and A. R. Ingraffea. Methods for calculating stress intensity factors in anisotropic materials: Part I - z=0 is a symmetric plane. *Engrg. Fracture Mech.*, 72:2328–2358, 2005.

[5] D. M. Barnett and R. J. Asaro. The fracture mechanics of slit-like cracks in anisotropic elastic media. *J. Mech. Phys. Solids*, 20:353–366, 1972.

[6] D. M. Barnett and J. Lothe. Dislocation and line charges in anisotropic piezoelectric insulators. *Physica Stutus Solidi (b)*, 67:105–111, 1975.

[7] E. Becache, J. C. Nedelec, and N. Nishimura. Regularization in 3D for anisotropic elastodynamic crack and obstacle problems. *J. Elasticity*, 31:25–46,

1993.

[8] G. Bonnet. A general regularization of the hypersingular integrals in the symmetric Galerkin boundary element method. *Internat. J. Numer. Methods Engrg.*, 80:1110–1123, 2009.

[9] M. Bonnet and M. Guiggiani. Direct evaluation of double singular integrals and new free terms in 2D (symmetric) Galerkin BEM. *Comput. Methods Appl. Mech. Engrg.*, 192:2565–2596, 2003.

[10] T. J. Boone, P. A. Wawrzynek, and A. R. Ingraffea. Finite element modeling of fracture propagation in orthotropic materials. *Engng. Fract. Mech.*, 26:185–201, 1987.

[11] O. L. Bowie and C. D. Fresse. Central crack in plane orthotropic rectangular sheet. *Int. J. Fract.*, 8:49–58, 1972.

[12] G. E. Cardew, M. R. Goldthorpe, I.C. Howard, and A. P. Kfouri. On the elastic T-Term, Fundamentals of deformation and fracture. In: B. A. Bilby, K. J. Miller, J. R. Willis, editors. *Proceedings of the Eshelby Memorial Symposium, Sheffield, 2-5 April 1984. Cambridge University Press*, pages 465–476, 1985.

[13] A. Carini, M. Diligenti, P. Maranesi, and M. Zanella. Analytical integrations for two-dimensional elastic analysis by the symmetric Galerkin boundary element method. *Comp. Mech.*, 23:308–323, 1999.

[14] C. Chang and M. E. Mear. A boundary element method for two dimensional linear elastic fracture analysis. *Int. J. Fract.*, 74:219–251, 1995.

[15] C.-S. Chen, R. Krause, R. G. Pettit, L. Banks-Sills, and A. R. Ingraffea. Numerical assessment of T-stress computation using a p-version finite element method. *Internat J. Fractures*, 107:177–199, 2001.

[16] B. Cotterell and J. R. Rice. Slightly curved or kinked cracks. *Internat J. Fracture*, 16:155–169, 1980.

[17] T. A. Cruse. *Boundary Element Analysis in Computational Fracture Mechanics.* Kluwer Academic Publishers, 1988.

[18] G. Davi and A. Milazzo. Multidomain boundary integral formulation for piezoelectric materials fracture mechanics. *Int. J. Solids Struct.*, 38:7065–7078, 2001.

[19] S. R. Deans. *The Radon transform and some of its applications.* John Wiley & Sons, 1983.

[20] M. Denda. Mixed Mode I, II and III analysis of multiple cracks in plane anisotropic solids by the BEM: a dislocation and point force approach. *Engrg. Anal. Bound. Elem.*, 25:267–278, 2001.

[21] M. Denda, Y. Araki, and Y.K. Yong. Time-harmonic BEM for 2-D piezoelectricity applied to eigenvalue problems. *Internat. J. Solids and Structures*, 41:7241–7265, 2004.

[22] M. Denda and C.-Y. Wang. 3D BEM for general piezoelectric solids. *Comput. Methods Appl. Mech. Engrg.*, 198:2950–2963, 2009.

[23] F. Erdogan. On the stress distribution in plates with linear cuts under arbitrary loads. *Proceedings of The Fourth U.S. National Congress of Applied Mechanics*, pages 547–553, 1962.

[24] A. Frangi and G. Novati. Symmetric BE method in two-dimensional elasticity: evaluation of double integrals for curved elements. *Comp. Mech.*, 19:58–68, 1996.

[25] A. Frangi and G. Novati. Regularized symmetric Galerkin BIE formulations in the Laplace transform domain for 2D problems. *Comp. Mech.*, 22:50–60, 1998.

[26] C.F. Gao, H. Kessler, and H. Balke. Crack problems in magnetoelectroelastic solids. Part I: exact solution of a crack. *Int. J. Engng. Sci.*, 41:969–981, 2003.

[27] C.F. Gao, H. Kessler, and H. Balke. Crack problems in magnetoelectroelastic solids. Part II: general solution of collinear cracks. *Int. J. Engng. Sci.*, 41:983–994, 2003.

[28] H. Gao and C.-H. Chiu. Slightly curved or kinked cracks in anisotropic elastic solids. *Internat. J. Solids and Structures*, 29:947–972, 1992.

[29] F. Garcia, A. Saez, and J. Dominguez. Traction boundary elements for cracks in anisotropic solids. *Engrg. Anal. Bound. Elem.*, 28:667–676, 2004.

[30] F. Garcia-Sanchez, R. Rojas-Diaz, A. Saez, and Ch. Zhang. Fracture of magnetoelectroelastic composite materials using boundary element method (BEM). *Theoretical and Applied Fracture Mechanics*, 47:192–204, 2007.

[31] F. Garcia-Sanchez, A. Saez, and J. Dominguez. Anisotropic and piezoelectric materials fracture analysis by BEM. *Comput. Struct.*, 83:804–820, 2005.

[32] N. Ghosh, H. Rajiyah, S. Ghosh, and S. Mukherjee. A new boundary element method formulation for linear elasticity. *J. Applied Mechanics*, 53:69–76, 1986.

[33] U. Groh and M. Kuna. Efficient boundary element analysis of cracks in 2D piezoelectric structures. *Int. J. Solids Struct.*, 42:2399–2416, 2005.

[34] B. S. Henry and A. R. Luxmoore. Three-dimensional evaluation of the T-stress in centre cracked plates. *Internat. J. Fracture*, 70:35–50, 1995.

[35] P. J. Hirth and J. Lothe. *Theory of dislocations.* A Wiley-Interscience Publication, New York, 2nd edition, 1982.

[36] A.P. Kfouri. Some evaluations of the elastic T-term using Eshelby's method. *Int. J. Fract.*, 30:301–315, 1986.

[37] J. Kim and G. H. Paulino. T-stress, mixed-mode stress intensity factors, and crack initiation angles in functionally graded materials: a unified approach using the interaction integral method. *Comput. Methods Appl. Mech. Engrg*, 192:1463–1494, 2003.

[38] J. Kim and G. H. Paulino. T-stress in orthotropic functionally graded materials: Lekhnitskii and Stroh formalisms. *Int. J. Fracture*, 126:345–384, 2004.

[39] S. G. Larsson and A. J. Carlsson. Influence of non-singular stress terms and specimen geometry on small-scale yielding at crack tips in elastic-plastic materials. *J. Mech. Phys. Solids*, 21:263–277, 1973.

[40] P. S. Leevers and J. C. Radon. Inherent stress biaxiality in various fracture specimen geometries. *Internat. J. Fracture*, 19:311–325, 1982.

[41] S. Li and M. E. Mear. Singularity-reduced integral equations for discontinuities in three-dimensional linear elastic media. *Internat. J. Fracture*, 93:87–114, 1998.

[42] S. Li, M. E. Mear, and L. Xiao. Symmetric weak-form integral equation method for three dimensional fracture analysis. *Comput. Methods Appl. Mech. Engrg*, 151:435–539, 1998.

[43] K. M. Liew, Yuzhou Sun, and S. Kitipornchai. Boundary element-free method for fracture analysis of 2-D anisotropic piezoelectric solids. *Int. J. Numer. Methods Engrg.*, 69:729–749, 2007.

[44] J. Liu, X. Liu, and Y. Zhao. Green's functions for anisotropic magnetoelectroelastic solids with an elliptical cavity or a crack. *Internat. J. Engrg. Science*, 39:1405–1418, 2001.

[45] J. Lothe. Dislocations in anisotropic media: The interaction energy. *Phil. Mag. A*, 46:177–180, 1982.

[46] P. A. Martin and F. J. Rizzo. Hypersingular integrals: how smooth must the density be. *Internat. J. Numer. Methods Engrg.*, 39:687–704, 1996.

[47] S. Melin. The influence of the T-stress on the directional stability of cracks. *Internat J. Fracture*, 114:259–265, 2002.

[48] T. Nakamura and D. M. Parks. Determination of T-stress along three-dimensional crack fronts using an interaction integral method. *Internat J. Solids Struct.*, 29:1597–1611, 1992.

[49] Y. E. Pak. Linear electro-elastic fracture mechanics of piezoelectric materials. *Int. J. Fract.*, 54:79–100, 1992.

[50] E. Pan. A BEM analysis of fracture mechanics in 2D anisotropic piezoelectric solids. *Engrg. Anal. Bound. Elem.*, 23:67–76, 1999.

[51] P. Parreira and M. Guiggiani. On the implementation of the Galerkin approach in the boundary element method. *Computers & Structures*, 33:269–279, 1989.

[52] J.J. Perez-Gavilan and M. H. Aliabadi. A symmetric Galerkin BEM for multi-connected bodies: a new approach. *Engrg. Anal. Bound. Elem.*, 25:633–638, 2001.

[53] J.J. Perez-Gavilan and M. H. Aliabadi. Symmetric Galerkin BEM for multi-connected bodies. *Commun. Numer. Meth. Engrg.*, 17:761–770, 2001.

[54] R.K.N.D. Rajapakse and X.-L. Xu. Boundary element modeling of cracks in piezoelectric solids. *Engrg. Anal. Bound. Elem.*, 25:771–781, 2001.

[55] J. D. Richardson and T. A. Cruse. Weakly singular stress-BEM for 2D elastostatics. *Internat. J. Numer. Methods Engrg.*, 45:13–35, 1999.

[56] J. Rungamornrat and M. E. Mear. A weakly-singular SGBEM for analysis of cracks in 3D anisotropic media. *Comput. Methods Appl. Mech. Engrg.*, 197:4319–4332, 2008.

[57] J. Rungamornrat and M. E. Mear. Analysis of fractures in 3D piezoelectric media by a weakly singular integral equation method. *Int. J. Fract*, 151:1–27, 2008.

[58] J. Rungamornrat and M. E. Mear. Weakly-singular, weak-form integral equations for cracks in three-dimensional anisotropic media. *Internat. J. Solids and Structures*, 45:1283–1301, 2008.

[59] A. Salvadori. Analytical integrations in 2D BEM elasticity. *Internat. J. Numer. Methods Engrg.*, 53:1695–1719, 2002.

[60] P. D. Shah, C. L. Tan, and X. Wang. T-stress solutions for two-dimensional crack problems in anisotropic elasticity using boundary element method. *Fatigue Fract. Engng. Mater. Struct.*, 29:342–356, 2005.

[61] T. L. Sham. The determination of the elastic T-term using higher order weight functions. *Internat. J. Fracture*, 48:81–102, 1991.

[62] S Sirtori, G Maier, G Novati, and S Miccoli. A Galerkin symmetric boundary-element method in elasticity: formulation and implementation. *Internat. J. Numer. Methods Engrg.*, 35:255–282, 1992.

[63] J. Sladek, V. Sladek, and P. Fedelinski. Contour integrals for mixed-mode crack analysis: effect of nonsingular terms. *Theor. Appl. Fract. Mech.*, 27:115–127, 1997.

[64] J. Sladek, V. Sladek, P. Solek, and E. Pan. Fracture analysis of cracks in magneto-electro-elastic solids by the MLPG. *Comput. Mech.*, 42:697–714,

2008.

[65] A. H. Stroud and D. Secrest. *Gaussian quadrature formulas.* Englewood Cliffs, N.J., Prentice-Hall, 1966.

[66] R.K.L Su and H.Y. Sun. Numerical solutions of two-dimensional anisotropic crack problems. *Internat. J. Solids and Structures*, 40:4615–4635, 2003.

[67] R.K.L Su and H.Y. Sun. A brief note on elastic T-stress for centred crack in anisotropic plate. *Internat. J. Fracture*, 131:53–58, 2005.

[68] Z. Suo, C.-M. Kuo, D. M. Barnett, and J. R. Willis. Fracture mechanics for piezoelectric ceramics. *J. Mech. Phys. Solids*, 40:739–765, 1992.

[69] A. Sutradhar and G. H. Paulino. Symmetric Galerkin boundary element computation of T-stress and stress intensity factors for mixed-mode cracks by the interaction integral method. *Engrg. Anal. Bound. Elem.*, 28:1335–1350, 2004.

[70] H. Tada, P. C. Paris, and G. R. Irwin. *The stress analysis of cracks handbook.* The American Society of Mechanical Engineers, 3rd edition, 2000.

[71] Wen-Ye Tian and U. Gabbert. Multiple crack interaction problem in magnetoelectroelastic solids. *European J. Mech. A/Solids*, 23:599–614, 2004.

[72] T. C. T. Ting. *Anisotropy elasticity: theory and applications.* Oxford University Press, 1996.

[73] Y. Ueda, K. Ikeda, T. Yao, and M. Aoki. Characteristics of brittle failure under general combined modes including those under bi-axial tensile loads. *Engrg. Fracture Mech.*, 18:1131–1158, 1983.

[74] B.-L. Wang and Y.-W. Mai. Fracture of piezoelectromagnetic materials. *Mech. Research Communications*, 31:65–73, 2004.

[75] C.-Y. Wang. Two-dimensional elastostatic Green's functions for general anisotropic solids and generalization of Stroh's formalism. *Int. J. Solids Structures*, 31:2591–2597, 1994.

[76] C.-Y. Wang. Green's functions and general formalism for 2D piezoelectricity. *Appl. Math. Lett.*, 9:1–7, 1996.

[77] C.-Y. Wang and J. D. Achenbach. Elastodynamic fundamental solutions for anisotropic solids. *Geophys. J. Int.*, 118:384–392, 1994.

[78] C.-Y. Wang and M. Denda. 3D BEM for general anisotropic elasticity. *Internat. J. Solids and Structures*, 44:7073–7091, 2007.

[79] C.-Y. Wang and Ch. Zhang. 3-D and 2-D Dynamic Green's functions and time-domain BIEs for piezoelectric solids. *Engrg. Anal. Bound. Elem.*, 29:454–465, 2005.

[80] X. Wang. Determination of weight functions for elastic T-stress from reference T-stress solutions. *Fatigue Fracture Engrg. Mater. Structs.*, 25:965–973, 2002.

[81] X. Wang. Elastic T-stress for cracks in test specimens subjected to non-uniform stress distributions. *Engrg. Fracture Mech.*, 69:1339–1352, 2002.

[82] J. G. Williams and P. D. Ewing. Fracture under complex stress - the angled crack problem. *Internat. J. Fracture*, 8:416–441, 1972.

[83] M. L. Williams. On the stress distribution at the base of a stationary crack. *J. Appl. Mech.*, 24:109–114, 1957.

[84] L. Xiao. *Symmetric weak-form integral equation method for three dimensional fracture analysis.* PhD. Dissertation, The University of Texas at Austin, 1998.

[85] G. Xu. A variational boundary integral method for the analysis of three-dimensional cracks of arbitrary geometry in anisotropic elastic solids. *J. Appl. Mech.*, 67:403–408, 2000.

[86] G. Xu and M. Ortiz. A variational boundary integral method for the analysis for 3-D cracks of arbitrary geometry modeled as continuous distributions of dislocation loops. *Internat. J. Numer. Methods Engrg.*, 36:3675–3701, 1993.

[87] B. Yang and K. Ravi-Chandar. Evaluation of elastic T-stress by the stress difference method. *Engng. Fract. Mech.*, 64:589–605, 1999.

[88] S. Yang and F.-G. Yuan. Determination and representation of the stress coefficient term by path-independent integrals in anisotropic cracked solids. *Internat. J. Solids and Structures*, 37:6635–6682, 2000.

[89] S. Yang and F.-G. Yuan. Kinked crack in anisotropic bodies. *Internat. J. Solids and Structures*, 37:6635–6682, 2000.

Vita

Han Duc Tran was born in Da Nang, Vietnam. After his work at Le Quy Don High School, he entered Ho Chi Minh City University of Architecture in 1992, where he received the degree of Bachelor of Science in 1997. He received the degree of Master of Science from Université de Liège in 2001. He was admitted to the Graduate School of The University of Texas at Austin in August 2004 and enrolled in the Aerospace Engineering and Engineering Mechanics Department.

Permanent address: 124 Thanh Long
Da Nang, Vietnam

This dissertation was typeset with LaTeX[†] by the author.

[†] LaTeX is a document preparation system developed by Leslie Lamport as a special version of Donald Knuth's TeX Program.